RĪGAS TEHNISKĀ UNIVERSITĀTE

Madara Dārziņa

ELEKTROĶĪMISKAS OKSIDĒŠANAS INDUCĒTA *C–O* UN *C–N* SAIŠU VEIDOŠANA FURĀNA UN CIKLOPROPĀNA ATVASINĀJUMOS

Promocijas darbs

ELECTROCHEMICAL OXIDATION INDUCED FORMATION OF *C–O* AND *C–N* BONDS IN FURAN AND CYCLOPROPANE DERIVATIVES

Doctoral Thesis

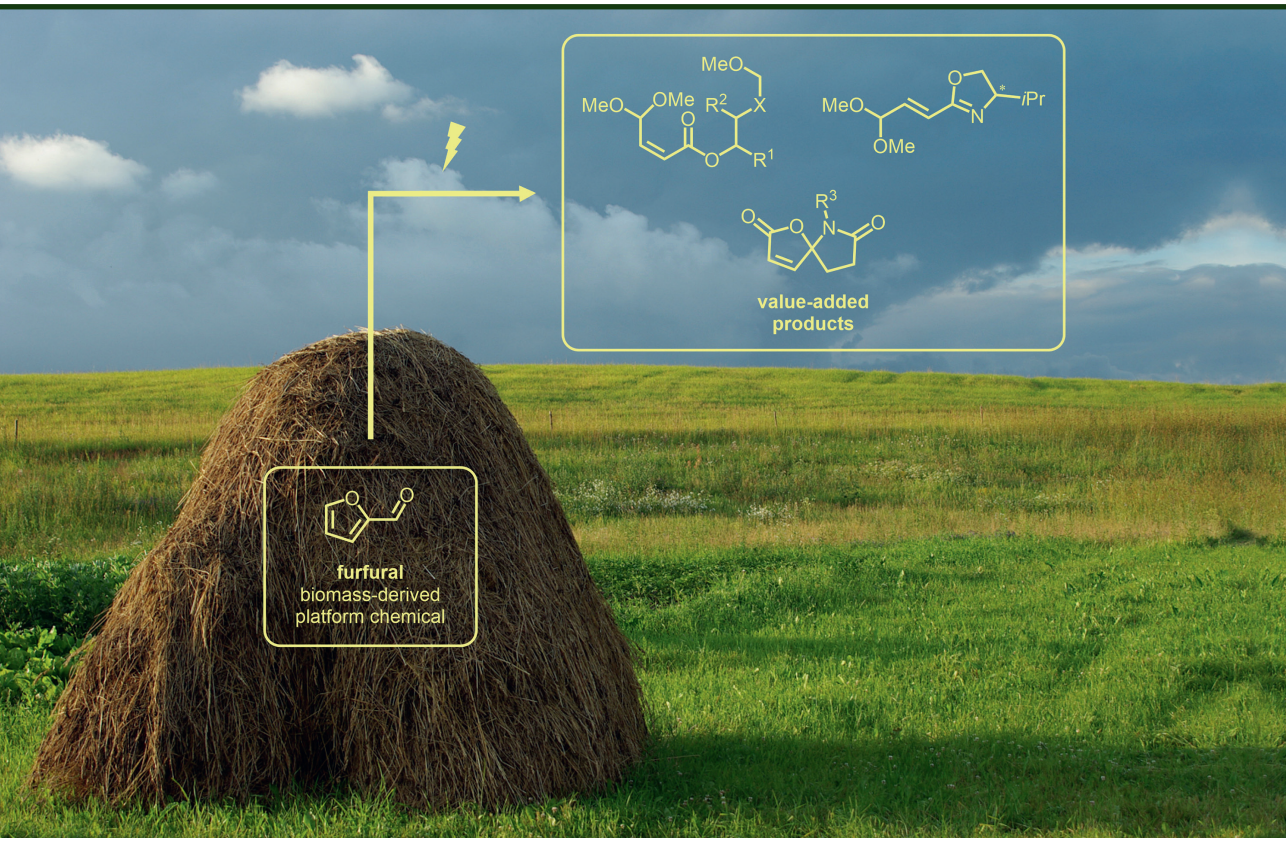

RTU Izdevniecība
RTU Press
Rīga 2026

RĪGAS TEHNISKĀ UNIVERSITĀTE
Dabaszinātņu un tehnoloģiju fakultāte
Ķīmijas un ķīmijas tehnoloģijas institūts

RIGA TECHNICAL UNIVERSITY
Faculty of Natural Sciences and Technology
Institute of Chemistry and Chemical Technology

Madara Dārziņa
Doktora studiju programmas "Ķīmijas, materiālzinātne un tehnoloģijas" doktorante
Doctoral Student of the Study Programme "Chemistry, Materials Science and Engineering"

ELEKTROĶĪMISKAS OKSIDĒŠANAS INDUCĒTA *C–O* UN *C–N* SAIŠU VEIDOŠANA FURĀNA UN CIKLOPROPĀNA ATVASINĀJUMOS

ELECTROCHEMICAL OXIDATION INDUCED FORMATION OF *C–O* AND *C–N* BONDS IN FURAN AND CYCLOPROPANE DERIVATIVES

Promocijas darbs
Doctoral Thesis

Zinātniskais vadītājs / Scientific supervisor

Profesors/Professor *Dr. chem.* AIGARS JIRGENSONS

RTU Izdevniecība / RTU Press
Rīga 2026

Dārziņa, M. Elektroķīmiskas oksidēšanas inducēta *C–O* un *C–N* saišu veidošana furāna un ciklopropāna atvasinājumos. Promocijas darbs. Rīga: RTU Izdevniecība, 2026. 103 lpp.

Dārziņa, M. Electrochemical Oxidation Induced Formation of *C–O* and *C–N* Bonds in Furan and Cyclopropane Derivatives. Doctoral Thesis. Riga: RTU Press, 2026. 103 p.

Publicēts saskaņā ar promocijas padomes "RTU P-01" 2025. gada 27. novembra lēmumu, protokols Nr. 244.26.

Published in accordance with the decision of the Promotion Council "RTU P-01" of 27th November 2025, Minutes No. 244.26.

Vāka attēla autore – Inga Sudāre-Špune
Cover photo by Inga Sudāre-Špune

PROMOCIJAS DARBS IZVIRZĪTS ZINĀTNES DOKTORA GRĀDA IEGŪŠANAI RĪGAS TEHNISKAJĀ UNIVERSITĀTĒ

Promocijas darbs zinātnes doktora (*Ph. D.*) grāda iegūšanai tiek publiski aizstāvēts 2026. gada 15. janvārī plkst. 17.00 Rīgas Tehniskās universitātes Dabaszinātņu un tehnoloģiju fakultātē, Rīgā, Paula Valdena ielā 3, 272. auditorijā.

OFICIĀLIE RECENZENTI

Asociētā profesore *Dr. chem*. Nelli Batenko,
Rīgas Tehniskā universitāte

Docents *Ph. D*. Maksim Ošeka,
Tallinas Tehnoloģiju universitāte, Igaunija

Asociētais profesors *Ph. D*. Vladislav Ivaništšev,
Latvijas Universitāte, Latvija

APSTIPRINĀJUMS

Apstiprinu, ka esmu izstrādājusi šo promocijas darbu, kas iesniegts izskatīšanai Rīgas Tehniskajā universitātē zinātnes doktora (*Ph. D.*) grāda iegūšanai. Promocijas darbs zinātniskā grāda iegūšanai nav iesniegts nevienā citā universitātē.

Madara Dārziņa ……. (paraksts)
Datums: ……

Promocijas darbs ir sagatavots kā tematiski vienota zinātnisko publikāciju kopa, kas papildināta ar kopsavilkumu latviešu un angļu valodā. Promocijas darbs apvieno četras zinātniskās publikācijas. Zinātniskās publikācijas ir angļu valodā, to kopējais apjoms ir 362 lappuses, ieskaitot pielikumus.

PATEICĪBAS/ACKNOWLEDGMENTS

Īpašs paldies:

- manam darba vadītājam profesoram *Dr. chem*. Aigaram Jirgensonam;
- *Ph. D.* Annai Lielpēterei, kura iepazīstināja mani ar elektroķīmiju un sniedza vērtīgus zinātniskos padomus šo gadu laikā;
- visiem OSM grupas kolēģiem par atbalstu doktorantūras laikā;
- profesoram *Dr. sc. ing*. Sergejam Gaidukovam un viņa grupai par veiksmīgo sadarbību biopolimēru sintēzē;
- Gentes Universitātes profesoram *Dr. ir*. Christian Stevens un *Dr. ir*. Anna Vanluchene, kuri uzņēma mani kā viespētnieci SynBioC grupā;
- bakalaurantiem, kuri šo gadu laikā ir strādājuši kopā ar mani: Olavam Rāciņam, Albertam Šeinam, Renātei Strazdiņai, Dmitrijam Černobrovkinam un Amālijai Gusarovai;
- *Dr. chem*. Jurim Popelim, *Dr. chem*. Baibai Turovskai, profesoram *Dr. sci. nat*. Jānim Velikam un *Dr. phys*. Sergejam Beļakovam par palīdzību un vērtīgajām konsultācijām darba izstrādes laikā;
- Fizikāli organiskās ķīmijas laboratorijai par KMR, AIMS un rentgenstruktūranalīzēm, un Hromatogrāfijas laboratorijai par AEŠH analīzēm un īpatnējās optiskās griešanas mērījumiem!

Promocijas darbs izstrādāts ar Latvijas Organiskās sintēzes institūta iekšējo grantu IG-2020-05, IG-2021-03, IG-2022-06, IG-2023-07, IG-2025-08, Atveseļošanas un noturības mehānisma (5.2.1.1.i.) doktorantu grantu Nr. 08/OSI/DG (2024) un Nr. 34/OSI/DG (2025) un projekta *TRANSPHARM* (Eiropas Savienības Horizon Europe pētniecības un inovāciju programmas granta Nr. 101057816) finansiālu atbalstu.

Special thanks to:

- My supervisor, Professor Dr. chem. Aigars Jirgensons;
- Anna Lielpētere, PhD, who introduced me to electrochemistry and has given a lot of invaluable advice over the years;
- All of my OSM group colleagues for their support during my doctoral studies;
- Professor Dr. sc. ing. Sergejs Gaidukovs and his group for successful collaboration in biopolymer synthesis;
- Professor Dr. ir. Christian Stevens and Dr. ir. Anna Vanluchene from Ghent University, who hosted me as a visiting researcher in the SynBioC group;
- Undergraduate students, who have worked with me during my doctoral studies: Olavs Rāciņš, Alberts Šeins, Renāte Strazdiņa, Dmitrijs Černobrovkins and Amālija Gusarova;
- Dr. chem. Juris Popelis, Dr. chem. Baiba Turovska, Professor Dr. sci. nat. Jānis Veliks and Dr. phys. Sergejs Beļakovs for help and invaluable advice during my doctoral studies;

- Laboratory of Physical Organic Chemistry for NMR, HRMS and X-ray analysis, and Laboratory of Chromatography for HPLC analysis and specific optical rotation measurements.

This Doctoral Thesis has been funded by Latvian Institute of Organic Synthesis internal grants IG-2020-05, IG-2021-03, IG-2022-06, IG-2023-07, IG-2025-08, Recovery and Resilience Facility (5.2.1.1.i.) doctoral career grants No. 08/OSI/DG (2024) and No. 34/OSI/DG (2025), and project TRANSPHARM (European Union Horizon Europe research and innovation program grant No. 101057816).

SATURS/CONTENTS

SAĪSINĀJUMI/ABBREVIATIONS AND ACRONYMS

9-BBN	9-borabiciklo[3.3.1]nonāns / 9-borabicyclo[3.3.1]nonane
A:	anods / anode
Ac	acetil- / acetyl-
AEŠH/HPLC	augstas efektivitātes šķidrumu hromatogrāfija / high-performance liquid chromatography
Alloc	aliloksikarbonil- / allyloxycarbonyl-
Ar	aril- / aryl-
ARO	akrilēta rapšu eļļa / acrylated rapeseed oil
BDD	ar boru leģēta dimanta elektrods / boron doped diamond electrode
BINAP	(2,2′-*bis*(difenilfosfīn)-1,1′-binaftils) / (2,2′-*bis*(diphenylphosphino)-1,1′-binaphthyl)
Boc	*terc*-butiloksikarbonil- / *tert*-butyloxycarbonyl-
Bz	benzoil- / benzoyl-
C_{Gr}	grafīta elektrods / graphite electrode
Cy	cikloheksil- / cyclohexyl-
DIPEA	*N*,*N*-diizopropiletilamīns / *N*,*N*-diisopropylethylamine
dr	diastereomēru attiecība / diastereomeric ratio
ee	enantiomērais pārākums / enantiomeric excess
E_p	potenciāla maksimums / peak potential
FTIR	Furjē transformācijas infrasarkanā spektroskopija / Fourier transform infrared spectroscopy
GC	stiklveida grafīta elektrods / glassy carbon electrode
HFIP	1,1,1,3,3,3-heksafluorpropān-2-ols / 1,1,1,3,3,3-hexafluoro-2-propanol
K:	katods / cathode
*m*CPBA	*meta*-hlorperoksibenzoskābe / *meta*-chloroperoxybenzoic acid
Me	metil- / methyl-
mol%	molprocenti / mole percent
MOM	metoksimetil- / methoxymethyl-
Ms	mezil- / mesyl-
NFSI	*N*-fluorbenzsulfonimīds / *N*-fluorobenzenesulfonimide
Nu	nukleofīls / nucleophile
ORTEP	*Oak Ridge Thermal-Ellipsoid Plot*
ox	anodiska oksidēšana / anodic oxidation
PG	aizsarggrupa / protecting group
PPTS	piridīnija *para*-toluolsulfonāts / pyridinium *para*-toluenesulfonate
*q*KMR/*q*NMR	kvantitatīvā kodolmagnētiskās rezonanses spektroskopija / quantitative nuclear magnetic resonance spectroscopy
SS	nerūsējošā tērauda elektrods / stainless steel electrode
TASF	*tris*(dimetilamino)sulfonija difluortrimetilsilikāts / *tris*(dimethylamino)-sulfonium difluorotrimethylsilicate
TBA	tetra-*n*-butilamonija katjons / tetra-*n*-butylammonium cation
TEA	trietilamīns / triethylamine
Teoc	2-(trimetilsilil)etoksikarbonil- / trimethylsilylethoxycarbonyl-
tfa	trifluoracetil- / trifluoroacetyl-
Troc	2,2,2-trihloretoksikarbonil- / 2,2,2-trichloroethoxycarbonyl-
Ts	tozil- / tosyl-
UEŠH/UPLC	ultraefektīvā šķidrumu hromatogrāfija / ultra-performance liquid chromatography

IEVADS

Elektroorganiskā sintēze ir organiskās sintēzes joma, kas ļauj veidot jaunas metodes organisku savienojumu iegūšanai, izmantojot elektrisko strāvu. Elektroķīmiskās sintēzes priekšrocības ir iespēja samazināt vai izvairīties no reducēšanas un oksidēšanas reaģentu izmantošanas, spēja kontrolēt reakcijas selektivitāti, regulējot pievadīto potenciālu, kā arī iespēja veikt transformācijas, kuras nevar panākt ar tradicionāli izmantotajiem ķīmiskajiem reaģentiem.[1]

Elektriskā strāva ir lēts enerģijas avots, ko iespējams iegūt no atjaunojamajiem resursiem, līdz ar to elektroķīmiskā sintēze atbilst pieprasījumam pēc ilgtspējīgas ķīmijas risinājumiem.[2] Elektroķīmiskās sintēzes jomas attīstību pēdējā desmitgadē ir veicinājis arī plašāks komerciāli pieejamā aprīkojuma piedāvājums, piemēram, *IKA ElectraSyn* potenciostats, kas tirgū parādījās 2017. gadā.[3] Rezultātā kopš 2014. gada ik gadu publicēto zinātnisko rakstu daudzums, kuros tiek izmantotas elektroķīmiskās sintēzes metodes, ir pieaudzis vairāk nekā 10 reizes.[4]

Elektrolīzes gaitā notiek heterogēna elektronu apmaiņa starp elektroda virsmu un substrātu. Anodreakcijā notiek elektronu pārnese no substrāta uz elektrodu jeb oksidēšana, savukārt katodreakcijā notiek pretējais process – elektronu pārnese no elektroda uz substrātu jeb reducēšana. Abas reakcijas ir saistītas vienotā procesā; elektrolīze bez oksidēšanās vai reducēšanās pusreakcijas nav iespējama.

Svarīgākie elektroķīmiskie parametri ir pievadītais strāvas stiprums un potenciāls. Strāvas stiprums raksturo elektronu pārneses ātrumu, savukārt potenciāls – tiem piemītošo enerģiju.[5] Nozīmīgs ir arī pievadītais lādiņa daudzums, ko nosaka strāvas stiprums laika vienībā. Lādiņa daudzumu izsaka faradejos (F), kur 1 F atbilst 96 485 C/mol lielam lādiņam. Tas ļauj noteikt, cik elektronu ekvivalentu (z F, kur z ir elektronu skaits uz substrāta molekulu) ir pievadīts reakcijas maisījumam, analoģiski reaģenta stehiometrijai.[5]

Promocijas darba izstrādes gaitā tika pētīta anodiskas oksidēšanas izmantošana jaunu ķīmisko savienojumu sintēzē. Reakcijas substrātu oksidēšana tika veikta uz anoda, savukārt uz katoda tika veikta protonu reducēšana līdz ūdeņradim, tādējādi mazinot reakcijas laikā ģenerēto atkritumu daudzumu. Elektroķīmiskās reakcijas tika veiktas tilpuma elektrolīzes apstākļos, kur reakcijas maisījums visu elektrolīzes laiku atrodas elektroķīmiskajā šūnā. Elektrolīzes veikšanai tika izmantots komerciāli pieejams standartizēts aprīkojums: potenciostats *IKA ElectraSyn 2.0*, kā arī *IKA* elektroķīmiskās šūnas un elektrodi.

Promocijas darba mērķis ir izstrādāt jaunas elektroķīmiskās sintēzes metodes *C-O* un *C-N* saišu veidošanai. Darbu veido divas daļas: 1) furāna atvasinājumu elektroķīmiska oksidēšana un iegūto produktu funkcionalizēšana; 2) ciklopropāna atvasinājumu elektroķīmiska oksidēšana. Katrā no pētītajiem virzieniem vismaz vienā sintēzes stadijā produkts tika iegūts, veicot izejvielas elektroķīmisku oksidēšanu.

Furāna atvasinājums furfurols **1** ir viens no produktiem, ko biomasas pārstrādes procesā iegūst lielos apjomos.[6] 2004. gadā ASV Enerģētikas departaments iekļāva furfurolu 12 daudzsološāko platformķimikāliju sarakstā.[7] Balstoties mūsu grupā iepriekš veiktajos pētījumos par spirociklisku bisketālu un nepiesātināto esteru iegūšanu no furāna konjugātiem, šajā darbā vēlējāmies papildināt zināmo metožu klāstu, kas ļautu no biomasas iegūto furfurolu transformēt par daudzfunkcionāliem būvblokiem: modificētiem

akrilātiem **2**, enantiobagātinātiem nepiesātinātiem oksazolīniem **3** un spirocikliskiem hemiaminālēteriem **4** (1. attēls).

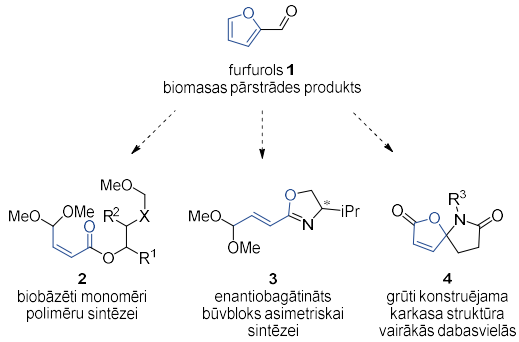

1. attēls. Promocijas darba pirmajā daļā definētie mērķsavienojumi **2**-**4**, kuru sintēze ietver furāna atvasinājumu elektroķīmisku oksidēšanu.

Promocijas darba otrā daļa veltīta elektroķīmiski inducētai neaktivētu ciklopropānu **5** *C*-*C* saites uzšķelšanai, lai iegūtu 1,3-difunkcionalizētus produktus **6** (1. shēma). Neaktivēta ciklopropāna gredzena oksidēšanās potenciāls ir pārāk augsts, lai varētu viegli veikt tā tiešu elektroķīmisku oksidēšanu,[8] tāpēc mēs izvēlējāmies konstruēt substrātus **5**, kuros ciklopropāns būtu savienots ar elektroķīmiski oksidējamu funkcionālo grupu – benzamīdu.

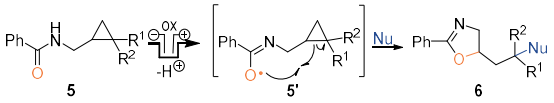

1. shēma. Elektroķīmiski inducēta neaktivētu ciklopropānu **5** uzšķelšana.

Paredzams, ka šādos substrātos elektroķīmiski iegūtais amidilradikālis **5'** spēj inducēt ciklopropāna *C*-*C* saites uzšķelšanu, veidojot jaunu *C*-*O* saiti. Uzšķelto starpproduktu oksidēšana un reakcija ar nukleofīlu ļautu iegūt ciklopropāna 1,3-difunkcionalizēšanas produktus **6**.

Pētījuma mērķis un uzdevumi

Promocijas darba mērķis ir izstrādāt jaunu metodoloģiju *C*-*O* un *C*-*N* saišu veidošanai, izmantojot elektroķīmisku oksidēšanu, un veikt iegūto produktu funkcionalizēšanu.

Promocijas darba uzdevumi:

1) biomasas izcelsmes furfurola konjugātu elektroķīmiska transformēšana par *α*,*β*-nepiesātinātiem esteriem un spirohemiaminālēteriem;
2) elektroķīmiski iegūto *α*,*β*-nepiesātināto esteru transformēšana par enantiobagātinātiem viniloksazolīniem;
3) elektroķīmiski inducēta neaktivētu ciklopropānu uzšķelšana un 1,3-difunkcionalizēšana.

Zinātniskā novitāte un galvenie rezultāti

Promocijas darbā izstrādātas trīs elektroķīmiskās metodes un viena sintēzes shēma daudzfunkcionālu būvbloku iegūšanai:

1) metode elektroķīmiskam viena reaktora procesam furfurilētu etilēnglikola atvasinājumu un furfurilētu aminospirtu transformēšanai par *α*,*β*-nepiesātinātiem esteriem;
2) sintēzes ceļš elektroķīmiski iegūto hirālo *α*,*β*-nepiesātināto esteru transformēšanai par enantiobagātinātiem viniloksazolīna būvblokiem;
3) metode elektroķīmiskai spirohemiaminālēteru iegūšanai no 3-(2-furil)propionskābes arilamīdiem;
4) metode elektroķīmiski inducētai neaktivētu ciklopropānu iekšmolekulārai uzšķelšanai ar amidilradikāli, un tai sekojošu monofluorēšanu.

Darba struktūra un apjoms

Promocijas darbs sagatavots kā tematiski vienota publikāciju kopa par elektroķīmiskās oksidēšanas izmantošanu jaunu *C-O/C-N* saišu veidošanā, kā arī par elektrolīzē iegūto produktu tālākas izmantošanas iespējām.

Darba aprobācija un publikācijas

Promocijas darba galvenie rezultāti apkopoti četrās oriģinālpublikācijās. Pētījumu rezultāti prezentēti 11 konferencēs.

Zinātniskās publikācijas

1. **Darzina**, **M**.; Lielpetere, A.; Jirgensons, A. Preparation of furfural derived enantioenriched vinyl oxazoline building block and exploring its reactivity. *Beilstein J. Org. Chem.* **2025**, *21*, 1737–1741. https://doi.org/10.3762/bjoc.21.136.
2. **Darzina**, **M**.; Jirgensons, A. Electrochemical Formation of Oxazolines by 1,3-Oxyfluorination of Non-activated Cyclopropanes. *Org. Lett*. **2024**, *26*, 2158–2162. https://doi.org/10.1021/acs.orglett.4c00143.
3. Briede, S.; Platnieks, O.; **Darzina**, **M**.; Jirgensons, A.; Gaidukovs, S. Effect of novel furan-based ester reactive diluent on structure and properties of UV-crosslinked acrylated rapeseed oil. *J. Polym. Sci*. **2023**, *61*, 3318–3328. https://doi.org/10.1002/pol.20230451.
4. **Darzina**, **M**.; Lielpētere, A.; Jirgensons, A. Torii-type electrosynthesis of *α*,*β*-unsaturated esters from furfurylated ethylene glycols and amino alcohols. *Eur. J. Org. Chem*. **2021**, 4224–4228. https://doi.org/10.1002/ejoc.202100605.

Konferences

1. **Darzina**, **M**.; Jirgensons, A. Electrochemical Formation of Oxazolines by 1,3-Oxyfluorination of Non-activated Cyclopropanes. *76th Annual Meeting of the International Society of Electrochemistry*. Vācija, 7.–12. septembris, **2025**. Stenda referāts.
2. **Darzina**, **M**.; Jirgensons, A. Electrochemical Formation of Oxazolines by 1,3-Oxyfluorination of Non-activated Cyclopropanes. *Electrifying Organic Synthesis.* Vācija, 3.–5. septembris, **2025**. Stenda referāts.
3. **Darzina**, **M**.; Černobrovkins, D.; Jirgensons, A. Electrochemical Formation of Oxazolines by 1,3-Oxyfluorination of Non-activated Cyclopropanes. *Electrochemistry 2024*. Vācija, 16.–19. septembris, **2024**. Stenda referāts.
4. **Darzina**, **M**.; Jirgensons, A. Electrochemical Formation of Oxazolines by 1,3-Oxyfluorination of Non-activated Cyclopropanes. *Balticum Organicum Syntheticum 2024*. Latvija, 7.–10. jūlijs, **2024**. Stenda referāts.
5. **Darzina**, **M**.; Černobrovkins, D.; Jirgensons, A. Electrochemical cleavage and subsequent oxyfluorination of cyclopropane *C*-*C* bond. *13th Paul Walden Symposium on Organic Chemistry*. Latvija, 14.–15. septembris, **2023**. Stenda referāts.
6. **Darzina**, **M**.; Lielpētere, A.; Jirgensons, A. Electrosynthesis of *α*,*β*-unsaturated esters from furfurylated ethylene glycols and amino alcohols. *73rd Annual Meeting of the International Society of Electrochemistry*. Tiešsaistē, 12.–16. septembris, **2022**. Virtuālais stenda referāts.
7. **Darzina**, **M**.; Lielpētere, A.; Jirgensons, A. Electrosynthesis of *α*,*β*-unsaturated esters from furfurylated ethylene glycols and amino alcohols. *Balticum Organicum Syntheticum 2022*. Lietuva, 3.–6. jūlijs, **2022**. Stenda referāts.
8. **Darzina**, **M**.; Lielpētere, A.; Jirgensons, A. Electrosynthesis of *α*,*β*-unsaturated esters from furfurylated ethylene glycols and amino alcohols *12th Paul Walden Symposium on Organic Chemistry*. Tiešsaistē, 28.–29. oktobris, **2021**. Virtuālais stenda referāts.
9. **Darzina**, **M**.; Lielpētere, A.; Jirgensons, A. Electrosynthesis of *α*,*β*-unsaturated esters from furfurylated ethylene glycols and amino alcohols. *72nd Annual Meeting of the International Society of Electrochemistry*. Tiešsaistē, 29. augusts–3. septembris, **2021**. Mutiska prezentācija.
10. **Darzina**, **M**.; Lielpētere, A.; Jirgensons, A. Electrosynthesis of *α*,*β*-unsaturated esters from furfuryl alcohol and furfurylamine derivatives. *Electrochemistry undercover 2020*. Tiešsaistē, 23.–24. septembris, **2020**. Virtuālais stenda referāts.
11. **Dārziņa**, **M**.; Lielpētere, A.; Jirgensons, A. Electrosynthesis of *α*,*β*-unsaturated esters from furfuryl alcohol and furfurylamine derivatives. *Graduate Student Symposium on Advantageous Electrochemistry 2020 online edition*. Tiešsaistē, 10.–11. septembris, **2020**. Mutiska prezentācija.

PROMOCIJAS DARBA GALVENIE REZULTĀTI

1. Torī (*Torii*) esteru elektrosintēze no furfurilētiem etilēnglikola atvasinājumiem un furfurilētiem aminospirtiem

1.1. Torī esteru elektrosintēzes viena reaktora procesa izveide

Iepriekš mūsu grupā tika izstrādāta metode elektroķīmiskai furāna atvasinājumu **7** transformēšanai par nepiesātinātajiem esteriem **9** divos atsevišķos elektrolīzes soļos galvanostatiskos tilpuma elektrolīzes apstākļos nedalītajā šūnā (2. shēma). Anodreakcijā tika veikta savienojumu **7** un **8** oksidēšana, katodreakcijā – protonu reducēšana līdz ūdeņradim. Katrā elektroķīmiskajā reakcijā tika izmantotas dažādas piedevas un fona elektrolīti.

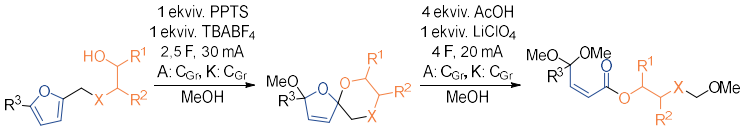

2. shēma. Elektroķīmiska furāna atvasinājumu **7** transformēšana par spirocikliem **8** un nepiesātinātajiem esteriem **9**.

Saskaņā ar piedāvāto reakcijas mehānismu (3. shēma) pirmajā elektrolīzes stadijā savienojumā **7a** notiek furāna cikla anodiska oksidēšana. Furāna katjonradikālim **10** uzbrūk iekšmolekulārais spirts, un, saslēdzot spirociklu, veidojas *C*-centrētais radikālis **11**. Tas tiek oksidēts par oksonija jonu **12**, kas reakcijas vidē pievieno metanolu, veidojot spirociklisko produktu **8a**.[9] Mehānisma pētījumi parādīja, ka otrajā elektrolīzes stadijā spirocikla uzšķelšanas pirmais solis ir substrāta **8a** oksidēšana par katjonradikāli **13**/**13'**. Pievienojot metanolu, veidojas oksiradikālis **14**, kurā *β*-fragmentēšanās rezultātā notiek *C*-*C* saites šķelšana. Iegūtais acikliskais *C*-centrētais radikālis **15** tiek oksidēts līdz oksonija jonam **16**, kas pievieno metanolu un veido nepiesātināto esteri **9a**.

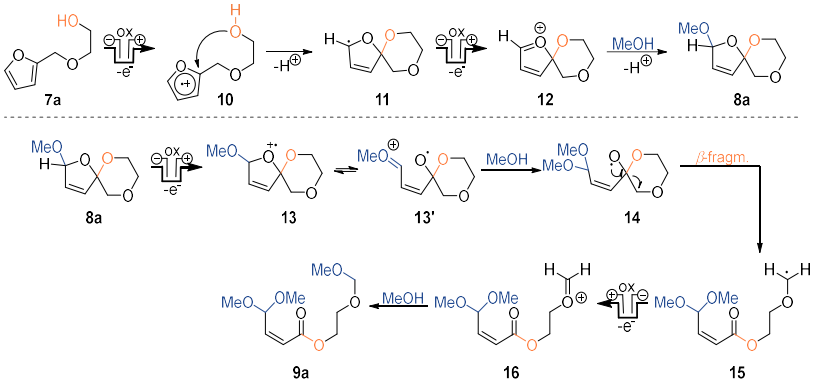

3. shēma. Iespējamais mehānisms spirta **7a** elektroķīmiskai transformēšanai par esteri **9a**.

Promocijas darbā tika izstrādāts viena reaktora process spirtu **7** transformēšanai par esteriem **9** divu soļu tilpuma elektrolīzē galvanostatiskos apstākļos nedalītajā šūnā (4. shēma). Veicot reakcijas apstākļu izpēti, tika noskaidrots, ka elektrolīzi var veikt divos posmos, neizolējot starpproduktu **8**. Pirmajā solī spirti **7** tika transformēti par spirocikliem **8**, kā piedevu izmantojot 1,1,1,3,3,3-heksafluorpropān-2-olu (HFIP). Reakcijas maisījumam tika pievadīts 2,2 F liels lādiņš, tad tika pievienoti 4 ekvivalenti etiķskābes, kam sekoja vēl 4 F liela lādiņa pievadīšana. Gala rezultātā tika iegūti esteri **9**.

No furāna atvasinājumiem **7a-c**, kas sānu ķēdē saturēja etilēnglikola fragmentu, produktus **9a-c** izdevās iegūt ar vidējiem iznākumiem (39–47 %), kas bija līdzvērtīgi vai zemāki, nekā veicot divas atsevišķas elektrolīzes, izolējot starpproduktus **8a-c**. Savukārt aminospirta fragmentu saturošo substrātu **7d-e** elektrolīzē esteru **9d-e** iznākumi bija ievērojami labāki (69–75 %; 4. shēma).

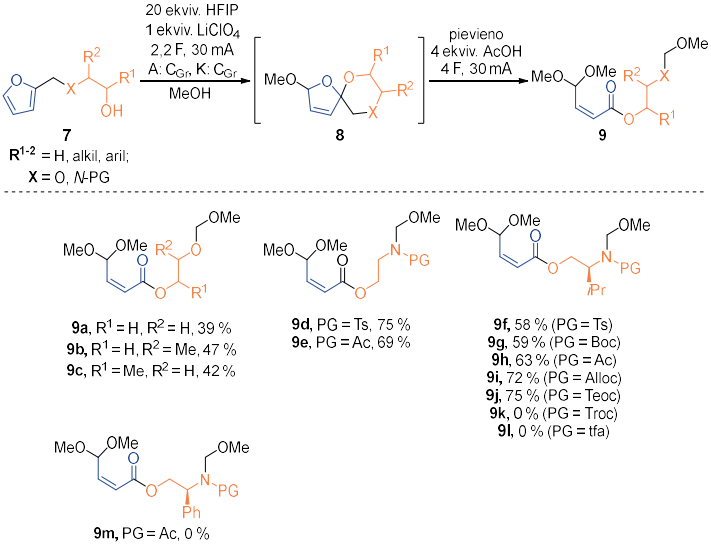

4. shēma. Nepiesātinātu esteru **9** iegūšana no furāna atvasinājumiem **7** viena reaktora procesā.

Lai paplašinātu produktu klāstu, tika sintezēti substrāti **7f-l**, kuros furāna gredzenam sānu ķēdē tika pievienots hirāls aminospirts – L-valinols. Amīniem ir zems oksidēšanās potenciāls (līdz 1,0 V, salīdzinot ar piesātinātu kalomela elektrodu (SCE)),[10] tāpēc, lai novērstu iespējamās blakusreakcijas, amīna grupa tika aizsargāta. Tika noskaidrots, ka Ts, Ac, Boc, Alloc un Teoc aizsarggrupas ir saderīgas ar elektrolīzes apstākļiem, kas ļāva iegūt produktus **9f-j**, savukārt halogēnus saturošās aizsarggrupas Troc un tfa elektrolīzes apstākļiem nebija piemērotas (4. shēma). Aizstājot valinola fragmentu ar fenilglicinola fragmentu, elektrolīzē veidojās sarežģīts produktu maisījums, no kura gaidīto produktu **9m** izolēt neizdevās (4. shēma).

Darba gaitā tika pētīts, kā aizvietotāju ievadīšana furāna gredzenā ietekmē elektrolīzes iznākumu. 4-Fenilfurānu saturošais savienojums **19** tika iegūts trīs soļos no komerciāli pieejamā 4-bromfurfurola **17** (5. shēma). Fenilgrupa furāna gredzenā tika ievadīta Suzuki-Mijauras reakcijā, veidojot produktu **18**, kuram reducējošās aminēšanas reakcijā tika pievienots valinols, un tika aizsargāta amīna funkcija. Spirta **19** elektrolīzē tika iegūts produktu maisījums, no kura gaidītais produkts **21** tika izolēts ar 8 % iznākumu (5. shēma).

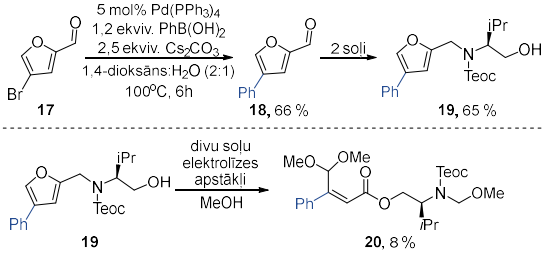

5. shēma. Fenilaizvietota furāna atvasinājuma **19** sintēze un elektrolīze.

Šajā nodaļā aprakstītie rezultāti apkopoti publikācijā "*Torii-type electrosynthesis of α,β-unsaturated esters from furfurylated ethylene glycols and amino alcohols*".

1.2. Biobāzēta akrilāta monomēra iegūšana polimerizācijas reakcijām

Promocijas darba izstrādes gaitā tika pētītas furāna atvasinājumu elektrolīzē iegūto produktu tālākas izmantošanas iespējas. Viens no darba virzieniem bija elektrolīzē iegūto esteru izmantošana polimēru sintēzē.

Pirmajiem pētījumiem kā potenciālais monomērs tika izvēlēts nepiesātinātais esteris **9a**. Tas tika iegūts divās secīgās elektrolīzēs no spirta **7a**, izolējot spirociklisko starpproduktu **8a**, jo viena reaktora procesā esteris **9a** veidojās ar zemu iznākumu (6. shēma). Tā kā izejvielas **7a** iekrāvums (422 mg; 3,0 mmol) bija lielāks nekā optimizētajos apstākļos (103 mg; 0,7 mmol (4. shēma)), bija iespējams samazināt nepieciešamā elektrolīta $TBABF_4$ daudzumu līdz 0,5 ekvivalentiem.

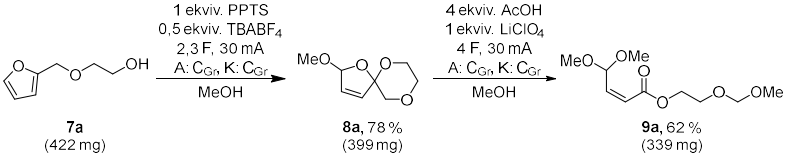

6. shēma. Estera **9a** elektrosintēze polimerizācijas pētījumiem.

Iegūtais esteris **9a** tika nodots sadarbības partneriem profesora S. Gaidukova laboratorijā (RTU), kuri to izmantoja kā reaktīvo atšķaidītāju, polimerizējot kopā ar akrilētu rapšu eļļu (ARO). Reaktīvā atšķaidītāja uzdevumi polimerizācijas procesā ir samazināt iegūtā polimēra viskozitāti un palielināt šķērssaišu veidošanos, kas spēj uzlabot iegūtā materiāla izturības un stiepes īpašības. Sadarbības partneru laboratorijā tika sintezēti vairāki kopolimēri, kuros reaktīvais atšķaidītājs **9a** tika pievienots 5 un 20 masas procentu daudzumā, attiecīgi iegūstot kopolimērus ARO/**9a** (5 %) un ARO/**9a** (20 %).

Polimēru iegūšana tika veikta divos soļos. Vispirms, sajaucot akrilēto rapšu eļļu ar attiecīgo estera **9a** daudzumu (5 vai 20 masas procenti), tika pagatavoti sveķi, tad maisījumam tika pievienots nelielā acetona daudzumā izšķīdināts radikāļu fotoiniciators (2,4,6-trimetilbenzoil)fosfīna oksīds (3 masas procenti). Maisījums tika atstāts uz nakti istabas temperatūrā, lai ļautu acetonam iztvaikot. Nākamajā solī šķidrais sveķu maisījums

tika uznests uz stikla substrāta 508 µm biezumā un pakļauts UV starojumam (405 nm), lai panāktu sacietēšanu. Rezultātā tika iegūtas polimēra filmas.

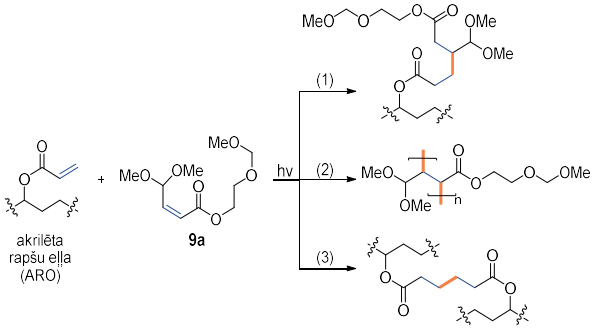

2. attēls. Akrilētas rapšu eļļas (ARO) un estera **9a** iespējamie kopolimerizēšanās produkti.

Radikāļu polimerizēšanās laikā kopolimērā var veidoties trīs dažādu veidu saites (2. attēls): reakcijā starp ARO un **9a** veidojas brīvi svārstīgas ķēdes fragmenti (1); vairākiem **9a** monomēriem reaģējot savās starpā, var veidoties (2) attēlotie fragmenti; trešā veida šķērssaišu veidošanās notiek starp diviem ARO fragmentiem (3), kas ir visvarbūtīgākā un notiek visātrāk, jo šajā gadījumā tiek savienotas divas terminālās dubultsaites.

FTIR spektroskopiskie mērījumi parādīja, ka iegūtajos polimēros ARO/**9a** (5 %) un ARO/**9a** (20 %) ir notikusi estera **9a** iekļaušana un pēc sacietēšanas UV staru ietekmē dubultsaišu signāli ir gandrīz pilnībā pazuduši. Estera **9a** iekļaušana redzama arī ar skenēšanas elektronu mikroskopu (SEM), par ko liecina tas, ka kopolimēru virsma ir ievērojami raupjāka nekā tīra ARO polimēra virsma.

Salīdzinot ar neatšķaidītu ARO polimēru, iegūtajiem kopolimēriem piemita līdz 1,6 reizēm zemāka viskozitāte (ARO/**9a** (20 %)) un uzlabots šķērssaišu savienošanās blīvums (no 1,07 mol/m^3 ARO polimērā līdz 1,65 mol/m^3 ARO/**9a** (5 %) kopolimērā).

Šis pētījums parādīja, ka no biomasas furāna un etilēnglikola konjugāta iegūtais nepiesātinātais esteris **9a** var veiksmīgi aizstāt no fosilās bāzes iegūtus akrilāta monomērus, veicot kopolimerizēšanu ar augu eļļām. Šajā nodaļā iegūtie rezultāti apkopoti publikācijā "*Effect of novel furan-based ester reactive diluent on structure and properties of UV-crosslinked acrylated rapeseed oil*".

1.3. No furfurola un valinola atvasināta enantiobagātināta viniloksazolīna būvbloka iegūšana un reaģētspējas izpēte

Nākamais apskatītais virziens elektroķīmiski iegūto esteru funkcionalizēšanā bija hirālo centru saturošo esteru **9i** transformācija par enantiobagātinātiem viniloksazolīniem **23**, ko varētu izmantot kā būvblokus asimetriskā sintēzē.

Saskaņā ar piedāvāto stratēģiju (7. shēma), izmantojot mūsu izstrādāto elektrolīzes metodi, no definētu hirālo centru saturošā furfurola un valinola konjugāta **7i** tiktu iegūts enantiobagātināts nepiesātinātais esteris **9i**. Nākamajā solī, veicot *N*-aizsarggrupu nošķelšanu, tika sagaidīts, ka atbrīvotais amīns **21** *in situ* pārgrupētos par amīdu **22**, ko

varētu tālāk transformēt par enantiobagātinātu viniloksazolīnu **23**. Tika pieļauta iespēja, ka kādā no sintēzes soļiem iespējama arī dubultsaites izomerizēšanās no *cis*- uz stabilāko *trans*-konfigurāciju. Amīna grupas aizsargāšanai tika izvēlēta Alloc-grupa, jo tā bija saderīga ar elektrolīzes apstākļiem, kā arī tās nošķelšanas apstākļos netika skarta acetāla funkcija.

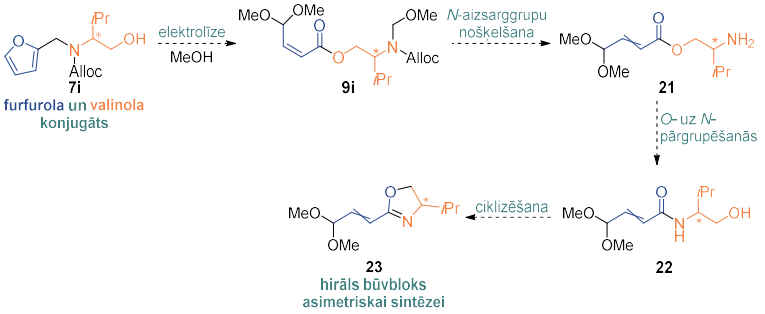

7. shēma. Stratēģija furfurola un valinola konjugāta **7i** transformēšanai par enantiobagātinātu viniloksazolīnu **23**.

Izmantojot 1.1. apakšnodaļā aprakstītos divu soļu elektrolīzes apstākļus, nepiesātināto esteri **9i** bija iespējams sintezēt preparatīvā mērogā (500 mg (2 mmol) un 1 grama (4 mmol) apjoma reakcijās) ar labiem iznākumiem (8. shēma).

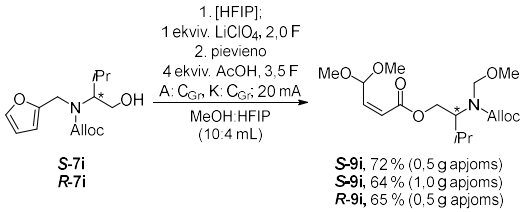

8. shēma. Nepiesātinātā estera **9i** iegūšana divu soļu elektrolīzes apstākļos preparatīvā mērogā.

Lai arī iepriekš atrastie elektrolīzes apstākļi bija piemēroti nepiesātinātā estera **9i** iegūšanai, tika izvēlēts vienkāršot elektrolīzes procesu, pārejot no divu soļu elektrolīzes uz nepārtrauktu elektrolīzi, kā arī samazināt dārgo vai bīstamo reaģentu izmantošanu (HFIP, $LiClO_4$), tāpēc tika veikta savienojuma ***S***-/***R***-**7i** elektrolīzes apstākļu optimizēšana (1. tabula).

Samazinot HFIP daudzumu no 4 mL līdz 1 mL vai 0,5 mL, nepārtrauktā elektrolīzē ar 5,5 F liela lādiņa pievadīšanu, veiksmīgi izdevās iegūt nepiesātināto esteri ***S***-**9i** (1. tabula, 2.–3. aile). Procesu iznākumi būtiski neatšķīrās no divu soļu sintēzes iznākumiem (72 % divu soļu sintēzē, 71 % un 70 % ar attiecīgi 1 mL un 0,5 mL HFIP nepārtrauktā sintēzē).

Aizstājot HFIP ar trīs ekvivalentiem AcOH arī izdevās veiksmīgi iegūt nepiesātinātos esterus ***S***-**9i** un ***R***-**9i** (1. tabula, 4.–6. aile). Elektrolīzes iznākums bija līdzvērtīgs divu soļu sintēzei 1 mmol apjomā (72 %), taču 2 mmol apjomā tas samazinājās līdz 68 %. Reakcijā izmantotā elektrolīta $LiClO_4$ daudzumu samazinājām no 1 līdz 0,5 ekvivalentiem (no 0,14 M uz 0,07 M). Palielinot AcOH daudzumu līdz 1 mL (~ 18 ekviv.) elektrolīzes iznākums

samazinājās līdz 55 %, kas liecināja, ka AcOH nav piemērots košķīdinātājs šai reakcijai (1. tabula, 7. aile). Savukārt, veicot elektrolīzi bez piedevām, produkts ***S*-9i** veidojās ar 60 % iznākumu (1. tabula, 8. aile). Aizstājot fona elektrolītu $LiClO_4$ ar LiOAc, tika novērots, ka elektrolīzes apstākļos veidojas spirocikls ***S*-8i**, taču nenotiek tā tālāka konversija par nepiesātināto esteri ***S*-9i** (1. tabula, 9. aile).

Optimizēšanas rezultātā izdevās modificēt elektrolīzes metodi, pārejot no divu soļu uz nepārtrauktu procesu. Iepriekš izmantotā piedevu kombinācija HFIP (4 mL) un AcOH (4 ekviv.) tika aizstāta ar vienu piedevu AcOH (3 ekviv.), kā arī izmantotā elektrolīta $LiClO_4$ daudzums tika samazināts uz pusi reakcijai 2 mmol apjomā (0,07 M). Turpmākajā darbā nepiesātinātā estera **9i** iegūšanai tika izmantoti 1. tabulas 5.–6. ailē aprakstītie apstākļi.

1. tabula

Savienojuma **7i** elektrolīzes apstākļu optimizēšana

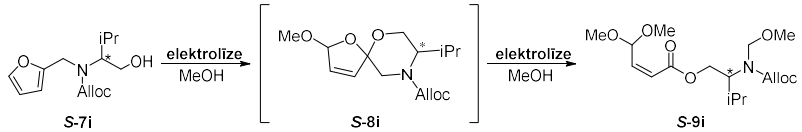

S-7i *R*-7i | *S*-8i *R*-8i | *S*-9i *R*-9i

Nr.	Apstākļi[a]	Iznākums 9i
1.[b]	1. solis: MeOH:HFIP (10:4 mL), $LiClO_4$ (1 ekviv.), 2,0 F; 2. solis: pievieno AcOH (4 ekviv.), 3,5 F	72 % (***S*-9i**)
2.	Nepārtraukta elektrolīze: MeOH:HFIP (13:1 mL), $LiClO_4$ (1 ekviv.), 5,5 F	71 % (***S*-9i**)
3.	Nepārtraukta elektrolīze: MeOH:HFIP (13,5:0,5 mL), $LiClO_4$ (1 ekviv.), 5,5 F	70 % (***S*-9i**)
4.	Nepārtraukta elektrolīze: MeOH (14 mL), AcOH (3 ekviv.), $LiClO_4$ (1 ekviv.), 5,5 F	72 % (***S*-9i**)
5.[b]	Nepārtraukta elektrolīze: MeOH (14 mL), AcOH (3 ekviv.), $LiClO_4$ (0,5 ekviv.), 5,5 F	68 %[c] (***S*-9i**)
6.[b]	Nepārtraukta elektrolīze: MeOH (14 mL), AcOH (3 ekviv.), $LiClO_4$ (0,5 ekviv.), 5,5 F	68 % (***R*-9i**)
7.	Nepārtraukta elektrolīze: MeOH:AcOH (13:1 mL), $LiClO_4$ (1 ekviv.), 5,5 F	55 % (***S*-9i**)
8.	Nepārtraukta elektrolīze: MeOH (14 mL), $LiClO_4$ (1 ekviv.), 5,5 F	60 % (***S*-9i**)
9.	Nepārtraukta elektrolīze: MeOH (14 mL), AcOH (3 ekviv.), LiOAc (1 ekviv.), 5,5 F	0 %[d] (***S*-9i**)

[a]Apjoms: 1 mmol. [b]Apjoms: 2 mmol; [c]Faradejiskā efektivitāte 49,5 %; šūnas produktivitāte 0,09 mmol/h; [d]mažorais produkts ir spirocikls ***S*-8i**.

Alloc grupas nošķelšanai tika izmantots palādija katalizators un pirolidīns (9. shēma). Tika novērots, ka reakcijas apstākļos tiek nošķelta arī *N*-MOM grupa un notiek gaidītā *O*- uz *N*- pārgrupēšanās. Izmantojot katalizatoru $Pd(PPh_3)_4$, pilna izejvielas ***S*-9i** konversija tika sasniegta 30 minūtēs, taču reakcijas apstākļos notika daļēja dubultsaites izomerizēšanās un

veidojās produktu *cis*-***S*-24** un *trans*-***S*-24** maisījums (9. shēma). Pārbaudot citus palādija katalizatorus un bāzes, neizdevās atrast apstākļus, kuros selektīvi varētu iegūt tikai *cis*-**24** produktu, savukārt, izmantojot Pd(*S*-BINAP)Cl_2 katalizatoru, izdevās panākt selektīvu produkta *trans*-**24** veidošanos. Atvasinot amīdu *trans*-***S*-24** par 4-brombenzoilesteri ***S*-25**, tika veikta iegūtā produkta rentgenstruktūranalīze, kas apstiprināja gaidīto atomu konektivitāti, dubultsaites izomerizēšanos un stereocentra absolūto konfigurāciju.

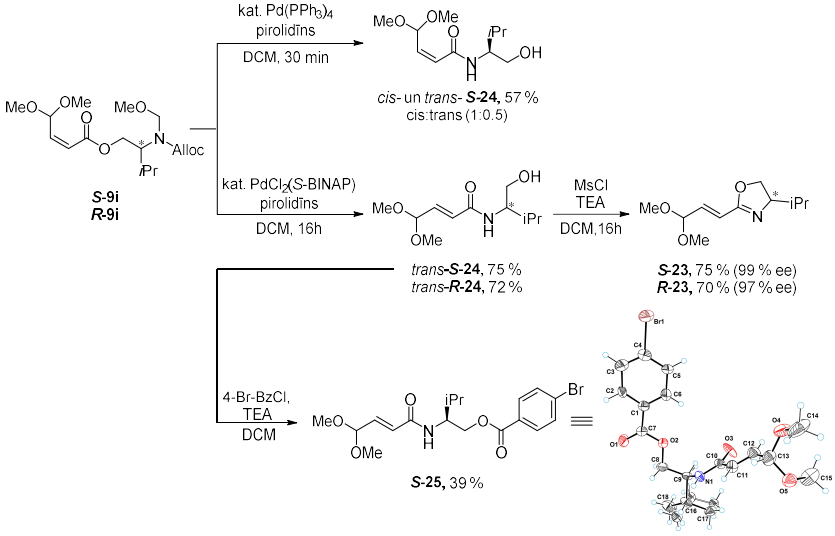

9. shēma. Elektrolīzē iegūtā estera **9i** transformācija par enantiobagātinātu viniloksazolīnu ***S*-/*R*-23** un *trans*-***S*-24** par 4-brombenzoilesteri ***S*-25**.

Iegūtie hidroksietilamīdi *trans*-***S*-/*R*-24** tika transformēti par attiecīgajiem oksazolīniem ***S*-/*R*-23**, izmantojot mezilhlorīdu un trietilamīnu (9. shēma). Hirālās AEŠH analīzes apstiprināja, ka iegūtajos oksazolīnos ***S*-/*R*-23** nav notikusi hirālā centra racemizācija.

Nākamajā darba posmā tika pētīta viniloksazolīna **23** izmantošana asimetriskā sintēzē, paredzot, ka oksazolīna cikls varētu kalpot kā hirāla virzītājgrupa.

Veicot aza-Dīlsa-Aldera reakciju ar oksazolīnu ***S*-23** un tozilizocianātu, tika iegūts oksazolo[3,2-*c*]pirimidīna atvasinājums **26** ar 86 % iznākumu (10. shēma). Produkts veidojās kā viens diastereomērs.

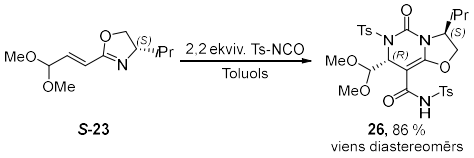

10. shēma. Oksazolo[3,2-*c*]pirimidīna **26** iegūšana aza-Dīlsa-Aldera reakcijā ar oksazolīnu ***S*-23**.

Saskaņā ar Eliota (*Elliott*) *et al*. piedāvāto reakcijas mehānismu,[11] produkta **26** veidošanās ietver asinhronu ciklopievienošanos (11. shēma). Vispirms, imidāta slāpeklim uzbrūkot izocianāta ogleklim, tiek ģenerēts intermediāts **27**, kam seko stereoselektīva cikla saslēgšana, veidojot dihidropirimidin-2-onu **28**. Savienojuma **28** nukleofīlā dubultsaite iesaistās reakcijā ar otru izocianāta molekulu, veidojot starpproduktu **29**/**29'**, kam seko protona pārnese, un tiek iegūts oksazolo[3,2-*c*]pirimidīns **26**.

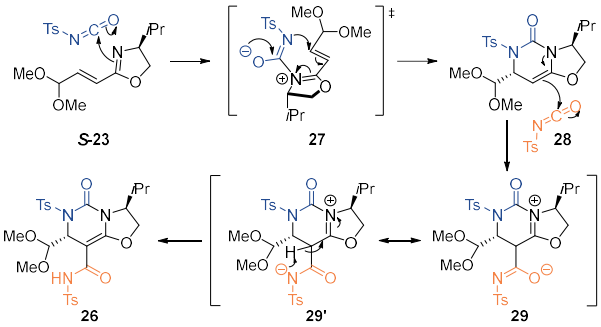

11. shēma. Iespējamais oksazolo[3,2-*c*]pirimidīna **26** veidošanās mehānisms.

Vēloties paplašināt oksazolo[3,2-*c*]pirimidīna atvasinājumu klāstu, tika mēģināts iesaistīt viniloksazolīnu ***S*-23** aza-Dīlsa-Aldera reakcijā arī ar citiem izocianātiem vai izotiocianātu, lai iegūtu produktus **30a-c**, taču šīs reakcijas bija neveiksmīgas (12. shēma).

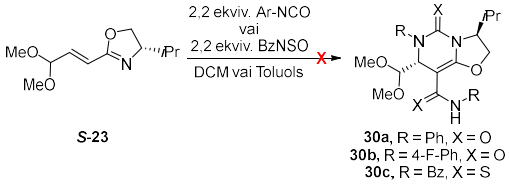

12. shēma. Aza-Dīlsa-Aldera reakcijas ar viniloksazolīnu ***S*-23** un dažādiem izo- vai izotiocianātiem.

Enantiobagātināto viniloksazolīnu ***S*-23** tika mēģināts iesaistīt arī dažādās dubultsaites transformācijās, tai skaitā 1,4-pievienošanas, ciklopropanēšanas, hidroborēšanas, Dīlsa-Aldera un Gīzes reakcijās, taču nevienā no tām neizdevās iegūt reakcijā gaidīto produktus **31-35** (13. shēma).

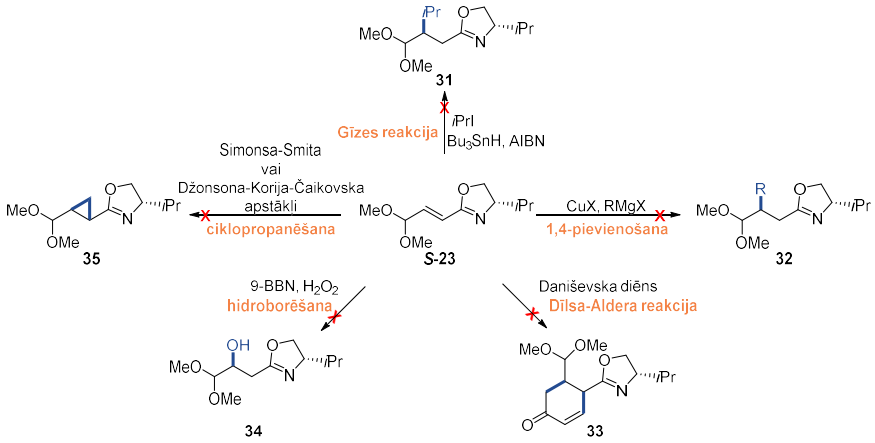

13. shēma. Viniloksazolīna ***S*-23** dubultsaites transformēšanas mēģinājumi.

Tālākā darba gaitā tika pētīta arī iespēja iegūto viniloksazolīnu ***S*-23** izmantot Heka reakcijā, lai ievadītu aizvietotāju pie dubultsaites. Tika veikta reakcijas apstākļu optimizēšana substrāta ***S*-23** arilēšanas reakcijā ar jodbenzolu. Labāko produkta **36** iznākumu (20 %) izdevās iegūt, izmantojot katalizatoru $Pd(dppf)Cl_2$ un bāzi Cs_2CO_3 (14. shēma).

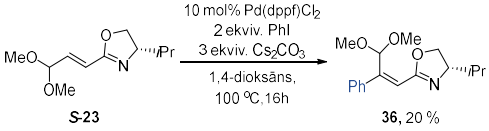

14. shēma. Heka reakcija ar oksazolīnu ***S*-23** un jodbenzolu.

Galvenie šajā nodaļā iegūtie rezultāti apkopoti publikācijā "*Preparation of furfural derived enantioenriched vinyl oxazoline building block and exploring its reactivity*".

2. Elektroķīmiska spirohemiaminālēteru sintēze no furfurola atvasinājumiem

[4.4]-Spirocikliska hemiaminālētera motīvs ir sastopams vairākās dabas vielās **37-41**, no kurām dažām ir zināma arī bioloģiska aktivitāte. Piemēram, likoplanīns A (**37**) ir kalcija kanālu inhibitors, elmenols H (**41**) spēj nomākt TRAIL rezistenci kuņģa adenokarcinomas šūnās, savukārt šihunīna (**40**) ekstrakts ir tradicionāli izmantots ķīniešu medicīnā, lai ārstētu diabētu (3. attēls).[12–14]

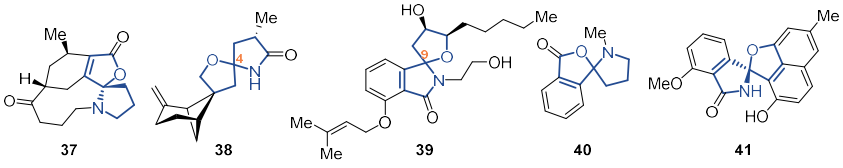

3. attēls. [4.4]-Spirohemiaminālētera substruktūru saturošas dabasvielas **37-41**.

Iepriekš mūsu grupā tika izstrādāta metode elektroķīmiskai [4.5]-spirobisketālu fragmentu saturošu savienojumu **43** iegūšanai no furāna atvasinājumiem **42** (15. shēma). Veicot furāna gredzenu saturošo spirtu **42** elektroķīmisku oksidēšanu vāji skābos apstākļos, tika panākta *C*-*O* saites veidošanās starp spirta skābekli un furāna gredzena C2 oglekli, saslēdzot spirociklu **43** (15. shēma). Visi spirocikli tika iegūti kā diastereomēru maisījumi.

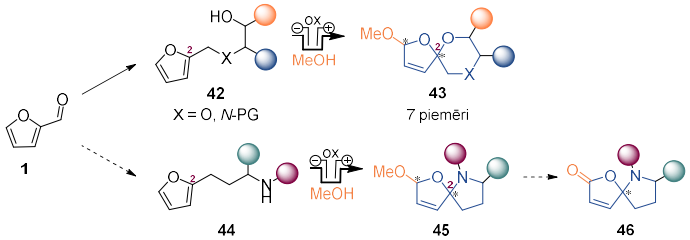

15. shēma. Elektroķīmiska [4.5]-spirobisketālu **43** un [4.4]-spirohemiaminālēteru **45** iegūšana no furāna atvasinājumiem.

Promocijas darbā tika attīstīta šī metodoloģija, lai konstruētu [4.4]-spirohemiaminālētera karkasu, saslēdzot spirociklu caur elektroķīmiski inducētu *C*-*N* saites veidošanos furāna atvasinājumos **44** (15. shēma). Pēc elektrolīzes tika plānots veikt metoksigrupas oksidēšanu par karbonilgrupu, tādējādi iegūstot produktu **46** ar vienu stereocentru.

Darba pirmajā posmā tika veikti koncepta pārbaudes eksperimenti, izmantojot modeļsubstrātu 3-(2-furil)propionskābes arilamīdu **47a**. Tā elektrolīze tika veikta nedalītajā šūnā galvanostatiskos apstākļos metanola vidē. Anodreakcijā tika veikta substrāta oksidēšana, katodreakcijā – protonu reducēšana līdz ūdeņradim. Substrāta **47a** elektrolīzē neitrālos apstākļos tika iegūts tikai furāna gredzena dimetoksilēšanās produkts **48**, savukārt substrāta **47a** elektrolīzē NaOMe klātbūtnē tika novērota selektīva spirocikliskā produkta **49a** veidošanās (16. shēma).

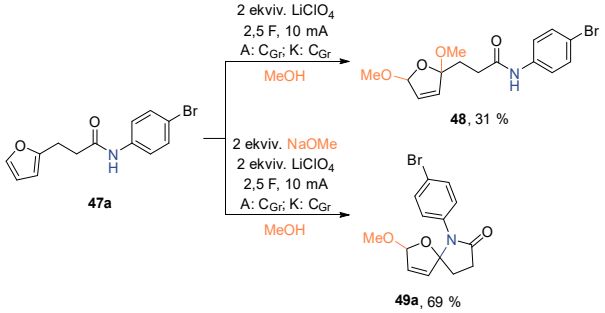

16. shēma. Savienojuma **47a** elektrolīzes produkti **48** un **49a**.

Lai noskaidrotu, kāda ir bāzes loma reakcijas produktu selektivitātē, tika uzņemtas cikliskās voltampērmetrijas līknes substrātam **47a** neitrālos apstākļos un bāziskā vidē (4. attēls). Mērījumi parādīja, ka neitrālos apstākļos pirmais oksidēšanās signāls ir novērojams pie E_p=1,1 V (4. attēls, zilā līkne), kas, visticamāk, atbilst furāna gredzena oksidēšanai. NaOMe klātbūtnē parādās jauns oksidēšanās signāls pie ievērojami zemāka potenciāla E_p = 0,64 V (4. attēls, zaļā līkne), kas liecina, ka bāzes klātbūtnē notiek amīda grupas deprotonēšana un cikliskās voltampērmetrijas līknē redzama amidāta anjona oksidēšana. Bāzes pārākumā uzņemtajā cikliskās voltampērmetrijas līknē aizvien ir redzams arī oksidēšanās signāls pie E_p = 1,1 V, kas liecina, ka šajos apstākļos nenotiek pilnīga substrāta **47a** deprotonēšana.

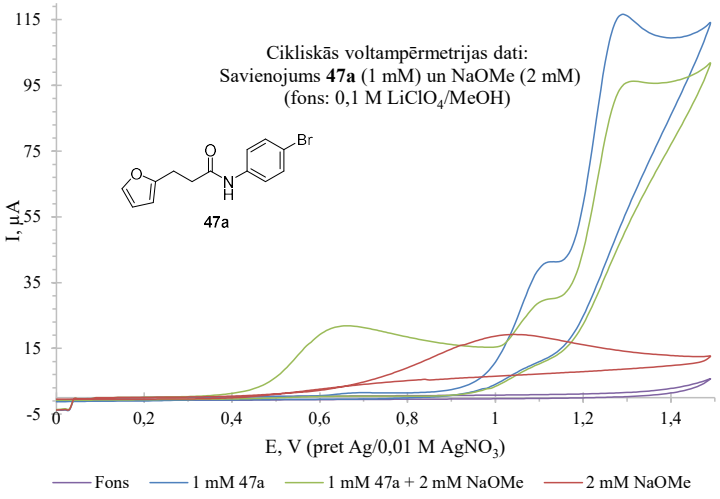

4. attēls. Savienojuma **47a** cikliskās voltampērmetrijas mērījumi neitrālos un bāziskos apstākļos.

Pamatojoties uz eksperimentālajiem novērojumiem, kā arī literatūras datiem,[15] tika definēts iespējamais mehānisms spirocikliskā hemiaminālētera **49a** iegūšanai (17. shēma).

Reakcijas pirmajā solī notiek amīda **47a** deprotonēšana, kam seko amidāta anjona **50** anodiska oksidēšana. Iegūtais amidilradikālis **51** ar slāpekļa centru veido *C*-*N* saiti ar furāna C2 oglekli un rodas *C*-centrētais radikālis **52**. Tam oksidējoties, veidojas oksonija jons **53**, kas, pievienojot metanolu, veido galaproduktu **49a**.

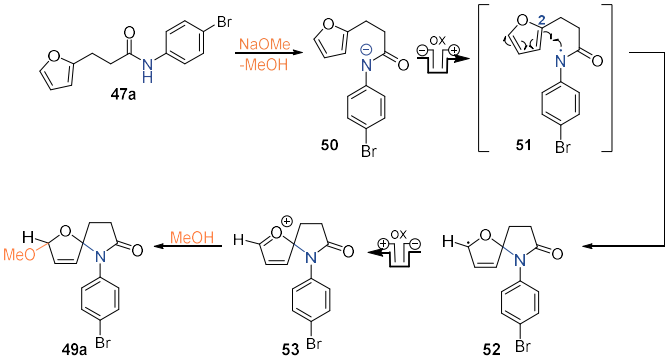

17. shēma. Izvirzītais spirohemiaminālētera **49a** veidošanās mehānisms.

Elektrolīzes substrātu klāsts tika paplašināts ar savienojumiem, kas saturēja dažādus aizvietotājus arilgrupā (18. shēma). Veicot substrātu **47** elektrolīzi NaOMe klātbūtnē, veiksmīgi tika iegūti spirocikli **49a-d**, kas benzola gredzenā saturēja gan elektronatvelkošus, gan elektrondonorus aizvietotājus. Visi spirocikli **49a-d** tika iegūti kā diastereomēru maisījumi. Nākamajā solī tika veikta spirociklu **49a-c** oksidēšana ar *m*CPBA un katalītisku daudzumu $BF_3{\cdot}Et_2O$, iegūstot spirociklus **54a-c** ar labiem iznākumiem (18. shēma).

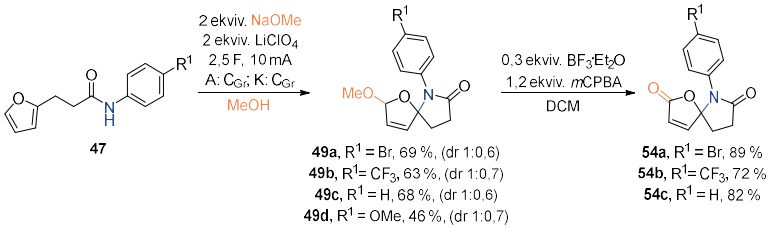

18. shēma. [4.4]-Spirohemiaminālēteru **49a-d** un **54a-c** iegūšana no 3-(2-furil)propionskābes atvasinājumiem **47a-d**.

Produkta **54b** rentgenstruktūranalīzes rezultāti apstiprināja gaidīto atomu konektivitāti (5. attēls), līdz ar to tika noslēgti koncepta pārbaudes eksperimenti.

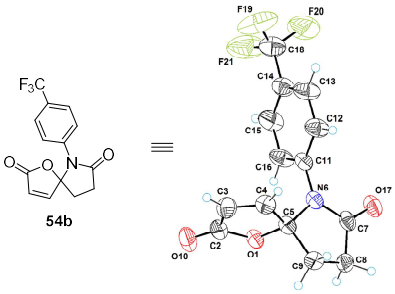

5. attēls. Savienojuma **54b** rentgenstruktūranalīzes *ORTEP* attēlojums ar 50 % kontūru varbūtību.

Nākamajā darba posmā tika sākta elektrolīzes apstākļu optimizēšana, vispirms pētot fona elektrolīta ietekmi uz reakcijas iznākumu (2. tabula). Spirocikla **49a** iznākums tika noteikts, izmantojot ^{1}H-*q*KMR spektroskopiju. Reakcijas tika veiktas nedalītajā elektroķīmiskajā šūnā galvanostatiskos tilpuma elektrolīzes apstākļos. Eksperimentālie rezultāti parādīja, ka reakcijai vispiemērotākie elektrolīti ir sārmu metālu perhlorāts ($LiClO_4$ un $NaClO_4$; 2. tabulas 1.–2., un 10. aile) un bromīds (LiBr; 2. tabula, 3. aile). Produkta iznākumi bija līdzīgi, izmantojot gan $LiClO_4$ (72 %), gan LiBr (74 %), tāpēc turpmākās eksperimentu sērijas tika veiktas ar abiem elektrolītiem.

2. tabula

Spirohemiaminālēteru **49a** veidošanās, izmantojot dažādus elektrolītus

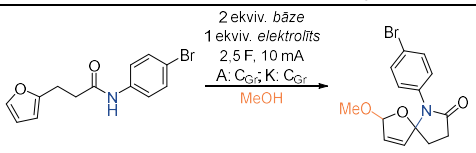

47a (0,5 mmol) **49a**

Nr.	Bāze	Elektrolīts	**49a**[a]
1.	NaOMe	$LiClO_4$	70 %
2.	LiO*t*Bu	$LiClO_4$	72 %
3.	LiO*t*Bu	LiBr	74 %
4.	LiO*t*Bu	LiCl	66 %
5.	LiO*t*Bu	$LiBF_4$	63 %
6.	LiO*t*Bu	LiOAc	62 %
7.	LiOH	--	64 %
8.	LiO*t*Bu	$TBAClO_4$	69 %
9.	LiO*t*Bu	$TBAPF_6$	64 %
10.	NaOMe	$NaClO_4$	72 %
11.	NaO*t*Bu	$NaClO_4$	63 %

[a]: iznākums noteikts, izmantojot ^{1}H-*q*KMR; iekšējais standarts 1,4-bis(trihlormetil)benzols.

Lai noskaidrotu, kā bāzes daudzums ietekmē substrāta **47a** deprotonēšanas pakāpi, tika veikti cikliskās voltampērmetrijas mērījumi. Substrātam **47a** tika pievienojti 0 līdz 6 ekvivalenti bāzes NaOMe, uzņemot cikliskās voltampērmetrijas līknes pēc katra pievienotā bāzes ekvivalenta (6. attēls). Pievienojot vienu ekvivalentu bāzes (6. attēls, zilā līkne), līknē nav novērojams izteikts amidāta oksidēšanās signāls pie $E_p = 0{,}6$ V, savukārt, pievienojot divus ekvivalentus bāzes (6. attēls, rozā līkne), amidāta oksidēšanās signāls kļūst skaidri redzams. Piesātinājuma strāva pie $E_p = 0{,}6$ V tiek sasniegta, pievienojot 4 līdz 5 ekvivalentus NaOMe, kas nozīmē, ka šāds ir nepieciešamais bāzes daudzums, lai pilnībā deprotonētu visu substrātu **47a** reakcijas maisījumā. Turpinot palielināt bāzes daudzumu, pie $E_p = 1{,}0$ V var novērot metoksīda oksidēšanās signālu (metoksīda oksidēšanās signāls redzams sarkanajā līknē 4. attēlā).

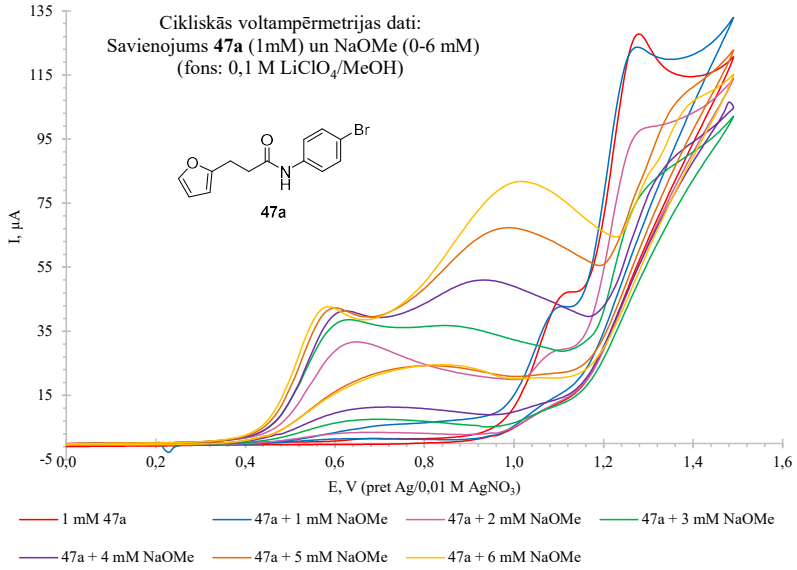

6. attēls. Cikliskās voltampērmetrijas līknes substrātam **47a** un NaOMe (0–6 ekvivalenti).

Pamatojoties uz šiem novērojumiem, tika izstrādāta eksperimentu sērija, pārbaudot pievienotā bāzes daudzuma ietekmi uz reakcijas produktu selektivitāti un iznākumu robežās no 0 līdz 4 ekvivalentiem. Eksperimentu sērijas tika veiktas ar diviem fona elektrolītiem – $LiClO_4$ un LiBr (3. tabula), kā bāzi izmantojot Li*O*t*B*u.

Tika noskaidrots, ka reakcija veiksmīgi norit arī tad, ja bāzi izmanto substehiometriskā daudzumā (0,5 ekvivalenti; 2. tabula, 3. un 8. ailes), turklāt bāzes pievienošana pārākumā (2–4 ekvivalenti; 2. tabula 1.–2., un 7. aile) produkta **49a** iznākumu būtiski neuzlabo. Tas liecina, ka veiksmīgai elektrolīzes norisei nav nepieciešams uzreiz deprotonēt visu reakcijas substrātu **47a**. Samazinot bāzes daudzumu no 0,5 līdz 0,2 ekvivalentiem, produkta **49a** iznākums nedaudz samazinās (3. tabula, 4. un 9. aile), bet, pievienojot 0,1 ekvivalentu bāzes, tika novērota arī dimetoksilētā blakusprodukta **48** veidošanās (3. tabula, 5. un 10. aile).

Elektrolīzi var veikt arī bāzes pārākumā (2 ekvivalenti) bez fona elektrolīta, taču tad produkta iznākums ir nedaudz zemāks nekā ar elektrolītu (3. tabula, 6. aile).

Šajā eksperimentu sērijā tika noskaidrots, ka selektīvai spirocikliskā produkta **49a** iegūšanai pietiek ar 0,5 ekvivalentiem bāzes. Produkta iznākumi ar LiBr un $LiClO_4$ bija līdzvērtīgi, bet, ņemot vērā, ka LiBr ir lētāks un drošāks reģents, nākamajos eksperimentos kā fona elektrolīts tika izmantots tikai tas.

3. tabula

Spirohemiaminālēteru **49a** veidošanās, pievienojot dažādus bāzes Li*O*t*B*u daudzumus

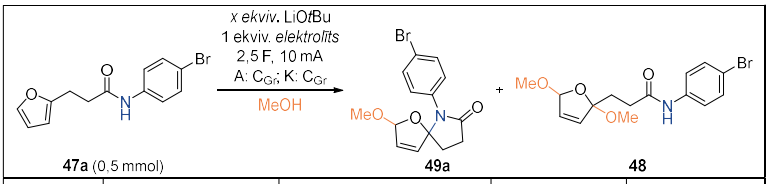

47a (0,5 mmol) 49a 48

Nr.	Li*O*t*B*u (ekviv.)	Elektrolīts	49a[a]	48[a]
1.	4,0	$LiClO_4$	73 %	–
2.	2,0		72 %	–
3.	0,5		72 %	–
4.	0,2		70 %	–
5.	0,1		61 %	5 %
6.	–		0 %	52 %
7.	2,0	LiBr	74 %	–
8.	0,5		74 %	–
9.	0,2		66 %	–
10.	0,1		17 %	49 %
11.	2,0	–	67 %	–

[a]: iznākums noteikts, izmantojot ^{1}H-*q*KMR; iekšējais standarts 1,4-bis(trihlormetil)benzols.

Nākamajā eksperimentu sērijā tika pārbaudīta katjona – Li^+, Na^+ un K^+ – ietekme uz reakcijas iznākumu, eksperimentos izmantojot attiecīgo katjonu saturošos alkoksīdus (MeO^- vai *t*BuO^-) un bromīdus (4. tabula). Vislabākais rezultāts tika iegūts, izmantojot litiju saturošu elektrolītu un bāzi (74 %; 4. tabula, 1. aile), taču arī pārējās katjonu kombinācijas deva līdzīgus rezultātus, kas liecina, ka katjona izvēle maz ietekmē reakcijas iznākumu.

4. tabula

Spirohemiaminālēteru **49a** veidošanās, izmantojot Li^+, Na^+ un K^+ saturošas bāzes un bromīdus

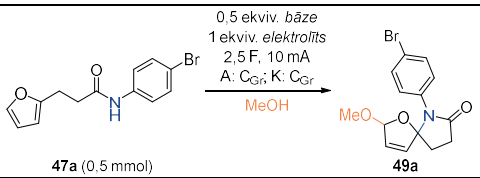

Nr.	Bāze	Elektrolīts	49a[a]
1.	LiO*t*Bu	LiBr	74 %
2.	LiO*t*Bu	NaBr	70 %
3.	NaOMe	LiBr	73 %
4.	NaOMe	NaBr	71 %
5.	KO*t*Bu	KBr	70 %

[a]: iznākums noteikts, izmantojot ^{1}H-*q*KMR; iekšējais standarts 1,4-bis(trihlormetil)benzols.

Noslēdzošajā elektrolīzes apstākļu optimizēšanas posmā tika pētīta elektroķīmisko parametru ietekme uz reakcijas iznākumu (5. tabula), pārbaudot dažādus anoda un katoda materiālus, kā arī strāvas stiprumu. No apskatītajiem anoda materiāliem, substrāta oksidēšanai vispiemērotākais bija grafīts (C_{Gr}), savukārt vislabākais katoda materiāls bija nerūsējošais tērauds (SS) (5. tabula, 6. aile). Svarīgs parametrs izrādījās strāvas stiprums – samazinot reakcijai pievadīto strāvu no 10 mA līdz 5 mA, produkta iznākums samazinājās no 76 % līdz 69 % (5. tabula, 7. aile), savukārt, palielinot strāvas stiprumu līdz 15–50 mA, produkta iznākums palielinājās līdz 78–84 % (5. tabula, 8.–12. aile).

5. tabula

Spirohemiaminālēteru **49a** veidošanās, variējot elektroķīmiskos parametrus

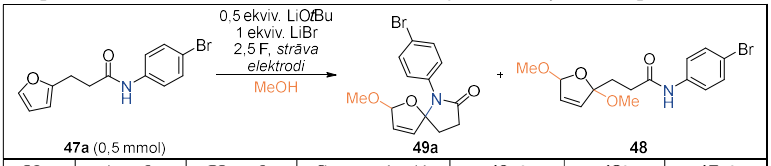

Nr.	Anods	Katods	Strāva (mA)	49a[a]	48[a]	47a[a]
1.	GC	C_{Gr}	10	65 %	–	–
2.	Pt	C_{Gr}		48 %	8 %	10 %
3.	BDD	C_{Gr}		7 %	37 %	–
4.	C_{Gr}	C_{Gr}		74 %	–	–
5.	C_{Gr}	Pt		75 %	–	–
6.	C_{Gr}	SS		76 %	–	–
7.			5	69 %	–	–
8.			15	80 %	–	–
9.			20	80 %	–	–
10.			30	78 %	–	–
11.			40	84 %	–	–
12.			50	82 %	–	–

[a]: iznākums noteikts, izmantojot ^{1}H-*q*KMR; iekšējais standarts 1,4-bis(trihlormetil)benzols.

Optimizēšanas rezultātā tika noskaidrots, ka labākie apstākļi spirohemiaminālētera **49a** iegūšanai ir, izmantojot 0,5 ekvivalentus LiO*t*Bu un 1 ekvivalentu (jeb 0,17 M) LiBr. Optimizētie elektroķīmiskie parametri bija 40 mA liela strāva (strāvas blīvums j = 25 mA/cm^2), 2,5 F liels lādiņš, grafīta anods un nerūsējošā tērauda katods.

Darba turpinājumā paredzēts veikt reakcijas substrātu klāsta izpēti un elektrolīzes produktu tālāku funkcionalizēšanu.

3. Oksazolīnu elektrosintēze ciklopropānu 1,3-oksifluorēšanas reakcijā

Otrs promocijas darba izstrādes gaitā pētītais virziens bija elektroķīmiski inducēta ciklopropāna *C*-*C* saites uzšķelšana. 2021. gadā Aivena Lei (*Aiwen Lei*) grupa publicēja rakstu, kurā viņi arilciklopropānu aktivēšanai izmantoja elektrisko strāvu (19. shēma).[8] Publicētajā metodē tika veikta arilciklopropānu **55** tieša anodiska oksidēšana, iegūstot katjonradikāļus **55'**. Šādos katjonradikāļos ciklopropāna *C*-*C* saite ir ievērojami vājāka nekā neitrālā ciklopropānā, un to var uzšķelt, izmantojot dažādus nukleofīlus X/Y, iegūstot 1,3-difunkcionalizētus produktus **58**. Viens no autoru izmantotajiem nukleofīliem bija fluorīds ($Et_3N{\cdot}3HF$), ļaujot iegūt mono- un difluorētus produktus **58**.

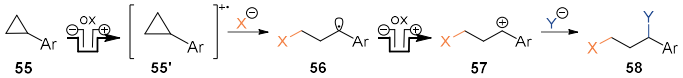

19. shēma. Aivena Lei grupas demonstrētā elektroķīmiskā arilciklopropānu 1,3-difunkcionalizēšana.[8]

Promocijas darba ietvaros vēlējāmies paplašināt elektroķīmisko ciklopropāna uzšķelšanas metožu klāstu, fokusējoties uz neaktivētiem ciklopropāniem, kuru tieša elektroķīmiska oksidēšana ir apgrūtināta. Šim nolūkam tika izstrādāta pieeja ciklopropāna uzšķelšanai ar anodiski oksidējamu funkcionālo grupu, kas pievienota ciklopropānam ar linkeri (20. shēma). Anodiski aktivētais intermediāts **59'** iekšmolekulāras ciklopropāna uzšķelšanas rezultātā veidotu *C*-centrēto radikāli **60**. Tas tiktu anodiski oksidēts par karbēnija jonu **61**, kura neitralizēšanai reakcijas maisījumā būtu nepieciešams arī ārējais nukleofīls (Nu). Galarezultātā tiktu iegūts ciklopropāna 1,3-difunkcionalizēšanas produkts **62**. Katodreakcijā tika plānots veikt protonu reducēšanu līdz ūdeņradim.

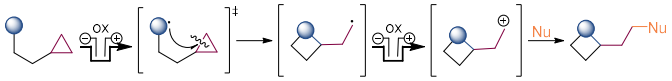

20. shēma. Stratēģija elektroķīmiski inducētai ciklopropāna uzšķelšanai.

Kā modeļsubstrāts metodes izstrādei tika izvēlēts savienojums **63a**, kas saturēja benzamīda un dimetilaizvietota ciklopropāna funkcijas. Elektroķīmiski oksidējot benzamīda fragmentu, veidotos amidilradikālis **63a'**, kas varētu inducēt ciklopropāna gredzena *C*-*C* saites uzšķelšanu, veidojot oksazolīnu **66** (21. shēma). Tika paredzēts, ka geminālās metilgrupas ciklopropāna fragmentā pēc tā uzšķelšanas varētu palīdzēt stabilizēt radikāli **64** un karbēnija jonu **65**.

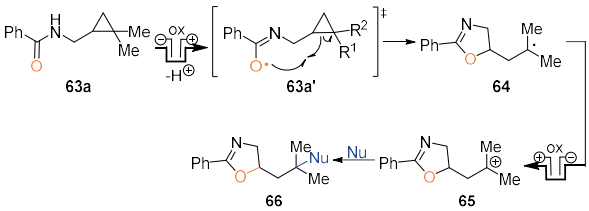

21. shēma. Elektroķīmiska benzamīda grupas oksidēšana ar sekojošu ciklopropāna uzšķelšanu savienojumā **63a**.

Pirmie mēģinājumi elektroķīmiskai ciklopropāna **63a** uzšķelšanai tika veikti nedalītajā šūnā galvanostatiskos tilpuma elektrolīzes apstākļos, kā reakcijas šķīdinātāju un ārējo nukleofīlu izmantojot metanolu (22. shēma). Tika gaidīts, ka reakcijā veidosies metilēteris **67**, taču, analizējot reakcijas maisījumu, tika noskaidrots, ka veidojas trīs produkti – metilēteris **67**, kā arī alkēns **68** un fluoru saturošais savienojums **69a**. Fluorētā produkta rašanās liecināja, ka elektrolīzē izmantotais elektrolīts $TBABF_4$ var kalpot arī kā fluora avots.

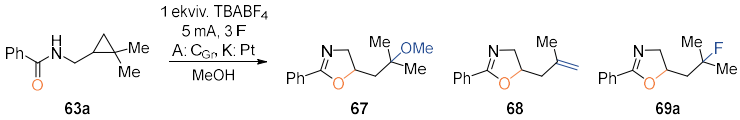

22. shēma. Elektroķīmiski inducēta ciklopropāna **63a** uzšķelšana metanolā.

Uzskatot, ka fluoru saturoši produkti varētu būt perspektīvi būvbloki, darba turpinājumā tika optimizēta sintēzes metode, lai varētu selektīvi ievadīt produktā fluora atomu.

Vispirms tika pētīts, kādi fluoru saturošie reaģenti elektrolīzes apstākļos vislabāk veic fluora pārnesi uz produktu. Tika apskatīti vairāki fluoru saturoši elektrolīti, kā arī dažādi nukleofīlie un elektrofīlie fluorēšanas reaģenti (6. tabula). Reakcijās kā šķīdinātājs tika izmantots HFIP, kas kā protona avots nodrošina katoda pusreakciju, taču ir vājš nukleofīls, novēršot šķīdinātāja pievienošanos karbēnija jonam **65** kā iespējamo blakusreakciju.

Elektrolīzes tika veiktas nedalītajā šūnā galvanostatiskos apstākļos, pievienojot 1 ekvivalentu fona elektrolīta un 2 ekvivalentus pārējās piedevas. Reakcijās, kurās tika izmantoti fluorēšanas reaģenti, kas paši nav labi elektrolīti, tika izmantots fona elektrolīts $TBAClO_4$. Elektrolīzē novērotie blakusprodukti bija alkēns **68**, spirts **70**, kā arī HFIP pievienošanās produkts **71**. Pēc elektrolīzes beigām tika noteikta iegūto produktu attiecība, izmantojot UEŠH analīzes; produktu iznākumi netika noteikti.

Visaugstākā selektivitāte fluorētā produkta iegūšanai tika novērota, izmantojot $TBABF_4$ sāli, nedaudz zemāka selektivitāte tika novērota $TBAPF_6$ klātbūtnē (6. tabula, 1.–2. aile). Šie sāļi ir ērti fluorēšanas reaģenti elektrolīzes apstākļos, jo spēj vienlaikus kalpot arī kā fona elektrolīts; tie arī nekorodē stikla elektroķīmiskās šūnas. Izmantojot tādus nukleofīlus fluorīda avotus kā CsF, TBAF un TASF, tika novērots, ka veidojas produktu

maisījums (6. tabula, 3.–5. aile). Elektrofīlā fluorēšanas reaģentu NFSI klātbūtnē kā mažorais produkts veidojās olefīns **68** (6. tabula, 6. aile).

Eksperimentu rezultātā tika noskaidrots, ka $TBABF_4$ ir piemērotākais fluorēšanas reaģents selektīvai fluorētā produkta **69a** iegūšanai elektrolīzes apstākļos, tāpēc tas tika izmantots turpmākajā darbā.

6. tabula

Modeļsubstrāta **63a** elektrolīzē iegūtie produkti, izmantojot dažādus fluora avotus

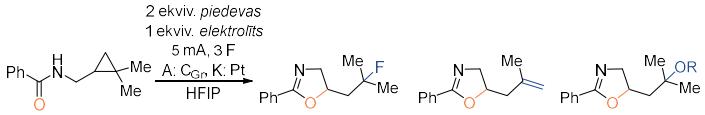

Nr.	Elektrolīts	Piedevas	Produktu attiecība[a]				
			69a, %	68, %	70, %	71, %	63a, %
1.	$TBABF_4$	--	> 95	< 2	< 2	0	0
2.	$TBAPF_6$	--	79	7	9	5	0
3.	$TBAClO_4$	CsF	8	40	6	20	26
4.		$TBAF \cdot 3H_2O$	11	31	40	18	0
5.		TASF	41	34	5	19	0
6.		NFSI	5	65	0	30	0
[a]: noteikta ar UEŠH (UV absorbcija).							

Nākamais solis bija elektrolīzes apstākļu optimizēšana. Reakcijas tika veiktas nedalītajā šūnā galvanostatiskos apstākļos (7. tabula). Produkta **69a** iznākumi tika noteikti ar ^{19}F-*q*KMR.

Vispirms tika pētīta $TBABF_4$ daudzuma ietekme uz elektrolīzes iznākumu. Elektrolīzē ar 1 ekvivalentu $TBABF_4$ produkts veidojās ar 69 % iznākumu (7. tabula, 1. aile). Palielinot $TBABF_4$ daudzumu līdz 3 ekvivalentiem, produkta **69a** iznākums pieauga līdz 82 % (7. tabula, 3. aile). Izmantojot 5 ekvivalentus $TBABF_4$, produkta iznākumu izdevās vēl nedaudz uzlabot (7. tabula, 5. aile), taču šajos apstākļos tika novērots, ka notiek grafīta elektroda šķīšana. Reakcijā, kurā tika izmantots elektrolītu $TBABF_4$ un $TBAClO_4$ maisījums 2 : 1 attiecībā, produkta **69a** iznākums samazinājās līdz 46 % (7. tabula, 6. aile).

Aizstājot grafīta anodu ar platīna anodu, produkta iznākums samazinājās līdz 53 % (7. tabula, 7. aile). Savukārt, platīna katodu aizstājot ar ievērojami lētāku grafīta katodu, reakcijas iznākums būtiski nemainījās (7. tabula, 8. aile).

Lai arī saskaņā ar 21. shēmā doto mehānismu substrāta **63a** transformēšanai par produktu **69a** ir nepieciešams 2 F liels lādiņš, tika noskaidrots, ka elektrolīzes apstākļos pilnai substrāta konversijai ir nepieciešams 3 F liels lādiņš (7. tabula, 9.–10. aile).

HFIP bija vienīgais protiskais šķīdinātājs, kurā ar augstu iznākumu veidojās produkts **69a**, taču līdzvērtīgu iznākumu varēja sasniegt, izmantojot arī DCM ar 20 ekvivalentiem HFIP katoda reakcijas nodrošināšanai (7. tabula, 11.–13. aile).

Bez strāvas pievades produkta **67a** veidošanās netika novērota (7. tabula, 14. aile).

Elektrolīzes apstākļu optimizēšanas rezultātā tika noskaidrots, ka reakcijai nepieciešami 3 ekvivalenti $TBABF_4$ un piemērotākais šķīdinātājs ir HFIP. Optimizētie elektroķīmiskie parametri bija 5 mA stipra strāva (strāvas blīvums j = 4,2 mA/cm^2), 3 F liels lādiņš, kā arī grafīta anods un platīna katods.

7. tabula

Elektroķīmiski inducētas ciklopropāna **63a** uzšķelšanas reakcijas apstākļu optimizēšana

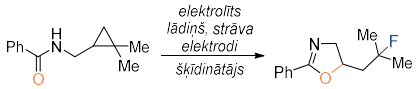

63a 69a

Nr.	Šķīdinātājs	Elektrolīts (ekviv.)	Strāva, mA	Lādiņš, F	A:K	69a[a]
1.	HFIP	$TBABF_4$ (1)	5	3	A: C_{Gr} K: Pt	69 %
2.		$TBABF_4$ (2)				79 %
3.		$TBABF_4$ (3)				82 %
4.		$TBABF_4$ (4)				82 %
5.		$TBABF_4$ (5)				84 %[b]
6.		$TBABF_4$ (2) $TBAClO_4$ (1)				46 %
7.		$TBABF_4$ (3)			A: Pt K: Pt	53 %
8.					A: C_{Gr} K: C_{Gr}	81 %
9.				2	A: C_{Gr} K: Pt	77 %
10.				2,5		79 %
11.	MeOH			3		11 %
12.	DCM 20 ekviv. HFIP					77 %
13.	MeCN 20 ekviv. HFIP					20 %
14.	HFIP	$TBABF_4$ (3)	0	0	–	0 %

[a]: iznākums noteikts ar ^{19}F-qKMR, iekšējais standarts 4,4'-difluorbenzofenons; [b]: anods tiek bojāts elektrolīzes laikā.

Reakcijas substrātu klāsta pētījumiem tika sintezētas trīs substrātu sērijas – substrāti **63a-f** ar dažādiem aizvietotājiem benzamīda funkcijā, substrāti **63h-m**, kuros ciklopropāns savienots ar vēl vienu karbociklu, un monoarilaizvietoti ciklopropāni **63o-t**. Iegūtie savienojumi tika pakļauti elektrolīzei optimizētajos apstākļos (23. shēma).

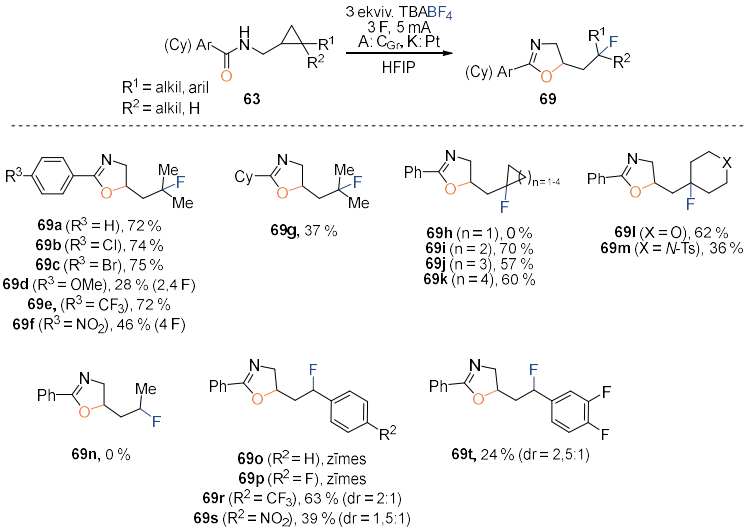

23. shēma. Ciklopropānu **63** elektrolīzē iegūtie 1,3-oksifluorētie produkti **69**.

Pirmās sērijas substrātu **63a-f** elektrolīzē tika pētīta benzamīda funkcijā ievadītu aizvietotāju ietekme uz ciklopropāna 1,3-oksifluorēšanas reakciju (produkti **69a-f**). Modeļsubstrāta **63a** elektrolīzē produkts **69a** tika iegūts ar 72 % iznākumu. Līdzīgu iznākumu varēja iegūt arī halogēn- un trifluorometil- aizvietotu analogu **63b-c** un **63e** elektrolīzēs (produkti **69b-c**, **69e**). Ievadot fenilgrupā elektrondonoro metoksigrupu, izejvielas **63d** konversijai bija nepieciešams mazāks pievadītais lādiņš, taču produkta **69d** iznākums bija ievērojami zemāks (28 %). Zems iznākums tika novērots arī nitrogrupu saturoša substrāta **63f** elektrolīzē, kur produkts **69f** tika iegūts ar 46 % iznākumu.

Benzamīda funkciju aizstājot ar cikloheksānkarboksamīdu (substrāts **63g**), tika iegūts elektrolīzes produkts **69g**, taču tā iznākums (37 %) bija ievērojami zemāks nekā benzamīdu saturošajam analogam **69a**.

Otrās sērijas substrāti bija spirocikliski analogi **63h-m** un analogs ar monometilaizvietotu ciklopropānu **63n**. Šajā sērijā veiksmīgi izdevās iegūt monofluorētu ciklobutānu **69i**, ciklopentānu **69j**, cikloheksānu **69k,** tetrahidropirānu **69l** un piperidīnu **69m**. Monofluorētu ciklopropānu saturošo produktu **69h** iegūt neizdevās, kā arī monometilaizvietota ciklopropāna **63n** elektrolīzē attiecīgais fluorētais savienojums **69n** netika iegūts.

Trešajā substrātu sērijā tika pētīta monoarilaizvietotu ciklopropānu **63o-t** elektroķīmiska 1,3-oksifluorēšana. Tika novērots, ka fluorētos produktus var iegūt tikai, ja arilgrupā pie ciklopropāna ievadīti elektronatvelkoši aizvietotāji (substrāti **63r-t**). Šādu selektivitāti varētu skaidrot ar to, ka neaizvietota arilciklopropāna oksidēšanās potenciāls ir zemāks nekā benzamīdam, līdz ar to tas tiek oksidēts pirmais. Elektronatvelkošo grupu ievadīšana ļauj kontrolēt oksidēšanās selektivitāti par labu benzamīda funkcijai.

Interesanti, ka tetrametilaizvietota ciklopropāna **72** elektrolīzē netika novērota gaidītā oksazolīna **73** veidošanās. Tā vietā kā galvenais produkts tika iegūts dihidrooksazīns **74**

(24. shēma). Šāda produkta veidošanās liecina, ka šajā gadījumā elektrolīzes gaitā tiek šķelta tetrametilaizvietotā ciklopropāna *C*-*C* saite.

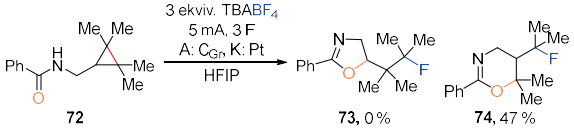

24. shēma. Tetrametilaizvietota ciklopropāna **72** elektrolīzes produkts dihidrooksazīns **74**.

Veicot tioamīdu saturošā ciklopropāna **75** elektrolīzi, izejvielas konversijai bija nepieciešams tikai 2,1 F liels lādiņš, taču tiazolīna produkta **76** iznākums bija zems (19 %, 25. shēma). Novērotie blakusprodukti liecināja, ka reakcijas apstākļos notiek izejvielas vai aktivēto intermediātu desulfurizēšana.

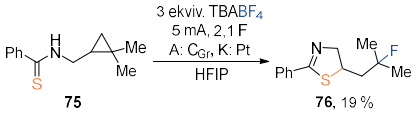

25. shēma. Tioamīdu saturošā ciklopropāna **75** elektrolīze.

Lai noskaidrotu, vai oksazolīna veidošanās laikā notiek hiralitātes pārnese no izejvielas uz produktu, tika izmantots enantiobagātināta brombenzamīda **63c** *S*-enantiomērs. Pakļaujot enantiotīru substrātu ***S*-63c** elektrolīzes apstākļiem, tika iegūts oksazolīns ***S*-69c** (26. shēma). Veicot hirālās AEŠH analīzes, tika noskaidrots, ka produkts ***S*-69c** ir iegūts kā viens enantiomērs, kas liecina par pilnīgu hiralitātes pārnesi.

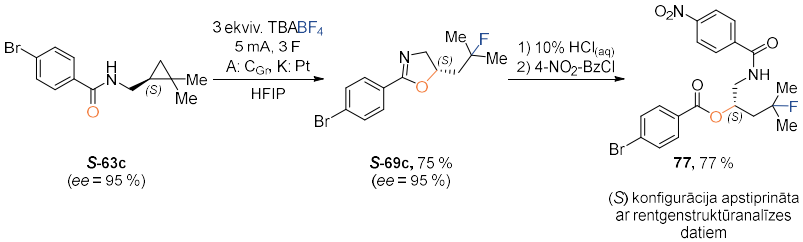

26. shēma. Enantiobagātinātā brombenzamīda ***S*-63c** elektrolīze un iegūtā produkta derivatizēšana.

Produkta ***S*-69c** absolūtā konfigurācija tika noteikta, veicot tā derivatizēšanu par savienojumu **77**, kuram tika veikta rentgenstruktūranalīze. Tā parādīja, ka produktā **77** hirālajam centram ir *S* konfigurācija; tas liecina par to, ka *C*-*C* saites uzšķelšanas laikā notiek konfigurācijas inversija (7. attēls).

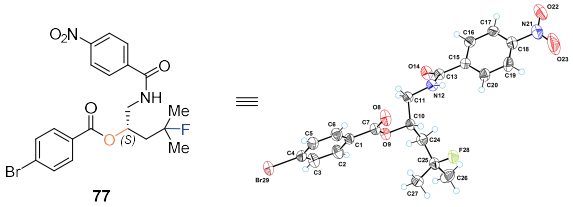

77

7. attēls. Savienojuma **77** rentgenstruktūranalīzes *ORTEP* attēlojums ar 50 % kontūru varbūtību.

Pamatojoties uz šiem datiem, bija iespējams piedāvāt iespējamo reakcijas mehānismu (27. shēma). Pirmais reakcijas solis ir elektroķīmiska benzamīda funkcijas oksidēšana, ģenerējot amidilradikāli **78'**. Nākamajā solī amidilradikālis ar skābekļa centru uzbrūk ciklopropāna *C*-*C* saites irdinošajai orbitālei saskaņā ar iekšmolekulārās homolītiskās aizvietošanas mehānismu (S_Hi). Ciklopropāna *C*-*C* saite tiek uzšķelta, un veidojas *C*-centrēts radikālis **80**, kas oksidējoties kļūst par karbēnija jonu **81**. Seko fluorīda pārnese no tetrafluorborāta anjona un veidojas galaprodukts – monofluorētais oksazolīns **82**.

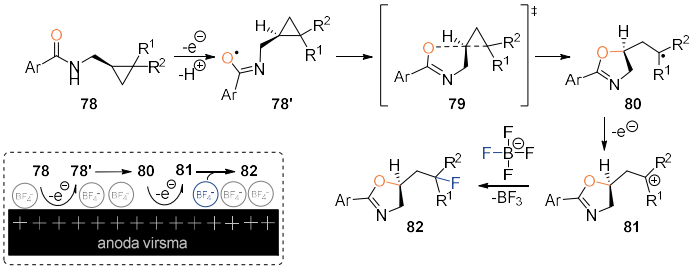

27. shēma. Piedāvātais oksazolīna **82** veidošanās mehānisms.

Reakcijas selektivitāti par labu fluorēšanai varētu skaidrot, ņemot vērā reakcijas vidi pie anoda virsmas, kur notiek elektronu pārnese. Anoda virsma ir pozitīvi lādēta, tāpēc tās tuvumā ir negatīvi lādētu jonu slānis, ko sauc par elektrisko dubultslāni. Elektrolīzes apstākļos to veido tetrafluorborāta joni (27. shēma). Šāda augsta nukleofīla koncentrācija tuvu karbēnija jonu ģenerēšanas vietai varētu sekmēt fluorēšanas norisi.

Analizējot reakcijas maisījuma ^{11}B-KMR spektru, tika secināts, ka elektrolīzes laikā ir izveidojies jauns boru saturošs savienojums, kas liecina, ka reakcijas gaitā atbrīvotais bora trifluorīds **83** tiek saistīts borāta kompleksā ar heksafluorizopropanolu (28. shēma). Bez strāvas pievadīšanas šāda apmaiņa notiek tikai zīmju līmenī.

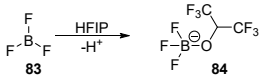

28. shēma. Elektrolīzes laikā atbrīvotā bora trifluorīda **83** saistīšana borāta kompleksā **84**.

Šajā nodaļā aprakstītie rezultāti apkopoti publikācijā "*Electrochemical Formation of Oxazolines by 1,3-Oxyfluorination of Non-activated Cyclopropanes*".

SECINĀJUMI

1. Furfurilētu etilēnglikolu un furfurilētu aminospirtu atvasinājumu **7** transformāciju par *α,β*-nepiesātinātiem esteriem **9** var veikt viena reaktora divpakāpju elektroķīmiskā sintēzē, kā piedevas izmantojot HFIP pirmajā solī un AcOH otrajā solī. Darba rezultātā tika izstrādāta jauna elektroķīmiska *C-O* saites veidošanas metode, kas ļauj iegūt funkcionalizētus Torī-tipa esterus.

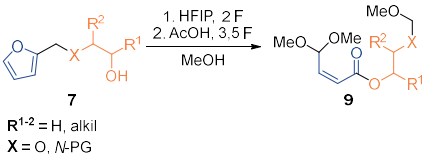

2. Elektroķīmiski iegūto *α,β*-nepiesātināto esteri **9a** var izmantot kā reaktīvo atšķaidītāju kopolimerizācijā ar akrilētu rapšu eļļu biobāzētu polimēru iegūšanai.

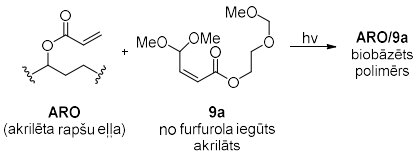

3. *N*-Alloc aizsargātu *α,β*-nepiesātināto esteri **9i** var iegūt no spirta **7i** nepārtrauktā elektrolīzē metanolā, izmantojot reakcijas piedevu AcOH. Šī metode ļauj iegūt hirālu būvbloku, kas atvasināts no biobāzētām izejvielām – furfurola un valinola.

4. Enantiobagātinātu *N*-Alloc aizsargātu *α,β*-nepiesātināto esteri **9i** ķīmiskās sintēzes ceļā var transformēt par enantiobagātinātu viniloksazolīnu **23**. *N*-Alloc nošķelšanas procesā notiek arī metoksimetilgrupas nošķelšana, *O*- uz *N*- pārgrupēšanās un daļēja vai pilnīga dubultsaites izomerizēšana. Rezultātā tiek iegūts hirāls viniloksazolīna būvbloks.

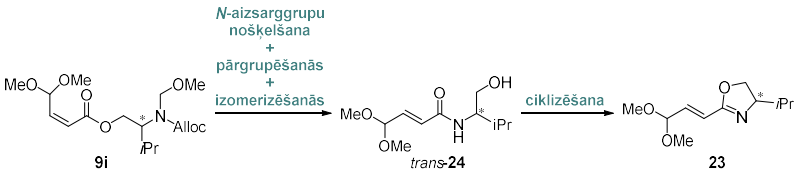

5. Viniloksazolīna atvasinājuma ***S*-23** aza-Dīlsa-Aldera reakcijā ar tozilizocianātu diastereoselektīvi veidojas oksazolo[3,2-*c*]pirimidīna atvasinājums **26**.

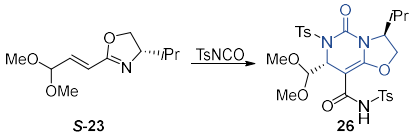

***S*-23** **26**

6. 3-(2-Furil)propionskābes arilamīdu **47a** elektrolīzē, pievienojot substehiometrisku bāzes daudzumu, notiek spirocikla **49a** saslēgšana, amīda funkcijai izveidojot *C*-*N* saiti ar furāna C2 oglekli. Metode ļauj konstruēt [4.4]-spirohemiaminālētera karkasu, kas ir sastopams vairākās dabasvielās.

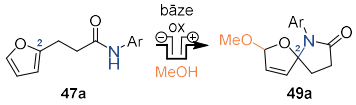

47a **49a**

7. Anodiskā oksidēšanā ģenerēti amidilradikāļi **63'** veic iekšmolekulāru neaktivēto ciklopropāna grupas *C*-*C* saites uzšķelšanu, veidojot oksazolīnus **69**. Šajā reakcijā $TBABF_4$ kalpo kā fluora avots. Rezultātā tiek izveidotas jaunas *C*-*O* un *C*-*F* saites, veidojot ciklopropāna 1,3-oksifluorēšanas produktus.

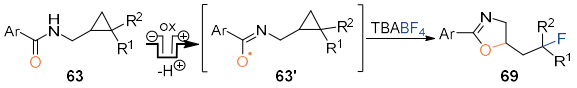

63 **63'** **69**

8. Veicot hirāla ciklopropāna ***S*-63c** elektroķīmiski inducētu uzšķelšanu, notiek pilnīga hiralitātes pārnese uz produktu ar konfigurācijas inversiju, rezultātā veidojot enantiobagātinātu oksazolīnu ***S*-69c**. Stereoķīmijas pētījumu rezultāti liecina par iekšmolekulārās homolītiskās aizvietošanas mehānismu (S_{HI}).

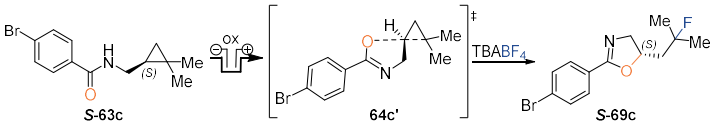

***S*-63c** (*ee* = 95 %) **64c'** ***S*-69c** (*ee* = 95 %)

DOCTORAL THESIS PROPOSED TO RIGA TECHNICAL UNIVERSITY FOR PROMOTION TO THE SCIENTIFIC DEGREE OF DOCTOR OF SCIENCE

To be granted the scientific degree of Doctor of Science (PhD), the present Doctoral Thesis has been submitted for defence at the open meeting of RTU Promotion Council on 15 January 2026 17.00 at the Faculty of Natural Sciences and Technology of Riga Technical University, Paula Valdena iela 3, Room 272.

OFFICIAL REVIEWERS

Associate Professor Dr. chem. Nelli Batenko,
Riga Technical University

Assistant Professor PhD Maksim Ošeka,
Tallinn University of Technology, Estonia

Associate Professor PhD Vladislav Ivaništšev,
University of Latvia, Latvia

DECLARATION OF ACADEMIC INTEGRITY

I hereby declare that the Doctoral Thesis submitted for review to Riga Technical University for promotion to the scientific degree of Doctor of Science (PhD) is my own. I confirm that this Doctoral Thesis has not been submitted to any other university for promotion to a scientific degree.

Madara Dārziņa ……. (signature)
Date: ……

The Doctoral Thesis has been prepared as a collection of thematically related scientific publications and summaries in both Latvian and English. The Doctoral Thesis consists of four scientific publications. The scientific publications have been written in English, with a total volume of 362 pages, including supplementary data.

INTRODUCTION

Electroorganic synthesis is a subfield of organic synthesis that enables the development of new methods for obtaining organic compounds, employing electric current. The advantages of electrochemical synthesis include the possibility to reduce or avoid the use of redox reagents and the ability to control reaction selectivity by tuning the applied potential.[1] In addition, electrochemical synthesis can expand the scope of chemical transformations, enabling reaction pathways that cannot be easily achieved with traditionally used chemical reagents.[1]

Electricity is a cheap source of energy that can be generated from renewable resources; hence electrochemical synthesis meets the demand for sustainable chemistry.[2] The rapid development of the field of electrosynthesis in the past decade has also been driven by increased supply of commercially available equipment, such as the IKA *ElectraSyn* potentiostat, which appeared on the market in 2017.[3] As a result, since 2014, the number of scientific articles published each year that employ electrochemical synthesis methods has increased more than tenfold.[4]

During electrolysis, a heterogeneous exchange of electrons takes place between the electrode surface and the substrate. In the anode reaction, electrons are transferred from the substrate to the electrode, i.e., oxidation, while in the cathode reaction, the opposite process takes place – electrons are transferred from the electrode to the substrate, i.e., reduction. Both transformations are linked in a joint process; it is not possible to carry out an electrolysis without the oxidation or reduction half-reaction.

The most important electrochemical parameters are the applied current and potential. Current strength characterizes the rate of electron transfer, while potential characterizes their inherent energy.[5] The most common modes of performing electrolysis are galvanostatic (controlling the current strength) or potentiostatic (controlling the potential) conditions. Another important variable is the amount of charge delivered, which is determined as the strength of the current per unit of time. Charge is expressed in faradays (F), where 1 F corresponds to a charge of 96,485 C/mol. It allows for determining, how many electron equivalents (z F, where z is the number of electrons per substrate molecule) have been added to the reaction mixture, analogous to reagent stoichiometry.[5]

During the Doctoral Thesis, the author explored the use of electrochemical oxidation to synthesize new compounds. Substrate oxidation was performed on the anode, while proton reduction to hydrogen was carried out on the cathode, thus reducing the amount of waste generated during the reaction. The electrochemical reactions were carried out in batch electrolysis conditions, where the reaction mixture remains in the electrochemical cell throughout the electrolysis process. Electrochemical reactions were performed using commercially available standardized equipment: the IKA *ElectraSyn 2.0* potentiostat, as well as IKA electrochemical cells and electrodes.

The aim of the Doctoral Thesis was to develop new electrochemical synthesis methods for the formation of *C-O* and *C-N* bonds. The study consists of two parts: 1) electrochemical oxidation of furan derivatives and electrochemically obtained product functionalization; and 2) electrochemical oxidation of cyclopropane derivatives. In each explored approach, at least one synthesis step was performed by electrochemical oxidation of the reaction substrate.

Furfural **1**, a furan derivative, is one of the products obtained in large quantities during biomass processing.[6] In 2004, the US Department of Energy included furfural in its list of 12 most promising platform chemicals.[7] Based on previous research conducted by our group on the synthesis of spirocyclic bisketals and unsaturated esters from furan derivatives, in this study, we wanted to expand the scope of known methods that would allow biomass-derived furfural **1** to be transformed into multi-functional building blocks: modified acrylates **2**, enantio-enriched unsaturated oxazolines **3**, and spirocyclic hemiaminal ethers **4** (Fig. 1).

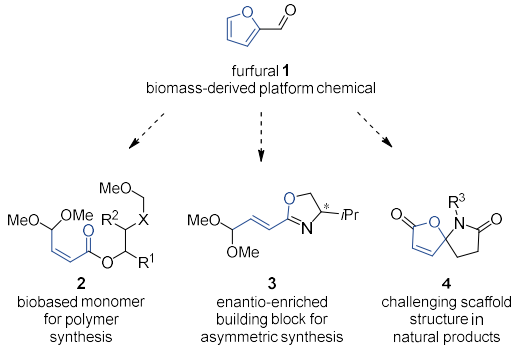

Fig. 1. Target compounds **2–4** proposed in the first part of the Doctoral Thesis, the synthesis of which involves electrochemical oxidation of furan derivatives.

The second part of the Doctoral Thesis is dedicated to electrochemically induced *C*-*C* bond cleavage of non-activated cyclopropanes **5** to obtain 1,3-difunctionalized products **6** (Scheme 1). The oxidation potential of the non-activated cyclopropane ring is too high to allow easy direct electrochemical oxidation,[8] so we chose to construct substrates **5** in which cyclopropane would be linked to an electrochemically oxidizable functional group, benzamide.

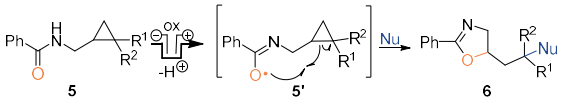

Scheme 1. Electrochemically induced cleavage of non-activated cyclopropanes **5** to obtain oxazolines **6**.

It is expected that the electrochemically obtained amidyl radical **5'** in such substrates is capable of inducing the cleavage of the cyclopropane *C*-*C* bond, forming a new *C*-*O* bond. Further oxidation of the cleaved intermediate and reaction with a nucleophile would lead to the formation of cyclopropane 1,3-functionalization products **6.**

Aims and objectives

The thesis aims to develop new methodology for the electrochemical formation of *C*-*O* and *C*-*N* bonds and explore further functionalization of the obtained products.

To achieve this aim, the following tasks were set:

1) electrochemical transformation of biomass-derived furfural conjugates into *α,β*-unsaturated esters and spiro-hemiaminal ethers;
2) transformation of electrochemically obtained *α,β*-unsaturated esters into enantio-enriched vinyl oxazolines;
3) electrochemically induced cleavage of non-activated cyclopropanes with subsequent 1,3-difunctionalization.

Scientific novelty and main results

Within the scope of the Thesis, three electrochemical methods and one synthesis route to obtain multi-functional building blocks were developed:

1) a method for an electrochemical one-reactor process for furfurylated ethylene glycol and furfurylated amino alcohol derivative transformation into *α,β*-unsaturated esters;
2) a synthesis route for the conversion of electrochemically obtained chiral *α,β*-unsaturated esters into enantio-enriched vinyl oxazoline building blocks;
3) a method for electrochemical synthesis of spiro-hemiaminal ethers from 3-(2-furyl)propionic acid aryl amide derivatives;
4) a method for electrochemically induced intramolecular cleavage of non-activated cyclopropanes by an amidyl radical, followed by monofluorination.

Structure and scope of the Thesis

The Doctoral Thesis is prepared as a collection of scientific publications on the use of electrochemical oxidation to form new *C-O*/*C-N* bonds, as well as exploration of further applications of the electrochemically obtained products.

Publications and approbation of the tTesis

The main results of the Doctoral Thesis are summarized in four scientific publications. The research results have been presented at 11 conferences.

Scientific publications

1. **Darzina**, **M**.; Lielpetere, A.; Jirgensons, A. Preparation of furfural derived enantioenriched vinyl oxazoline building block and exploring its reactivity. *Beilstein J. Org. Chem.* **2025,** *21,* 1737–1741. https://doi.org/10.3762/bjoc.21.136
2. **Darzina**, **M**.; Jirgensons, A. Electrochemical Formation of Oxazolines by 1,3-Oxyfluorination of Non-activated Cyclopropanes. *Org. Lett*. **2024**, *26*, 2158–2162. https://doi.org/10.1021/acs.orglett.4c00143
3. Briede, S.; Platnieks, O.; **Darzina**, **M**.; Jirgensons, A.; Gaidukovs, S. Effect of novel furan-based ester reactive diluent on structure and properties of UV-crosslinked acrylated rapeseed oil. *J. Polym. Sci*. **2023**, *61*, 3318–3328.

https://doi.org/10.1002/pol.20230451

4. **Darzina**, **M**.; Lielpetere, A.; Jirgensons, A. Torii-type electrosynthesis of *α,β*-unsaturated esters from furfurylated ethylene glycols and amino alcohols. *Eur. J. Org. Chem.* **2021,** 4224–4228. https://doi.org/10.1002/ejoc.202100605

Conferences

1. **Darzina**, **M**.; Jirgensons, A. Electrochemical Formation of Oxazolines by 1,3-Oxyfluorination of Non-activated Cyclopropanes. *76th Annual Meeting of the International Society of Electrochemistry*. Germany, September 7–12, **2025**. Poster presentation.
2. **Darzina**, **M**.; Jirgensons, A. Electrochemical Formation of Oxazolines by 1,3-Oxyfluorination of Non-activated Cyclopropanes. *Electrifying Organic Synthesis.* Germany, September 3–5, **2025**. Poster presentation.
3. **Darzina**, **M**.; Černobrovkins, D.; Jirgensons, A. Electrochemical Formation of Oxazolines by 1,3-Oxyfluorination of Non-activated Cyclopropanes. *Electrochemistry 2024*. Germany, September 16–19, **2024**. Poster presentation.
4. **Darzina**, **M**.; Jirgensons, A. Electrochemical Formation of Oxazolines by 1,3-Oxyfluorination of Non-activated Cyclopropanes. *Balticum Organicum Syntheticum 2024*. Latvia, July 7–10, **2024**. Poster presentation.
5. **Darzina**, **M**.; Černobrovkins, D.; Jirgensons, A. Electrochemical Cleavage and Subsequent Oxyfluorination of Cyclopropane *C-C* Bond. *13th Paul Walden Symposium on Organic Chemistry*. Latvia, September 14–15, **2023**. Poster presentation.
6. **Darzina**, **M**.; Lielpētere, A.; Jirgensons, A. Electrosynthesis of *α,β*-unsaturated esters from furfurylated ethylene glycols and amino alcohols. *73rd Annual Meeting of the International Society of Electrochemistry*. Online, September 12–16, **2022.** Virtual poster presentation.
7. **Darzina**, **M**.; Lielpētere, A.; Jirgensons, A. Electrosynthesis of *α,β*-unsaturated esters from furfurylated ethylene glycols and amino alcohols. *Balticum Organicum Syntheticum 2022*. Lithuania, July 3–6, **2022**. Poster presentation.
8. **Darzina**, **M**.; Lielpētere, A.; Jirgensons, A. Electrosynthesis of *α,β*-unsaturated esters from furfurylated ethylene glycols and amino alcohols *12th Paul Walden Symposium on Organic Chemistry*. Online, October 28–29, **2021**. Virtual poster presentation.
9. **Darzina**, **M**.; Lielpētere, A.; Jirgensons, A. Electrosynthesis of *α,β*-unsaturated esters from furfurylated ethylene glycols and amino alcohols. *72nd Annual Meeting of the International Society of Electrochemistry*. Online, August 29–September 3, **2021**. Oral presentation.
10. **Darzina**, **M**.; Lielpētere, A.; Jirgensons, A. Electrosynthesis of *α,β*-unsaturated esters from furfuryl alcohol and furfurylamine derivatives. *Electrochemistry Undercover 2020*. Online, September 23–24, **2020**. Virtual poster presentation.
11. **Dārziņa**, **M**.; Lielpētere, A.; Jirgensons, A. Electrosynthesis of *α,β*-unsaturated esters from furfuryl alcohol and furfurylamine derivatives. *Graduate Student*

Symposium on Advantageous Electrochemistry 2020 online edition. Online, September 10–11, **2020**. Oral presentation.

MAIN RESULTS OF THE THESIS

1. Electrosynthesis of *Torii-type* esters from furfurylated ethylene glycol derivatives and furfurylated amino alcohols

1.1. Development of a single-reactor process for the electrosynthesis of *Torii-type* esters

Previously, our group developed a method for electrochemical conversion of furan derivatives **7** into unsaturated esters **9** in two separate electrolysis steps under galvanostatic batch electrolysis conditions in an undivided cell (Scheme 2). Oxidation of compounds **7** and **8** was carried out in the anode reaction, while proton reduction to hydrogen was employed as the cathode reaction. Different additives and supporting electrolytes were required in each electrochemical reaction.

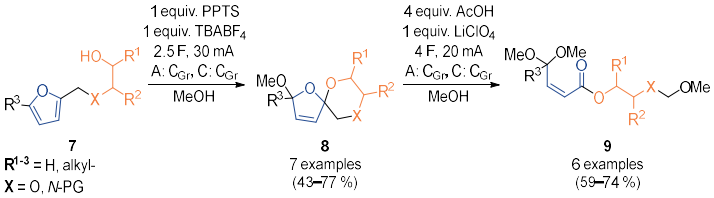

Scheme 2. Electrochemical conversion of furan derivatives **7** into spirocyclic compounds **8** and unsaturated esters **9**.

According to the proposed reaction mechanism (Scheme 3), in the first step, the furan ring in compound **7a** undergoes anodic oxidation, resulting in the formation of radical cation **10**, which is attacked by the intramolecular alcohol, closing the spirocycle. This results in the formation of a *C*-centered radical **11** that is further oxidized to an oxonium ion **12** and quenched with methanol, forming the spirocyclic product **8a**.[9] Mechanistic investigation revealed that spirocycle cleavage in the second stage of electrolysis begins with anodic oxidation to form the radical cation **13**/**13'**, followed by methanol addition to give the oxyradical **14**. In the next step, intermediate **14** undergoes *β-scission* forming acyclic *C*-centered radical **15**, that is oxidized to oxonium ion **16** and quenched by methanol to give the final product unsaturated ester **9a**.

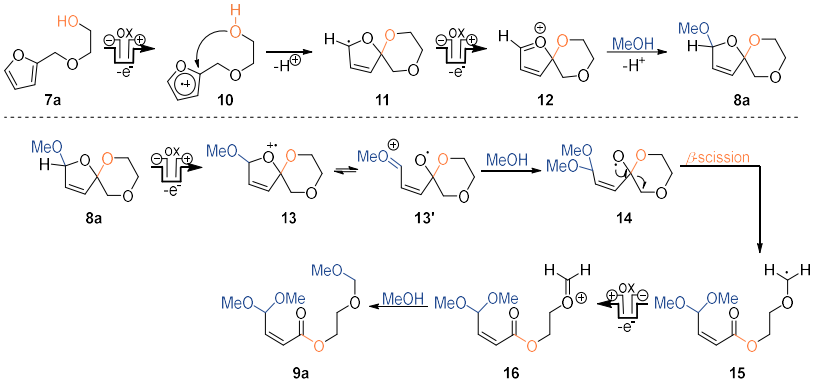

Scheme 3. Proposed mechanism for the electrochemical transformation of alcohol **7a** into ester **9a**.

As part of the Doctoral Thesis, a single-reactor process was developed for the conversion of alcohols **7** into esters **9** by two-step batch electrolysis under galvanostatic conditions in an undivided cell (Scheme 4). By studying the reaction conditions, it was found that electrolysis can be carried out in two steps without isolating the spirocyclic product **8**. In the first step, alcohols **7** were converted into spirocyclic compounds **8** in the presence of 1,1,1,3,3,3-hexafluoropropan-2-ol (HFIP) as an additive by applying 2.2 F of charge. Then, 4 equivalents of acetic acid were added to the reaction mixture, and electrolysis was continued until an additional 4 F was added to the cell. As a result, unsaturated esters **9** were formed.

Using furan derivatives **7a-c**, which contained an ethylene glycol fragment in the side chain, products **9a-c** were obtained with average yields (39–47 %), which were equivalent to or lower than those obtained by performing two separate electrolysis reactions, isolating spirocyclic intermediates **8a-c.** In contrast, the ester yield was significantly improved in the electrolysis of substrates **7d-e** containing an amino alcohol fragment, and esters **9d-e** could be obtained with yields of 69–75 % (Scheme 4).

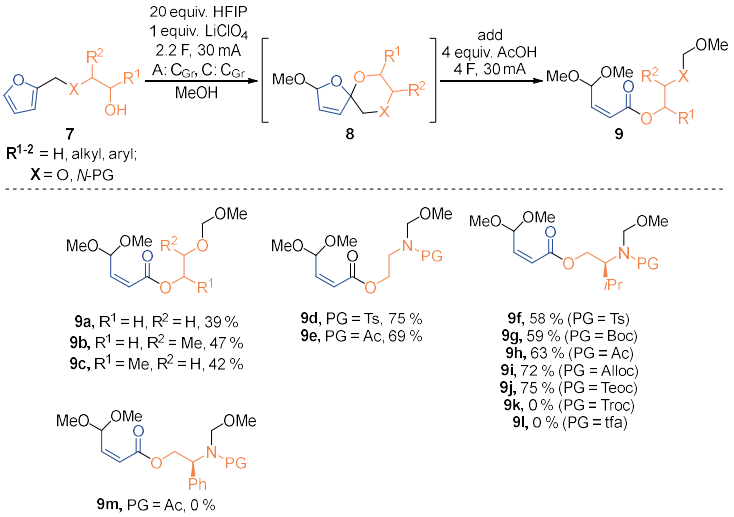

Scheme 4. Electrosynthesis of unsaturated esters **9** from furan derivatives **7** in a single-reactor process.

To expand the scope of products, we synthesized substrates **7f-l**, in which a chiral amino alcohol, L-valinol, was attached to the furan ring. Amine groups have a low oxidation potential (up to 1.0 V vs. saturated calomel electrode (SCE)[10]), thus a protecting group was installed on the amine function to prevent possible side reactions. We found that Ts, Ac, Boc, Alloc, and Teoc protecting groups are compatible with the electrolysis conditions, which allowed us to obtain products **9f-j**, while the halogen-containing protecting groups Troc and tfa were not suitable (Scheme 4). If valinol fragment was replaced with a phenylglycinol fragment, a complex mixture of products was formed during electrolysis, from which the expected product **9m** could not be isolated (Scheme 4).

We also explored how introducing a substituent in the furan ring affects the electrolysis outcome with substrate **19**. Compound **19** was obtained in three steps from commercially available 4-bromofurfural **17** (Scheme 6). In the first step, a phenyl group was installed by Suzuki-Miyaura coupling with phenylboronic acid, followed by reductive amination and amino group protection to give compound **19**. Electrolysis of alcohol **19** led to a mixture of products from which the expected ester **20** was isolated with an 8 % yield (Scheme 5).

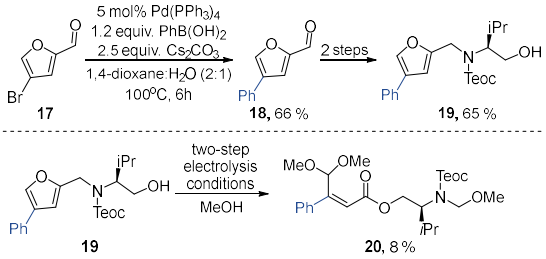

Scheme 5. Synthesis and electrolysis of 4-phenyl-substituted furan derivative **19**.

The main results obtained in this chapter are summarized in the publication "*Torii-type electrosynthesis of α,β-unsaturated esters from furfurylated ethylene glycols and amino alcohols*".

1.2. Obtaining bio-based acrylate monomer for polymerization reactions

Having developed a method for the electrochemical synthesis of unsaturated esters, we explored the prospects of further application of these compounds. One of the areas of interest was the use of the unsaturated esters in polymer synthesis as acrylate-type monomers.

For initial studies, we selected unsaturated ester **9a** as a potential monomer. Ester **9a** was obtained in two consecutive electrolysis steps from alcohol **7a,** isolating spirocyclic intermediate **8a**, because the single-reactor process was not suitable for obtaining product **9a** with a sufficiently high yield (Scheme 6). Since the substrate **7a** loading (422 mg; 3.0 mmol) was higher than under optimized conditions (103 mg; 0.7 mmol (Scheme 4)), we were able to reduce the amount of supporting electrolyte $TBABF_4$ from 1 to 0.5 equivalents.

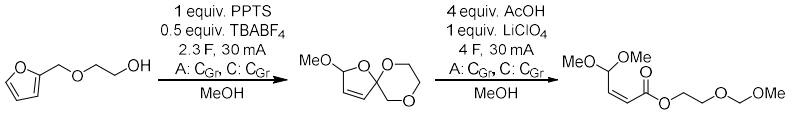

7a (422 mg) **8a**, 78 % (399 mg) **9a**, 62 % (339 mg)

Scheme 6. Synthesis of ester **9a** for polymerization studies.

The obtained ester **9a** was handed over to collaboration partners at Professor S. Gaidukovs' laboratory (RTU), where it was used as a reactive diluent to be copolymerized with acrylated rapeseed oil (ARO). The purpose of the reactive diluent in polymerization reactions is to reduce the viscosity of the obtained polymer and increase the formation of crosslinks, which can improve the strength and tensile properties of the material. Our collaboration partners prepared several polymer films, in which the reactive diluent **9a** was added in amounts of 5 % and 20 % by weight, yielding copolymers **ARO/9a**(5 %) and **ARO/9a**(20 %), respectively.

The polymer films were obtained in two steps. First, the resin was prepared by mixing acrylated rapeseed oil with the appropriate amount of ester **9a** (5 % or 20 % by weight), followed by the addition of a small amount of radical photoinitiator (2,4,6-trimethylbenzoyl)phosphine oxide (3 % by weight) solution in acetone to the mixture. The mixture was left overnight at room temperature to allow the solvent to evaporate. In the next step, the liquid resin mixture was applied to a glass substrate at a thickness of 508 μm and exposed to UV radiation (405 nm) to achieve curing. This resulted in the formation of polymer films.

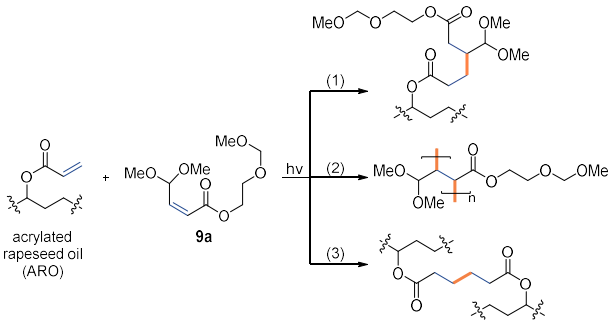

Fig. 2. Possible copolymerization products of acrylated rapeseed oil (ARO) and ester **9a**.

During radical polymerization, three different types of bonds can form in the copolymer (Fig. 2): the reaction between ARO and **9a** forms freely oscillating chain fragments (1); several **9a** monomers react with each other and the fragments shown in (2) can form; the third type of cross-linking occurs between two ARO fragments (3), which is the most likely and fastest, as in this case two terminal double bonds are connected.

FTIR spectroscopic measurements confirmed that ester **9a** was incorporated into the obtained polymers **ARO/9a**(5 %) and **ARO/9a**(20 %), because the double bond signals had almost completely disappeared after curing by UV rays. The incorporation of ester **9a** is also visible using a scanning electron microscope (SEM), as the surface of the copolymer is significantly rougher than that of a pure ARO polymer.

Compared to undiluted ARO polymer, the obtained copolymers had up to 1.6 times lower viscosity (**ARO/9a**(20 %)) and improved crosslink density (from 1.07 mol/m^3 in ARO polymer to 1.65 mol/m^3 in **ARO/9a**(5 %) copolymer).

This study demonstrated that the unsaturated ester **9a**, derived from biomass furan and ethylene glycol conjugate, can successfully replace fossil-based acrylate monomers in copolymerization with vegetable oils. The results obtained in this chapter are summarized in the publication "*The effect of a new furan-based ester reactive solvent on the structure and properties of UV-cured acrylated rapeseed oil*."

1.3. Obtaining a furfural and valinol derived enantio-enriched vinyl oxazoline building block and exploring its reactivity

The next explored approach of electrochemically obtained ester functionalization was the transformation of chiral center-containing esters **9i** into enantio-enriched vinyl oxazolines **23**, which could be used as building blocks in asymmetric synthesis.

According to the proposed strategy (Scheme 7), the electrolysis of the chiral center containing furfural and valinol conjugate **7i** would yield the enantio-enriched unsaturated ester **9i**. Upon amine protecting group removal in the next step, we expected the free amine **21** to undergo *in situ* rearrangement to amide **22,** which could be cyclized into enantio-enriched vinyl oxazoline **23**. We allowed for the possibility that double bond isomerization

from *cis*- to the more stable *trans*-configuration might also occur in one of the synthesis steps. We chose Alloc group as the amine protecting group, because it was compatible with the electrolysis conditions and the acetal function in the substrate was not affected during its removal.

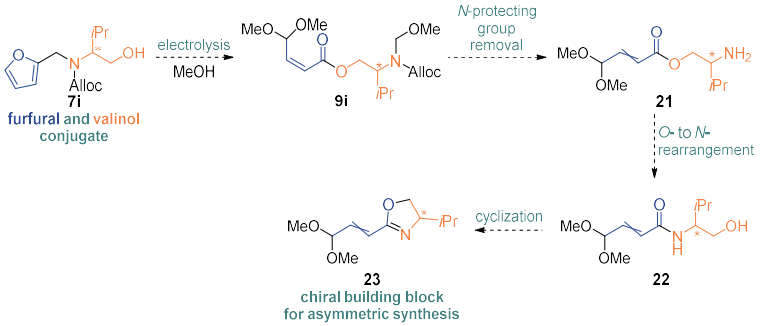

Scheme 7. Strategy for the transformation of the furfural and valinol conjugate **7i** into the enantio-enriched vinyl oxazoline **23**.

Using the two-step electrolysis conditions described in Section 1.1, we were able to synthesize the unsaturated ester **9i** on a preparative scale (500 mg (2 mmol) and 1 g (4 mmol) of substrate loading) with good yields (Scheme 8).

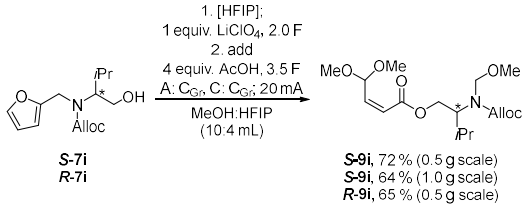

Scheme 8. Preparation of unsaturated ester **9i** on a preparative scale using two-step electrolysis conditions.

Although the previously developed reaction conditions were suitable for obtaining unsaturated ester **9i**, we wanted to simplify the electrolysis process by switching from two-step electrolysis to continuous electrolysis, as well as to reduce the use of expensive or hazardous reagents (HFIP, $LiClO_4$). To achieve this, we proceeded to optimize the electrolysis conditions for compounds ***S*-/*R*-7i** (Table 1).

First, we reduced the amount of HFIP from 4 mL to 1 mL and 0.5 mL and performed continuous electrolysis with a 5.5 F of added charge. Gratifyingly, we were able to successfully obtain the unsaturated esters ***S*-9i** (Table 1, rows 2–3). The yields in these reactions were comparable to previously established two-step conditions (72 % in the two-step electrolysis, 71 % and 70 % with 1 mL and 0.5 mL of HFIP in the continuous electrolysis, respectively).

Replacing HFIP with 3 equivalents of AcOH also resulted in the successful formation of unsaturated esters ***S*-9i** and ***R*-9i** (Table 1, rows 4–6). The yield of electrolysis was equivalent to that of the two-step synthesis on a 1 mmol scale (72 %), but decreased to 68 %

on a 2 mmol scale. Additionally, the amount of $LiClO_4$ electrolyte used in the reaction was reduced from 1 to 0.5 equivalents (from 0.14 M to 0.07 M). By increasing the amount of AcOH to 1 mL (~ 18 equiv.), the product yield decreased to 55 %, indicating that AcOH is not suitable as a co-solvent for this reaction (Table 1, row 7). In contrast, when electrolysis was performed without additives, product ***S*-9i** was formed with a 60 % yield (Table 1, row 8).

When replacing the supporting electrolyte $LiClO_4$ with LiOAc, we observed the formation of spirocycle ***S*-8i**, but no further conversion to unsaturated ester ***S*-9i** took place (Table 1, row 9).

As a result of optimization studies, it was possible to modify the electrolysis method, switching from a two-step to a continuous electrolysis process. The previously used additive combination of HFIP (4 mL) and AcOH (4 equiv.) was replaced with a single additive, AcOH (3 equiv.), and the amount of supporting electrolyte $LiClO_4$ was reduced by half on a 2 mmol scale.

Table 1

Optimization of the electrolysis conditions for compound **7i**

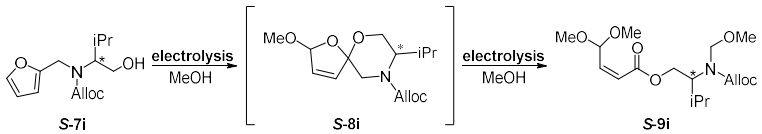

S-7i *R*-7i | *S*-8i *R*-8i | *S*-9i *R*-9i

No.	Conditions[a]	Yield of 9i
1.[b]	Step 1: MeOH: HFIP (10:4 mL), $LiClO_4$ (1 equiv.), 2.0 F; Step 2: Add AcOH (4 equiv.), 3.5 F	72 % (***S*-9i**)
2.	Continuous electrolysis: MeOH: HFIP (13:1 mL), $LiClO_4$ (1 equiv.), 5.5 F	71 % (***S*-9i**)
3.	Continuous electrolysis: MeOH: HFIP (13.5:0.5 mL), $LiClO_4$ (1 equiv.), 5.5 F	70 % (***S*-9i**)
4.	Continuous electrolysis: MeOH (14 mL), AcOH (3 equiv.), $LiClO_4$ (1 equiv.), 5.5 F	72 % (***S*-9i**)
5.[b]	Continuous electrolysis: MeOH (14 mL), AcOH (3 equiv.), $LiClO_4$ (0.5 equiv.), 5.5 F	68 %[c] (***S*-9i**)
6.[b]	Continuous electrolysis: MeOH (14 mL), AcOH (3 equiv.), $LiClO_4$ (0.5 equiv.), 5.5 F	68% (***R*-9i**)
7.	Continuous electrolysis: MeOH: AcOH (13:1 mL), $LiClO_4$ (1 equiv.), 5.5 F	55 % (***S*-9i**)
8.	Continuous electrolysis: MeOH (14 mL), $LiClO_4$ (1 equiv.), 5.5 F	60 % (***S*-9i**)
9.	Continuous electrolysis: MeOH (14 mL), AcOH (3 equiv.), LiOAc (1 equiv.), 5.5 F	0 %[d] (***S*-9i**)

[a] Scale: 1 mmol. [b] Scale: 2 mmol. [c] Faradaic efficiency 49.5 %; cell productivity 0.09 mmol/h. [d] The major product is spirocycle ***S*-8i**.

To cleave the Alloc group, we used a palladium catalyst and pyrrolidine as a nucleophile to scavenge the allyl group (Scheme 9). We observed that under reaction conditions, the *N*-MOM group was also cleaved and the expected *O*-to-*N* rearrangement took place. Using catalyst $Pd(PPh_3)_4$, a complete conversion of the starting material ***S*-9i** was achieved in 30 minutes, but partial double bond isomerization occurred, and a mixture of *cis*-***S*-24** and *trans*-***S*-24** products was obtained (Scheme 9). After additional screening of other palladium catalysts and bases, we were not able to find conditions under which the *cis*-**24** isomer could be obtained selectively, whereas using the Pd(*S*-BINAP)Cl_2 catalyst led to the selective formation of the *trans*-**24** isomer. Product *trans*-***S*-24** was derivatized to 4-bromo-benzoyl ester ***S*-25** to perform X-ray structural analysis, which confirmed the expected atom connectivity, double bond isomerization and absolute configuration of the stereocenter (Scheme 9).

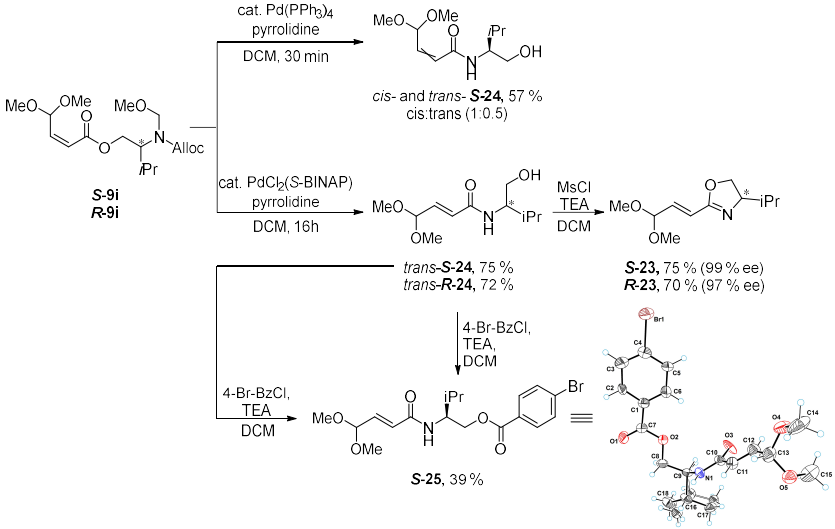

Scheme 9. Transformation of the electrochemically obtained esters ***S*-/*R*-9i** into enantio-enriched vinyl oxazolines ***S*-/*R*-23** and *trans*-***S*-24** to 4-bromobenzoic ester ***S*-25**.

The obtained amides *trans*-***S*-/*R*-24** were transformed into the corresponding oxazolines ***S*-/*R*-23**, using mesyl chloride and triethylamine (Scheme 9). Chiral HPLC analysis confirmed that no racemization had occurred in the oxazolines ***S*-/*R*-23**.

In the next stage of the study, we focused on exploring the reactivity of the obtained vinyl oxazolines **23**. We predicted that the oxazoline ring could serve as a chiral directing group, thus allowing asymmetric transformations.

Performing aza–Diels–Alder reaction with oxazoline ***S*-23** and tosyl isocyanate, we obtained oxazolo[3,2-*c*]pyrimidine derivative **26** with an 86 % yield (Scheme 10). The product was formed as a single diastereomer.

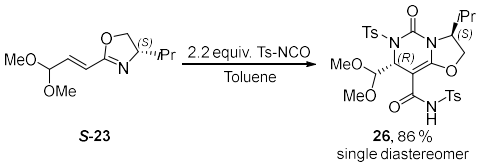

Scheme 10. Oxazoline ***S*-23** and tosyl isocyanate aza–Diels–Alder reaction product oxazolo[3,2-*c*]pyrimidine **26**.

Based on the reaction mechanism proposed by Elliott *et al*.,[11] the formation of product **26** involves asynchronous cycloaddition (Scheme 11). First, the attack of imidate nitrogen to isocyanate carbon generates intermediate **27**, followed by stereoselective ring closure to form dihydropyrimidine-2-one **28.** Intermediate **28** with its nucleophilic double bond attacks another isocyanate molecule, forming intermediate **29**/**29**', and proton transfer yields the final product oxazolo[3,2-*c*]pyrimidine **26.**

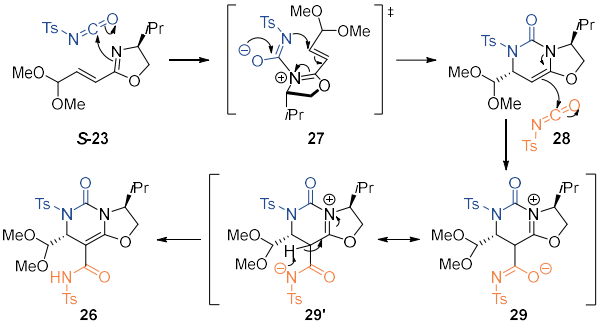

Scheme 11. Proposed mechanism for oxazolo[3,2-*c*]pyrimidine **26** formation.

We wanted to expand the scope of oxazolo[3,2-*c*]pyrimidine products, so we attempted to engage the vinyl oxazoline ***S*-23** in aza–Diels–Alder reaction with other isocyanates or isothiocyanates. However, these reactions were unsuccessful and products **30a-c** were not obtained (Scheme 12).

Scheme 12. Aza–Diels–Alder reactions with vinyl oxazoline ***S*-23** and various isocyanates or isothiocyanate.

We also attempted to explore asymmetric vinyl oxazoline ***S*-23** double bond transformations, including 1,4-addition, cyclopropanation, hydroboration, Diels–Alder, and Giese reactions. Unfortunately, none of them led to the formation of the desired products **31-35** (Scheme 13).

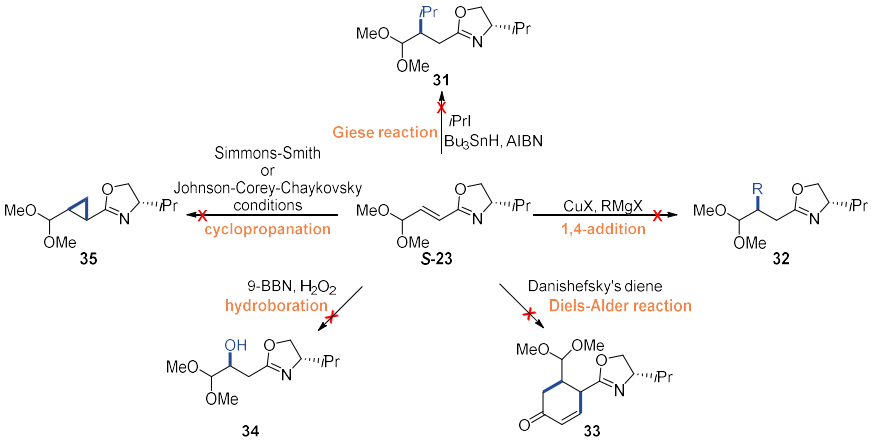

Scheme 13. Attempts to engage the vinyl oxazoline ***S*-23** in asymmetric double bond transformations.

We also investigated the prospect of using the vinyl oxazoline ***S*-23** in the Heck reaction. We attempted to optimize the reaction conditions for the arylation of substrate ***S*-23** with iodobenzene; however, the highest obtained yield of product **36** was only 20 % (Scheme 14).

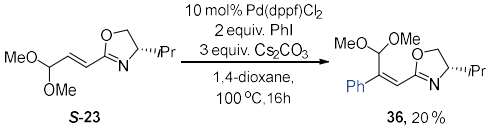

Scheme 14. Heck reaction with oxazoline ***S*-23** and iodobenzene.

The main results obtained in this chapter are summarized in the publication "*Preparation of furfural derived enantioenriched vinyl oxazoline building block and exploring its reactivity*".

2. Electrochemical synthesis of spiro-hemiaminal ethers from furfural derivatives

The [4.4]-spirocyclic hemiaminal ether motif is found in several natural products **37-41**, some of which are known to have biological activity. For example, *lycoplanine A* (**37**) is a calcium channel inhibitor, *elmenol H* (**41**) can suppress TRAIL resistance in gastric adenocarcinoma cells, while *shihunine* (**40**) extract has been traditionally used in Chinese medicine to treat diabetes (Fig. 3).[12–14]

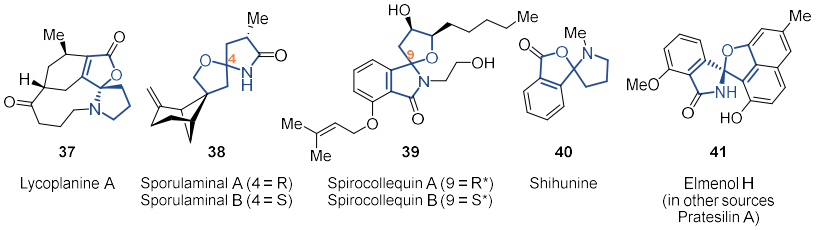

Fig. 3. Natural products **37-41** containing [4.4]-spiro-hemiaminal ether motif.

Previously, our group developed a method for electrochemical synthesis of [4.5]-spiro-bisketal scaffold containing compounds **43** (Scheme 15). Electrochemical oxidation of furfural derived alcohol **42** in weakly acidic conditions lead to *C-O* bond formation between the oxygen of the alcohol and the C2 carbon of the furan ring. As a result, spirocyclic products **43** were obtained, as mixtures of diastereomers (Scheme 15).

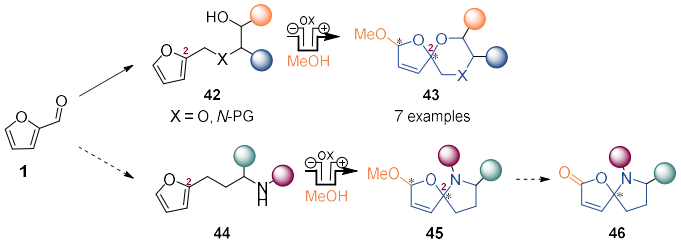

Scheme 15. Electrochemical synthesis of [4.5]-spiro-bisketals **43** and [4.4]-spiro-hemiaminal ethers **45** from furan derivatives.

As part of the Doctoral Thesis, we looked to extend this methodology to construct [4.4]-spiro-hemiaminal ether scaffolds by assembling spirocycles through electrochemically induced *C-N* bond formation in furan derivatives **44** (Scheme 15). After electrolysis, we planned to transform the methoxy group into a carbonyl group, thus obtaining product **46** with a single stereocenter.

In the first stage of the work, we carried out concept verification experiments, using 3-(2-furyl)propionic acid derived arylamide **47a** as the model substrate. Electrochemical reactions were carried out in an undivided cell under galvanostatic conditions. Substrate oxidation was performed on the anode, while proton reduction to hydrogen was employed as the cathode reaction. Electrolysis of substrate **47a** in methanol in neutral conditions gave

only the furan ring dimethoxylation product **48**, while electrolysis in the presence of NaOMe resulted in the selective formation of the spirocyclic product **49a** (Scheme 16).

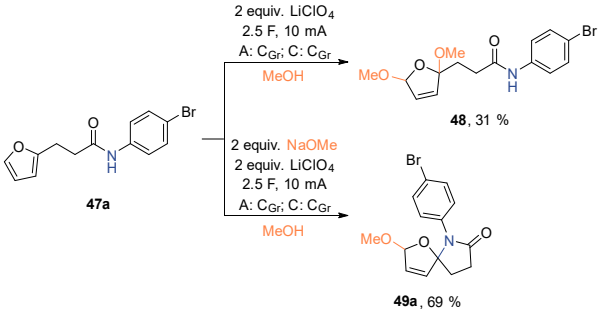

Scheme 16. Products **48** and **49a**, formed by electrolysis of compound **47a** in methanol.

To determine the role of base in the reaction product selectivity, we recorded cyclic voltammetry curves for substrate **47a** in neutral and basic conditions (Fig. 4). In neutral conditions, the first oxidation peak is observed at E_p = 1.1 V (Fig. 4, blue curve), which most likely corresponds to the oxidation of the furan ring. In the presence of NaOMe, a new oxidation peak appears at a significantly lower potential, E_p = 0.64 V (Fig. 4, green curve), which likely indicates that the amide group is deprotonated and the new oxidation peak corresponds to oxidation of the amidate anion. Even in the presence of excess base (2 equiv.), the cyclic voltammetry curve still shows an oxidation signal at E_p = 1.1 V (Fig. 4, green curve), suggesting that complete deprotonation of substrate **47a** does not occur under these conditions.

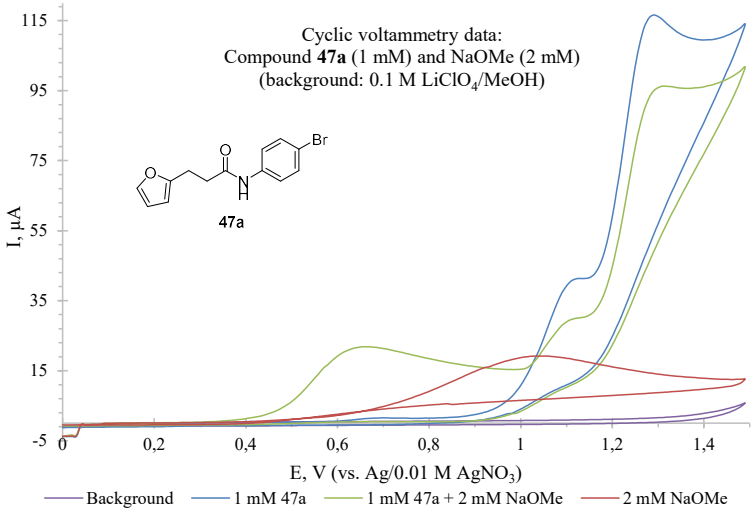

Fig. 4. Cyclic voltammetry curves of compound **47a** in neutral and basic conditions.

Based on experimental and literature[15] data, we proposed a possible mechanism for the formation of spirocyclic hemiaminal ether **49a** (Scheme 17). The first step is amide **47a** deprotonation, followed by anodic oxidation of amidate **50**. The resulting amidyl radical **51** with its nitrogen center forms a *C*-*N* bond with the C2 carbon of the furan ring, which leads to *C*-centered radical **52**. Subsequent oxidation produces oxonium ion **53**, which, upon addition of methanol, forms the final product **49a.**

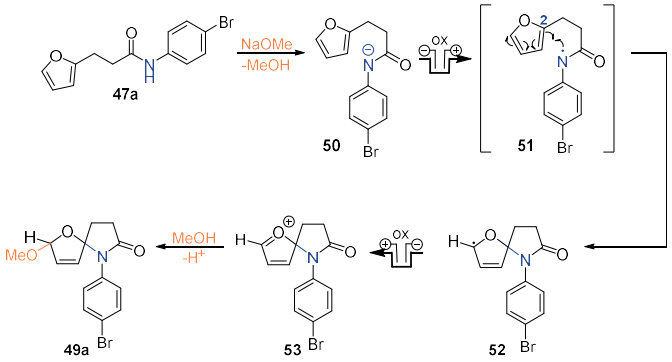

Scheme 17. Possible mechanism of formation of spiro-hemiaminal ether **49a**.

Next, we explored the electrolysis substrate scope with compounds containing various substituents in the arylamide function (Scheme 18). Electrolysis of substrates **47** in the presence of NaOMe successfully gave spirocycles **49a-d**, which contained both electron-withdrawing and electron-donating substituents in the benzene ring. All electrolysis products were obtained as a mixture of diastereomers. In the next step, we performed oxidation of spirocycles **49a-c** with *m*CPBA and a catalytic amount of $BF_3 \cdot Et_2O$, to obtain the respective spirocycles **54a-c** with good yields (Scheme 18).

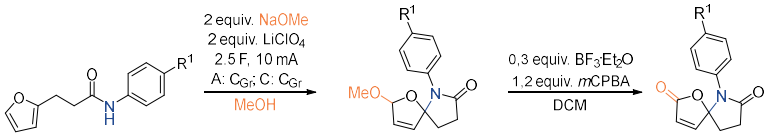

49a, R^1 = Br, 69 %, (dr 1:0.6)
49b, R^1= CF_3, 63 %, (dr 1:0.7)
49c, R^1 = H, 68 %, (dr 1:0.6)
49d, R^1 = OMe, 46 %, (dr 1:0.7)

54a, R^1 = Br, 89 %
54b, R^1= CF_3, 72 %
54c, R^1 = H, 82 %

Scheme 18. Synthesis of [4.4]-spiro-hemiaminal ethers **49a-d** and **54a-c** from 3-(2-furyl)propionic acid derivatives **47**.

X-ray structural analysis of product **54b** confirmed the expected atom connectivity (Fig. 5). With this, we concluded concept verification experiments.

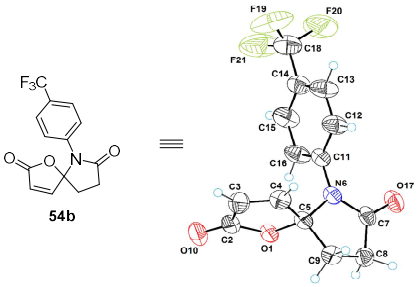

Fig. 5. ORTEP image of the X-ray structural analysis of compound **54b** with 50 % contour probability.

In the next stage of our work, we began optimizing the reaction conditions. First, we studied the effect of the supporting electrolyte on the reaction outcome (Table 2). The yield of spirocycle **49a** was determined using ^{1}H-*q*NMR spectroscopy. The reactions were carried out in an undivided electrochemical cell under galvanostatic conditions. The experimental results showed that the most suitable electrolytes for the reaction are alkali metal perchlorate ($LiClO_4$ and $NaClO_4$; Table 2, rows 1–2 and 10) and bromide (LiBr; Table 2, row 3). Since the product yields were similar when using both $LiClO_4$ (72 %) and LiBr (74 %), the next series of experiments was carried out with both supporting electrolytes.

Table 2

Formation of spiro-hemiaminal ether **49a** using different supporting electrolytes

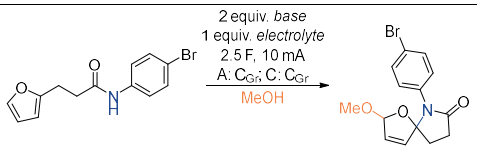

No.	Base	Electrolyte	49a[a]
1.	NaOMe	$LiClO_4$	70 %
2.	LiO*t*Bu	$LiClO_4$	72 %
3.	LiO*t*Bu	LiBr	74 %
4.	LiO*t*Bu	LiCl	66 %
5.	LiO*t*Bu	$LiBF_4$	63 %
6.	LiO*t*Bu	LiOAc	62 %
7.	LiOH	--	64 %
8.	LiO*t*Bu	$TBAClO_4$	69 %
9.	LiO*t*Bu	$TBAPF_6$	64 %
10.	NaOMe	$NaClO_4$	72 %
11.	NaO*t*Bu	$NaClO_4$	63 %

[a] Yield determined using ^{1}H-*q*NMR; internal standard 1,4-bis(trichloromethyl)benzene.

To determine how the amount of base affects the degree of amide deprotonation and oxidation potential of substrate **47a**, a cyclic voltammetry study was performed by adding 0 to 6 equivalents of the base NaOMe in increments of one equivalent to substrate **47a** (Fig. 6). When one equivalent of base is added (Fig. 6, blue curve), no pronounced amidate oxidation peak is observed at $E_p = 0.6$ V, whereas, when two equivalents of base are added (Fig. 6, pink curve), the amidate oxidation peak becomes clearly visible. The saturation current at $E_p = 0.6$ V is reached upon addition of 4 to 5 equivalents of NaOMe, which means that this is the amount of base required to completely deprotonate all of the substrate **47a** in the reaction mixture. By continuing to increase the amount of base, a methoxide oxidation peak becomes prominent at $E_p = 1.0$ V (the methoxide oxidation peak is shown in the red curve in Fig. 4).

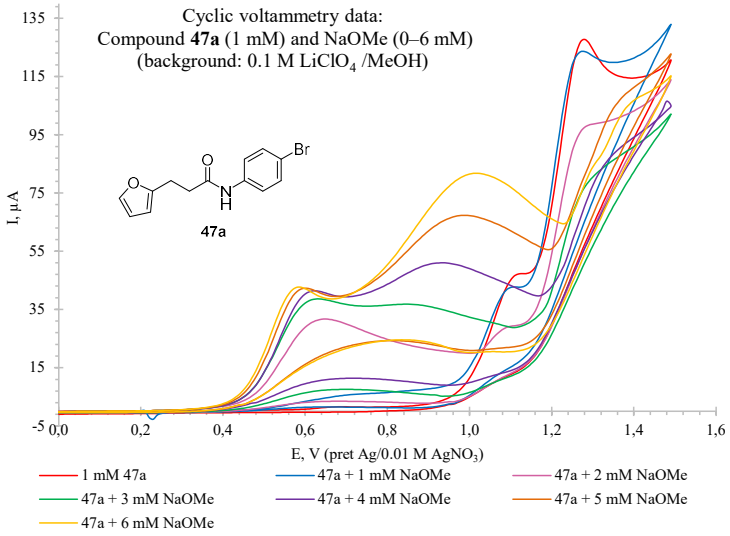

Fig. 6. Cyclic voltammetry curves for substrate **47a** with NaOMe (0 to 6 equivalents).

Based on cyclic voltammetry data, we developed a series of experiments to test how the amount of base added affects the selectivity and yield of the reaction products, exploring a range from 0 to 4 equivalents. The series of experiments was carried out with two supporting electrolytes – $LiClO_4$ and LiBr (Table 3), using Li*O*t*Bu* as the base.

We observed that adding a substoichiometric amount of base (0.5 equivalents; Table 2, rows 3 and 8) leads to selective formation of spirocyclic product **49a**, while adding an excess of base (2–4 equivalents; Table 2, columns 1–2 and 7) does not significantly improve the yield. This shows that it is not necessary to deprotonate all of substrate **47a** at the start of the reaction.

Reducing the amount of base from 0.5 to 0.2 equivalents caused the product **49a** yield to decrease slightly (Table 3, rows 4 and 9), while adding only 0.1 equivalent of base led to significant formation of the dimethoxylated side product **48** (Table 3, rows 5 and 10).

Electrolysis could also be performed with excess base (2 equivalents) without any additional supporting electrolyte, but the product yield was slightly lower than in the same conditions with electrolyte (Table 3, row 11).

In this series of experiments, we found that 0.5 equivalents of base are sufficient for selective formation of the spirocyclic product **49a**. The product yields using LiBr and $LiClO_4$ were comparable, but considering that LiBr is a cheaper and safer reagent, we used lithium bromide as the supporting electrolyte in further experiments.

Table 3

Formation of spiro-hemiaminal ether **49a** by adding different amounts of base LiO*t*Bu

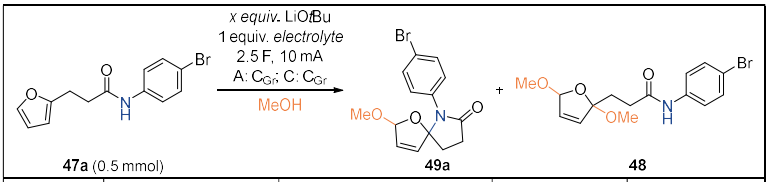

47a (0.5 mmol) **49a** **48**

No.	LiO*t*Bu (equiv.)	Electrolyte	**49a**[a]	**48**[a]
1.	4.0	$LiClO_4$	73 %	--
2.	2.0		72 %	--
3.	0.5		72 %	--
4.	0.2		70 %	--
5.	0.1		61 %	5 %
6.	--		0 %	52 %
7.	2.0	LiBr	74 %	--
8.	0.5		74 %	--
9.	0.2		66 %	--
10.	0.1		17 %	49 %
11.	2.0	--	67 %	--

[a] Yield determined using ^{1}H-*q*NMR; internal standard 1,4-bis(trichloromethyl)benzene.

In the next series of experiments, we tested the effect of cations – Li^+, Na^+ and K^+– on product yield. For reactions, we used alkoxides (MeO^- or $tBuO^-$) and bromides containing the respective cations (Table 4). The best results were obtained using a lithium-containing electrolyte and base (74 %; Table 4, row 1), but other cation combinations also gave similar results, indicating that the choice of cation in this case has little effect on the reaction outcome.

Table 4

Formation of spiro-hemiaminal ether **49a**, using Li^+, Na^+ and K^+ containing bases and bromides

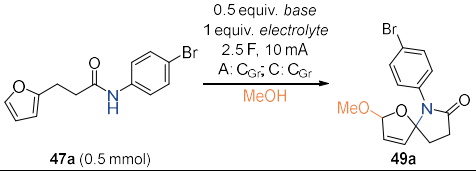

47a (0.5 mmol) 49a

No.	Base	Electrolyte	49a[a]
1.	LiO*t*Bu	LiBr	74 %
2.	LiO*t*Bu	NaBr	70 %
3.	NaOMe	LiBr	73 %
4.	NaOMe	NaBr	71 %
5.	KO*t*Bu	KBr	70 %

[a] Yield determined using ^{1}H-*q*NMR; internal standard 1,4-bis(trichloromethyl)benzene.

In the final stage of optimization, we studied the effect of electrochemical parameters on the reaction outcome (Table 5). We tested various anode and cathode materials, as well as current strength. Of the anode materials used, graphite (C_{Gr}) was best suited for substrate oxidation, while stainless steel (SS) was the best cathode material (Table 5, row 6). Current strength proved to be an important parameter – when the current supplied to the reaction was reduced from 10 mA to 5 mA, the product yield decreased from 76 % to 69 % (Table 5, row 7), while increasing the current to 15–50 mA increased the product yield to 78–84 % (Table 5, rows 8–12).

Table 5

Formation of spiro-hemiaminal ether **49a** by varying electrochemical parameters

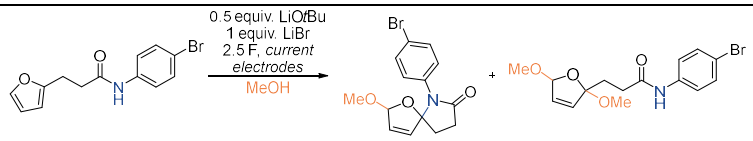

47a (0.5 mmol) 49a 48

No.	Anode	Cathode	Current (mA)	49a[a]	48[a]	47a[a]
1.	GC	C_{Gr}	10	65 %	--	--
2.	Pt	C_{Gr}		48 %	8 %	10 %
3.	BDD	C_{Gr}		7 %	37 %	--
4.	C_{Gr}	C_{Gr}		74 %	--	--
5.	C_{Gr}	Pt		75 %	--	--
6.	C_{Gr}	SS		76 %	--	--
7.			5	69 %	--	--
8.			15	80 %	--	--
9.			20	80 %	--	--
10.			30	78 %	--	--
11.			40	84 %	--	--
12.			50	82 %	--	--

[a] Yield determined using ^{1}H-*q*NMR; internal standard 1,4-bis(trichloromethyl)benzene.

During optimization studies, we found that synthesis of spiro-hemiaminal ether **49a** requires 0.5 equivalents of LiO*t*Bu and 1 equivalent (0.17 M) of LiBr. Optimized electrochemical parameters were a current of 40 mA (current density $j = 25$ mA/cm^2), applied charge of 2.5 F, as well as a graphite anode and a stainless steel cathode.

The next steps in this study include investigating the reaction substrate scope and further functionalization of electrolysis products.

3. Electrochemical formation of oxazolines by 1,3-oxyfluorination of cyclopropanes

The second part of the Doctoral Thesis focused on electrochemically induced cleavage of cyclopropane *C*-*C* bond. In 2021, Aiwen Lei's group published an article in which they used electric current to activate aryl cyclopropanes for reactions with nucleophiles (Scheme 19).[8] In the published method, direct anodic oxidation of aryl cyclopropane **55** leads to radical cations **55'**, in which the cyclopropane *C*-*C* bond is significantly weaker and which in turn can be cleaved using various nucleophiles X/Y, leading to 1,3-difunctionalized products **58.** One of the nucleophiles explored was fluoride (as $Et_3N{\cdot}3HF$), allowing the authors to obtain mono- and difluorinated products **58**.

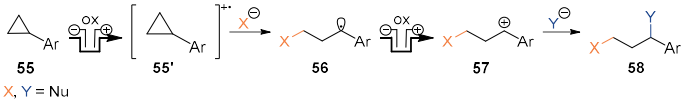

Scheme 19. Electrochemical 1,3-difunctionalization of arylcyclopropanes **55** as demonstrated by the group of Aiwen Lei.[9]

We wanted to expand the scope of electrochemical methods for cyclopropane *C*-*C* bond cleavage, focusing on cyclopropanes that are difficult to oxidize directly. For this purpose, we developed an approach for indirect electrochemical cyclopropane ring cleavage, employing an anodically oxidizable functional group attached to cyclopropane *via* a linker (Scheme 20). Anodic oxidation of compound **59** would lead to radical **59'**, in which the activated functional group could induce intramolecular cyclopropane *C*-*C* bond cleavage. Resulting *C*-centered radical **60** could be further oxidized to carbenium ion **61**, which, upon reaction with an external nucleophile (Nu), would give the final product **62**. In the cathode reaction, we planned to employ proton reduction to hydrogen.

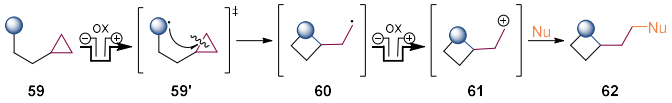

Scheme 20. Strategy for electrochemically induced cyclopropane *C*-*C* bond cleavage.

We chose compound **63a** as the model substrate for the reaction, which contained benzamide and dimethyl-substituted cyclopropane functions. Electrochemical oxidation of benzamide group would form amidyl radical **63a'**, which could induce cleavage of the *C*-*C* bond in cyclopropane, forming oxazoline **66** (Scheme 21). We predicted that the geminal methyl groups in cyclopropane function could help stabilize radical **64** and carbenium ion **65**.

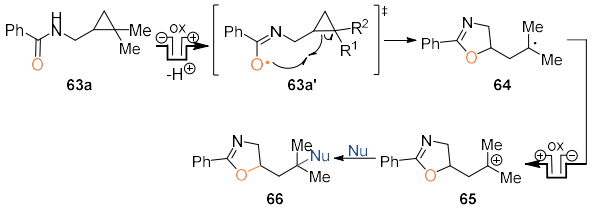

Scheme 21. Electrochemical oxidation of benzamide group, followed by intramolecular cyclopropane ring cleavage in compound **63a**.

The first attempts at electrochemical cyclopropane **63a** cleavage were carried out, using methanol as the reaction solvent and an external nucleophile (Scheme 22). We expected to obtain methyl ether **67**, but analysis of the reaction mixture revealed that three products were formed: methyl ether **67**, alkene **68**, and fluorine-containing compound **69a**. The formation of the fluorinated product suggested that the supporting electrolyte $TBABF_4$ could also serve as a source of fluorine.

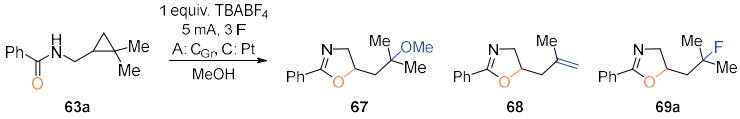

Scheme 22. Electrochemically induced cleavage of cyclopropane **63a** in methanol.

We believed that fluorine-containing products could be promising building blocks, so we focused on optimizing the synthesis method towards the selective introduction of a fluorine atom in the product.

Retaining dimethylcyclopropane **63a** as the model substrate, we first investigated which fluorine-containing reagents work best for product fluorination under electrolysis conditions. We examined several fluorine-containing supporting electrolytes, as well as nucleophilic and electrophilic fluorination reagents (Table 6). HFIP was used as the reaction solvent, while also serving as a proton source for the cathode reaction. Being a weak nucleophile, HFIP was unlikely to promote solvent addition to the carbenium ion intermediate **65** side reaction.

Substrate electrolysis was performed in an undivided cell under galvanostatic conditions. One equivalent of supporting electrolyte and two equivalents of other additives were used. In reactions where the fluorinating reagent in question was itself a poor electrolyte, we used $TBAClO_4$ as the supporting electrolyte. Identified side products were alkene **68**, alcohol **70**, and HFIP addition product **71.** After electrolysis, we determined the ratio of the products obtained using UPLC analysis; the product yields were not determined.

The highest selectivity towards fluorinated product **69a** formation was observed using $TBABF_4$ salt, while slightly lower selectivity was observed in the presence of $TBAPF_6$ (Table 6, rows 1–2). These salts are convenient fluorination reagents in electrochemical conditions, because they also serve as supporting electrolyte and don't corrode glass electrochemical cells. Using nucleophilic fluoride sources such as CsF, $TBAF \cdot 3H_2O$, and

TASF, we observed formation of a mixture of products (Table 6, rows 3–5). In the presence of electrophilic fluorination reagent NFSI, the major product was olefin **68** (Table 6, row 6).

Experimental results showed that $TBABF_4$ was the most suitable fluorination reagent for achieving selective formation of fluorinated product **69a** under electrolysis conditions.

Table 6

Products obtained by electrolysis of model substrate **63a** using different fluorine sources

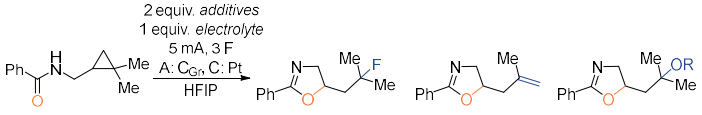

No.	Electrolyte	Additives	Product ratio[a]				
			69a, %	**68**, %	**70**, %	**71**, %	**63a**, %
1.	$TBABF_4$	--	> 95	< 2	< 2	0	0
2.	$TBAPF_6$	--	79	7	9	5	0
3.	$TBAClO_4$	CsF	8	40	6	20	26
4.		$TBAF{\cdot}3H_2O$	11	31	40	18	0
5.		TASF	41	34	5	19	0
6.		NFSI	5	65	0	30	0

[a] Determined by UPLC (UV absorption).

Next, we proceeded to optimize electrolysis conditions. Electrolysis of substrate **63a** was carried out in an undivided cell under galvanostatic conditions (Table 7). The yield of product **69a** was determined by ^{19}F-*q*NMR.

First, we studied the effect of $TBABF_4$ quantity on the product yield. Adding 1 equivalent of $TBABF_4$ led to a product **69a** yield of 69 % (Table 7, row 1). By increasing the amount of $TBABF_4$ to 3 equivalents, the yield of product **69a** increased to 82 % (Table 7, row 3). Using 5 equivalents of $TBABF_4$, the yield of the product was slightly improved to 84 % (Table 7, row 5), but we observed that the graphite anode was dissolving. When using a 2 : 1 mixture of $TBABF_4$ and $TBAClO_4$ salts, the yield of product **69a** decreased to 46 % (Table 7, row 6).

In the next series of experiments, we studied the effect of the electrode material on the reaction yield. When the graphite anode was replaced with a platinum anode, the product yield decreased to 53 % (Table 7, row 7). However, when the platinum cathode was replaced with a significantly cheaper graphite cathode, the reaction yield did not change significantly (Table 7, row 8).

Although, according to the mechanism shown in Scheme 21, a charge of 2 F is required for the transformation of substrate **63a** into product **69a**, we found that under electrolysis conditions, a charge of 3 F is required for complete substrate conversion (Table 7, rows 9–10).

HFIP was the only protic solvent in which compound **69a** was formed with a high yield, but a comparable yield could also be achieved using DCM with 20 equivalents of HFIP to supply reactant for the cathode reaction (Table 7, rows 11–13).

Without applying current, the formation of product **69a** was not observed (Table 7, row 14).

Reaction optimization studies revealed that 3 equivalents of $TBABF_4$ are required for efficient product formation, with HFIP being the most suitable reaction solvent. The optimized electrochemical parameters were a current of 5 mA (current density $j = 4.2$ mA/cm^2), a charge of 3 F, a graphite anode and a platinum cathode.

Table 7

Optimization of reaction conditions for oxazoline **69a** formation

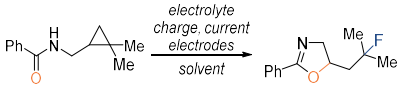

63a 69a

No.	Solvent	Electrolyte (equiv.)	Current, mA	Charge, F	A: C	69a[a]
1.	HFIP	$TBABF_4$ (1)	5	3	A: C_{Gr} C: Pt	69 %
2.		$TBABF_4$ (2)				79 %
3.		$TBABF_4$ (3)				82 %
4.		$TBABF_4$ (4)				82 %
5.		$TBABF_4$ (5)				84 %[b]
6.		$TBABF_4$ (2) $TBAClO_4$ (1)				46 %
7.		$TBABF_4$ (3)			A: Pt C: Pt	53 %
8.					A: C_{Gr} C: C_{Gr}	81 %
9.				2.0	A: C_{Gr} C: Pt	77 %
10.				2.5		79 %
11.	MeOH			3		11%
12.	DCM 20 equiv. HFIP					77 %
13.	MeCN 20 equiv. HFIP					20 %
14.	HFIP	$TBABF_4$ (3)	0	0	--	0 %

[a] Yield determined by ^{19}F-*q*NMR, internal standard 4,4'-difluorobenzophenone. [b] Anode damaged during electrolysis.

To explore the reaction substrate scope, we synthesized three substrate series – substrates **63a-f** with various substituents in the benzamide function, substrates **63h-m** in which cyclopropane was connected to another carbocycle to form spirocycles, and mono-

aryl substituted cyclopropanes **63o-t**. Compounds **63a-t** were subjected to electrolysis under optimized conditions (Scheme 23).

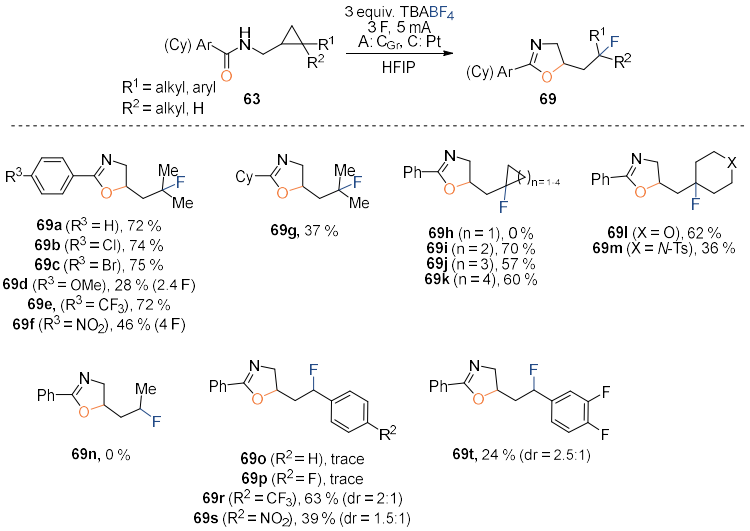

Scheme 23. 1,3-Oxyfluorinated products **69** obtained by electrolysis of cyclopropanes **63**.

In the first series of substrates **63a-f**, the effect of substituents in the benzene ring of the benzamide group was studied. Electrolysis of model substrate **63a** gave product **69a** with a 72 % yield. A similar yield was obtained in the electrolysis of halogen- and trifluoromethyl-substituted analogues **63b-c** and **63e** (products **69b-c, 69e)**. By introducing an electron-donating methoxy group in the benzene ring, a lower applied charge was required for the conversion of starting material **63d**, but the yield of product **69d** was significantly lower (28 %). A low yield was also observed in the electrolysis of substrate **63f** containing a nitro-phenyl group, where product **69f** was obtained with a yield of 46 %.

Replacing the benzamide function in the starting material with cyclohexanecarboxamide (substrate **63g**) gave product **69g**, but the yield (37 %) was significantly lower than that of the benzamide analogue.

The substrates in the second series were spirocyclic analogues **63h-m** and an analogue with monomethyl-substituted cyclopropane **63n**. In this series**,** fluorinated cyclobutane **69i,** cyclopentane **69j,** cyclohexane **69k,** tetrahydropyran **69l,** and piperidine **69m** were successfully obtained**.** Monofluorinated cyclopropane-containing product **69h** was not obtained. The corresponding fluorinated compound **69n** by electrolysis of monomethyl-substituted cyclopropane **63n** was also not obtained.

In the third substrate series, we explored electrochemical 1,3-oxyfluorination of mono-aryl substituted cyclopropanes **63o-t**. We observed that fluorinated products could only be obtained if the aryl group attached to cyclopropane contained electron-withdrawing substituents (substrates **63r-t**). This selectivity could be explained by the fact that the oxidation potential of unsubstituted aryl cyclopropane is lower than that of benzamide, so it

is oxidized first. The introduction of electron-withdrawing groups allows the oxidation selectivity to be controlled in favor of the benzamide group.

Interestingly, we did not observe the expected formation of oxazoline **73** in the electrolysis of tetra-methyl substituted cyclopropane **72**. Instead, dihydro-oxazine **74** was obtained as the main product (Scheme 24). The formation of product **74** indicates that in this case the tetra-methyl substituted *C*-*C* bond is cleaved during electrolysis.

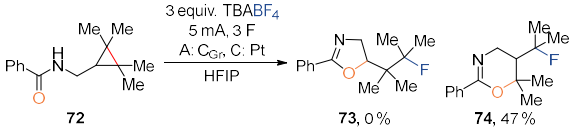

Scheme 24. Tetra-methyl substituted cyclopropane **72** electrolysis product dihydro-oxazine **74**.

For electrolysis of thioamide containing cyclopropane **75**, only 2.1 F of charge was required for full conversion of the starting material; however, the yield of the thiazoline product **76** was low – 19 % (Scheme 25). The observed by-products indicated that desulfurization of the starting material or intermediates occurs under the reaction conditions.

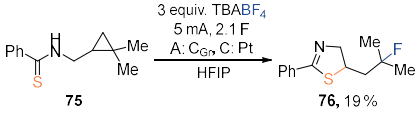

Scheme 25. Electrolysis of thioamide containing cyclopropane **75**.

To probe whether chirality transfer from the starting material to the product occurs during oxazoline ring formation, we chose an enantio-enriched 4-bromo-benzamide ***S*-63c** as the reaction substrate. By subjecting the enantiomerically pure cyclopropane ***S*-63c** (95 % ee) to electrolysis conditions, we obtained oxazoline ***S*-69c** (Scheme 26). Chiral HPLC analysis revealed that the product ***S*-69c** was obtained as a single enantiomer, indicating a complete chirality transfer.

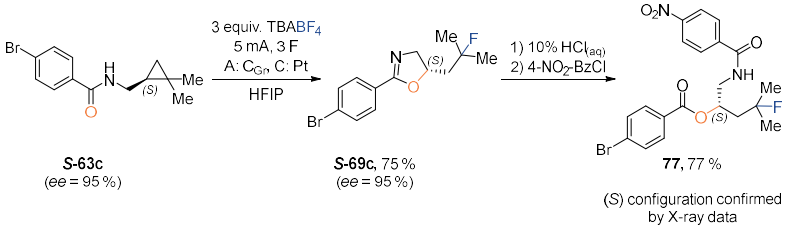

Scheme 26. Synthesis of enantio-enriched oxazoline ***S*-69c** and its derivatization to compound **77**.

The absolute configuration of product ***S*-69c** was determined by derivatizing it to compound **77**, which was subjected to X-ray structural analysis. This revealed, that the chiral center in product **77** had an *S*-configuration, indicating that configuration inversion occurs during the cleavage of the *C*-*C* bond (Fig. 7).

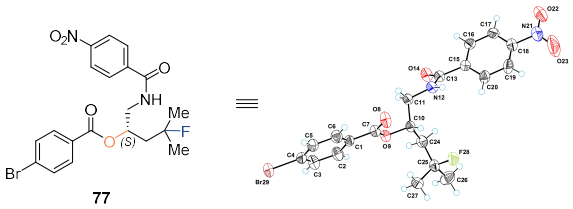

Fig. 7. ORTEP image of the X-ray structural analysis of compound **77** with a 50 % contour probability.

Based on these observations, we were able to propose a possible reaction mechanism (Scheme 27). In the first step, electrochemical oxidation of the benzamide group provides the amidyl radical **78'**. Next, the amidyl radical with its oxygen center attacks the cyclopropane *C*-*C* bond anti-bonding orbital, according to the intramolecular homolytic substitution mechanism (S_{Hi}). The *C*-*C* bond is cleaved, leading to *C*-centered radical **80**, which is further oxidized to carbenium ion **81.** In the last step, transfer of fluoride from the tetrafluoroborate anion gives the final product – monofluorinated oxazoline **82**.

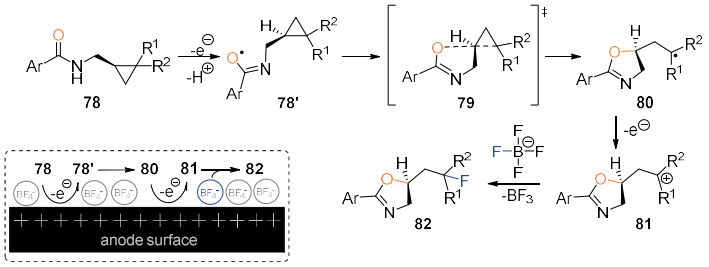

Scheme 27. Proposed mechanism of monofluorinated oxazoline **82** formation.

The reaction selectivity in favor of fluorination can be explained by considering the environment near the anode surface, where electron transfer takes place. Since the anode surface is positively charged, the liquid interface in its vicinity contains a layer of negatively charged ions, called the electric double layer. In our reaction, it is formed by tetrafluoroborate ions (Scheme 27). Such a high concentration of nucleophile near the site of carbenium ion generation could promote the fluorine transfer process.

Analyzing the ^{11}B-NMR spectrum of the reaction mixture, we observed that a new boron containing compound was formed during electrolysis. This suggests that the boron trifluoride released during the reaction is scavenged by HFIP (Scheme 28). Without the application of electric current, fluorine to HFIP exchange occurs only at trace level.

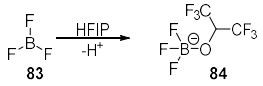

Scheme 28. Binding of released boron trifluoride **83** in a borate complex **84** with HFIP.

The results obtained in this chapter are summarized in the publication "*Electrochemical Formation of Oxazolines by 1,3-Oxyfluorination of Non-activated Cyclopropanes*".

CONCLUSIONS

1. Furfurylated ethylene glycol and furfurylated amino alcohol derivatives **7** can be transformed into *α,β*-unsaturated esters **9** in a two-step single-reactor electrochemical synthesis, using HFIP as an additive in the first step and AcOH in the second step. As a result, a new electrochemical *C-O* bond formation method was developed, which allowed to obtain functionalized *Torii-type* esters.

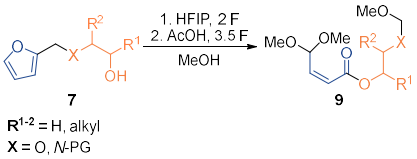

2. Electrochemically obtained *α,β*-unsaturated ester **9a** can be used as a reactive diluent in copolymerization with acrylated rapeseed oil to obtain a bio-based polymer.

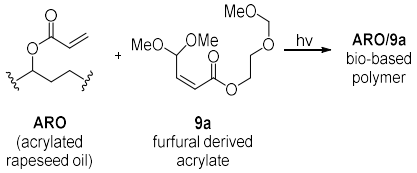

3. *N*-Alloc-protected *α,β*-unsaturated ester **9i** can be obtained by continuous electrolysis of furfural and valinol conjugate **7i** in methanol, using AcOH as the sole reaction additive. This method allows to obtain a chiral biomass-derived building block.

4. Enantio-enriched *N*-Alloc-protected *α,β*-unsaturated ester **9i** can be transformed into enantio-enriched vinyl oxazoline **23** in two steps. The *N*-Alloc cleavage also induces the cleavage of the methoxymethyl group, *O*- to *N*- rearrangement, and partial or full isomerization of the double bond. As a result, a chiral vinyl oxazoline building block is obtained.

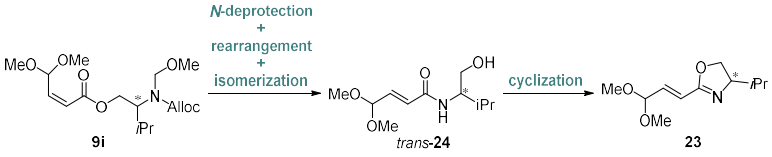

5. Aza–Diels–Alder reaction of the vinyl oxazoline derivative ***S*-23** and tosyl isocyanate, diastereoselectively furnishes the oxazolo[3,2-*c*]pyrimidine derivative **26**.

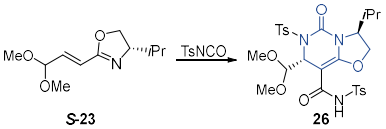

6. Electrolysis of 3-(2-furyl)propionic acid arylamide **47** in the presence of a substoichiometric amount of base induces a *C*-*N* bond formation between amide and the C2 carbon of furan to give spirocicle **49.** This method allows a rapid construction of [4.4]-spiro hemiaminal ether scaffold, which can be found in several natural products.

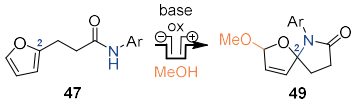

7. Anodically generated amidyl radicals **63'** intramolecularly cleave the *C*-*C* bond in non-activated cyclopropanes, forming oxazolines **69**. In this reaction, $TBABF_4$ serves as a fluorine transfer reagent. As a result, new *C*-*O* and *C*-*F* bonds are formed, resulting in the formation of cyclopropane 1,3-oxyfluorination products.

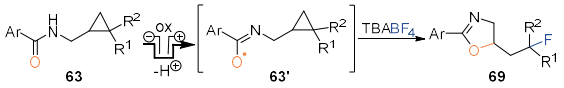

8. Electrochemically induced cleavage of chiral cyclopropane ***S*-63c** results in complete transfer of chirality to the product with configuration inversion, resulting in the formation of enantio-enriched oxazoline ***S*-69c**. Stereochemical studies suggest an intramolecular homolytic substitution mechanism (S_Hi).

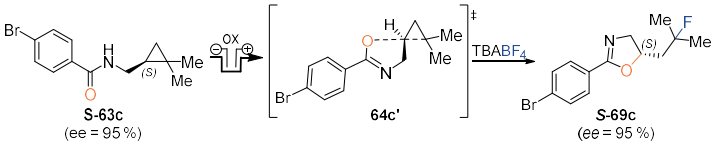

LITERATŪRAS SARAKSTS/ REFERENCES

1. Kingston, C.; Palkowitz, M. P.; Takahira, Y.; Vantourout, J. C.; Peters, B. K.; Yu Kawamata, Y.; Baran, P. S. A Survival Guide for the "Electro-curious". *Acc. Chem. Res.* **2020,** *53*, 72–83. https://doi.org/10.1021/acs.accounts.9b00539.
2. Wiebe, A.; Gieshoff, T.; Möhle, S.; Rodrigo, E.; Zirbes, M.; Waldvogel, S. R. Electrifying Organic Synthesis. *Angew. Chem. Int. Ed.* **2018**, *57*, 5594. https://doi.org/10.1002/anie.201711060.
3. Yan, M.; Kawamata, Y.; Baran, P. S. Synthetic Organic Electrochemistry: Calling All Engineers. *Angew. Chem. Int. Ed*. **2018**, *57*, 4149. https://doi.org/10.1002/anie.201707584.
4. Scopus datubāze/database. https://www.scopus.com/term/analyzer.uri?sort=plf-f&src=s&sid=48db715f0ba16fb8e044737c59d6e2b1&sot=a&sdt=a&sl=59&s=KEY%28electrosynthesis%29+AND+PUBYEAR+%3e+2013+AND+PUBYEAR+%3c+2025&origin=resultslist&count=10&analyzeResults=Analyze+results (lapa skatīta/site visited on 21.01.2025.) Izmantotais atslēgvārds: electrosynthesis; salīdzināti 2014. un 2024. gada dati. /Keyword: electrosynthesis; compared results from 2014 and 2024.
5. Schotten, C.; Nicholls, T. P.; Bourne, R. A.; Kapur, N.; Nguyen, B. N.; Willans, C. E. Making electrochemistry easily accessible to the synthetic chemist. *Green Chem.*, **2020**, *22*, 3358–3375. https://doi.org/10.1039/D0GC01247E.
6. Wang, Y.; Li, M.; Wang, Z.; Liu, S.; O'Young, L. Furfural production: A review on reaction mechanism and conventional production process. *Ind. Crops Prod*. **2025**, *230*, 121103. https://doi.org/10.1016/j.indcrop.2025.121103.
7. Bao, Y.; Du, Z.; Liu, X.; Liu, H.; Tang, J.; Qin, C.; Liang, C.; Huang, C.; Yao, S. Furfural production from lignocellulosic biomass: one-step and two-step strategies and techno-economic evaluation. *Green Chem.*, **2024**, *26*, 6318–6338. https://doi.org/10.1039/D4GC00883A.
8. Peng, P.; Yan, X.; Zhang, K.; Liu, Z.; Zeng, L.; Chen, Y.; Zhang, H.; Lei, A. Electrochemical C−C Bond Cleavage of Cyclopropanes Towards the Synthesis of 1,3-Difunctionalized Molecules. *Nat. Commun*. **2021**, *12*, 3075. https://doi.org/10.1038/s41467-021-23401-8.
9. Shipman, M. A.; Sproules, S.; Wilson, C.; Symes, M. D. Towards a better understanding of the electrosynthesis of 2,5-dicarboxy-2,5-dihydrofurans: structure, mechanism and influence over stereochemistry. *Soc. Open Sci*. **2019**, *6*, 190336. https://doi.org/10.1098/rsos.190336.
10. Roth, H. G.; Romero, N. A.; Nicewicz, D. A. Experimental and Calculated Electrochemical Potentials of Common Organic Molecules for Applications to Single-Electron Redox Chemistry. *Synlett*. **2016**, *27*, 714–723. https://doi.org/10.1055/s-0035-1561297.
11. Elliott, M. C.; Kruiswijk, E. Asymmetric hetero-Diels–Alder reactions of alkenyldihydrooxazoles. Synthesis of oxazolo[3,2-c]pyrimidines and related compounds. *J. Chem. Soc., Perkin Trans*. **1999**, *1*, 3157–3166. https://doi.org/10.1039/A905700E.

12. Zhang, Z.; Nian, Y.; Zhu, Q.; Li, X.; Su, J.; Wu, X.; Yang, J.; Zhao, Q. Lycoplanine A, a C16N Lycopodium Alkaloid with a 6/9/5 Tricyclic Skeleton from Lycopodium complanatum. *Org. Lett*. **2017**, *19*, 4668–4671. https://doi.org/10.1021/acs.orglett.7b02293.
13. Yixizhuoma, N. I.; Abdelfattah, M. S.; Ishibashi, M. Elmenols C-H, new angucycline derivatives isolated from a culture of Streptomyces sp. IFM 11490. *J. vv*. **2017**, *70*, 601–606. https://doi.org/10.1038/ja.2016.158.
14. Li, X.; Huang, M.; Lo, K.; Chen, W.; He, Y.; Xu, Y.; Zheng, H.; Hu, H.; Wang, J. Anti-Diabetic Effect of a Shihunine-Rich Extract of Dendrobium loddigesii on 3T3-L1 Cells and db/db Mice by Up-Regulating AMPK–GLUT4–PPARα. *Molecules.* **2019**, *24*, 2673. https://doi.org/10.3390/molecules24142673.
15. Zhu, L.; Xiong, P.; Mao, Z.; Wang, Y.; Yan, X.; Lu, X.; Xu, H. Electrocatalytic Generation of Amidyl Radicals for Olefin Hydroamidation: Use of Solvent Effects to Enable Anilide Oxidation. *Angew. Chem. Int. Ed*. **2016**, *55*, 2226–2229. https://doi.org/10.1002/anie.201510418.

PIELIKUMI

APPENDICES

Darzina, M.; Lielpetere, A.; Jirgensons, A.

Torii-type electrosynthesis of *α,β*-unsaturated esters from furfurylated ethylene glycols and amino alcohols.

Eur. J. Org. Chem. **2021**, 4224–4228.

https://doi.org/10.1002/ejoc.202100605

The Supporting Information is available free of charge on the Wiley website:

https://doi.org/10.1002/ejoc.202100605

EurJOC
European Journal of Organic Chemistry

Full Papers
doi.org/10.1002/ejoc.202100605

Chemistry Europe
European Chemical Societies Publishing

Torii-Type Electrosynthesis of α,β-Unsaturated Esters from Furfurylated Ethylene Glycols and Amino Alcohols

Madara Darzina,[a] Anna Lielpetere,[a] and Aigars Jirgensons*[a]

Electrosynthesis of unsaturated esters from furan derivatives, reported by Torii et al. in 1976, is an attractive method for the valorization of furanoic platform chemicals. Nevertheless, it has received practically no attention, presumably due to specific reaction conditions including the use of expensive Pt electrodes. With the aim of expanding the application of Torii-type ester electrosynthesis, we explored the electrochemical transformation of *O*-furfuryl ethylene glycols and N-furfuryl amino alcohols to esters **5**. These can be obtained in two consecutive electrochemical steps: bis-alkoxylation of the furan derived substrates **3** to give spirocycles **4**, followed by ring-opening involving oxidative fragmentation of the C–C bond. Both steps can be carried out at ambient conditions, using inexpensive graphite electrodes; however, each step required a different supporting electrolyte and acidic additive to achieve good yields of the product. Additionally, conditions were found for efficient one-pot transformation of N-furfuryl amino alcohols to esters **5** while O-furfuryl ethylene glycols under the same conditions gave esters **5** in moderate yields.

Introduction

The utilization of biomass has received increasing attention as an alternative to replace the dwindling fossil resources for the production of value-added products.[1] Biomass-derived platform chemicals are central to this initiative. Among them, furanoics, accessible in bulk amounts from lignocellulosic feedstocks, are versatile starting materials to achieve a range of chemicals with an application in material science, drug discovery, and agriculture.[2] Electrochemistry has been demonstrated as a useful tool for valorization of biomass-derived compounds.[3] Furanoics are particularly suitable substrates for electrochemical functionalization due to the low oxidation potential of the furan ring[4] (see also Supporting Information). Notable examples include oxidative dihydroxylation[5] and dialkoxylation[6] of furan derivatives. Anodic oxidative dialkoxylation was also employed in electrochemical synthesis of unsaturated ester **2** from furfuryl alcohol **1a**, furfural **1b**, and 2-furoic acid **1c** in the presence of methanol, first demonstrated by Torii *et al* (Figure 1).[7] According to their proposed mechanism, oxidative dimethoxylation of the furan ring leads to intermediate **A**. Further oxidation leads to cleavage of the *C–C* bond resulting in oxonium ion **B** and subsequent ring opening by methanol gives ester **2**. Despite the high potential value of the Torii ester electrosynthesis products, surprisingly limited application of this transformation has been demonstrated in the scientific literature.[8] Our work was focused on the electrochemical oxidation of furylmethyl derivatives **3** bearing hydroxyl group as an internal nucleophile (Figure 1). In this case, oxidative methoxylation should provide spirocyclic derivatives **4** which would undergo fragmentation to give products **5** with functionalized ester moiety. These products are valuable building blocks for further chemical transformations, including tailored polymer synthesis.

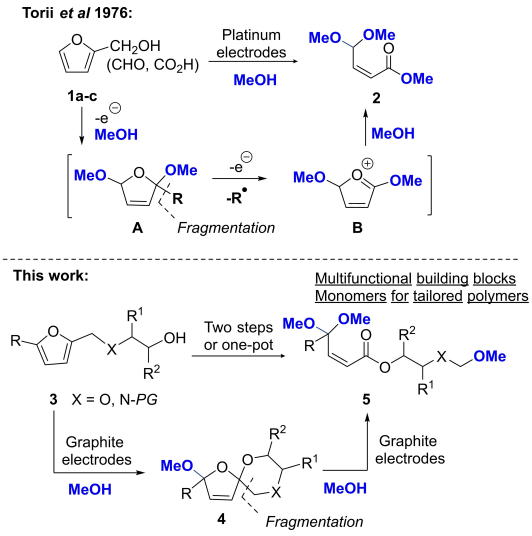

Figure 1. Torii-type electrosynthesis of unsaturated esters.

Results and Discussion

O-Furfuryl ethylene glycol (**3a**) was used as the model substrate to find efficient conditions for the spirocycle (**4a**) formation by

[a] *M. Darzina, A. Lielpetere, Prof. Dr. A. Jirgensons*
Latvian Institute of Organic Synthesis
Aizkraukles 21, Riga, LV-1006, Latvia
E-mail: aigars@osi.lv
https://osmg.osi.lv/

Supporting information for this article is available on the WWW under https://doi.org/10.1002/ejoc.202100605

electrochemical oxidation of the furan ring (Table 1). The reaction previously has been described using one-pot two-step transformation which includes electrochemical bromination of furan using NH_4Br and a carbon anode/nickel cathode, followed by addition of sodium methoxide.[9] Given the low oxidation potential of furan, we explored direct spirocycle formation[6a] with a simple electrochemical setup using undivided cell and graphite electrodes. Methanol was used as a solvent and proton reduction as the cathode reaction. We found that the addition of PPTS (1 equiv.) was beneficial to achieve a good yield of the product **4a** (Table 1, entry 1). Decreasing or increasing the amount of PPTS led to a reduced yield of the product **4a** (Table 1, entries 2–4). It can be hypothesized that the addition of PPTS prevents formation of methoxide as the reduction product of methanol which may decrease the dimethoxylation of furane favoring formation of spirocycle **4a**.[6a] A slight increase of the total charge passed through the solution (measured in faradays per mole of substrate (F/mol)) led to a slightly higher yield (Table 1, entry 5), while significant increase of the charge was detrimental to the product **4a** formation (Table 1, entry 6). $LiClO_4$ as an electrolyte was less efficient compared to $TBABF_4$ (Table 1, entry 7). If HFIP was used as an additive instead of PPTS, a relatively good yield of product **4a** was observed at increased charge. However, in this case, a significant amount of ester **5a** formed as a by-product (Table 1, entry 8). If HFIP was used as an additive and $LiClO_4$ as an electrolyte, poor yield of spirocycle **4a** was obtained due to competing dimethoxylation of the furane (Table 1, entry 9). Optimal conditions were suitable also for the oxidation of alcohol **3a** to spirocycle **4a** in 0.5 g scale (Table 1, entry 10).

Table 1. Oxidative cyclization of alcohol **3a** to spirocycle **4a**.

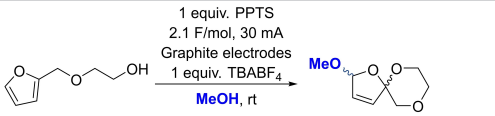

3a (0.7 mmol) **4a** (mix of diastereomers ~1:1)

Entry	Conditions[a]	Yield of **4a**[b]
1	none	70%
2	no PPTS	50%
3	0.5 equiv. PPTS	58%
4	2.0 equiv. PPTS	55%[c]
5	2.5 F/mol	77%
6	4.0 F/mol	59%
7	$LiClO_4$ instead of $TBABF_4$	59%
8	no PPTS, 20 equiv. HFIP, 4 F/mol	52%[d]
9	no PPTS, 20 equiv. HFIP, $LiClO_4$ instead of $TBABF_4$,	38%[e]
10	45 mA, 500 mg scale	71%

[a] Deviation from the conditions given in the scheme. [b] Isolated yields are given; [c] Precipitate deposition on cathode observed; [d] Formation of **5a** was observed, isolated yield 15%. [e] dimethoxylation product of furane is a major by-product according to ^{1}H-NMR of a crude mixture

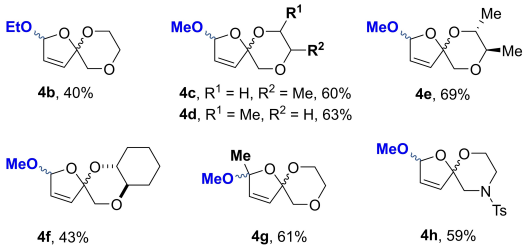

4b, 40%

4c, R^1 = H, R^2 = Me, 60%
4d, R^1 = Me, R^2 = H, 63%

4e, 69%

4f, 43%

4g, 61%

4h, 59%

Scheme 1. Scope of spirocycle **4** synthesis.

The scope for spirocycle **4b–h** synthesis was investigated for a wider range of ethylene glycol and amino ethanol derivatives **3a–h** bearing furfuryl substituent (Scheme 1). Ethanol was also found to be a competent nucleophile to form ethoxy-substituted product **4b**, although in a lower yield than **4a** formed with methanol as nucleophile. Moreover, electrolysis in ethanol led to precipitate formation on the cathode. Substitution at ethylene glycol linker in starting materials **3c–f** gave products **4c–f** with good yields. Methyl substitution at furan 5th position in the starting material did not significantly affect the yield of the product **4g**. *N*-substituted amino ethanol derivative **3h** was also subjected to electrochemical cyclization to give spirocycle **4h** in good yield.

With spirocycles **4** in hand, their electroxidative fragmentation was investigated with an aim to obtain esters **5**. Spirocycle **4a** was used as a model compound to establish the conditions for this step (Table 2). PPTS as an additive and $TBABF_4$ as an electrolyte used for spirocycle **4a** formation were not suitable for obtaining ester **5a** due to precipitation of the PPTS decomposition products on the cathode during prolonged electrolysis (Table 2, Entry 1).

When acetic acid and HFIP were used as additives, the yield of product **5a** was considerably increased, however, the formation of an inseparable side-product along ester **5a** was observed (Table 2, entry 2). To obtain ester **5a** in a good yield, AcOH (4 equiv.) as an additive and $LiClO_4$ as electrolyte were

Table 2. Conditions for the oxidative fragmentation of spirocycle **4a**.

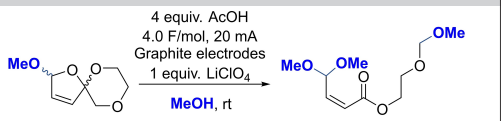

4a (0.6 mmol) **5a**

Entry	Conditions[a]	Yield of **5a**[b]
1	1 equiv. PPTS instead of AcOH $TBABF_4$ instead of $LiClO_4$	9%[c]
2	Add 20 equiv. HFIP $TBABF_4$ instead of $LiClO_4$	58%[d]
3	None	68% (77%)[e]
4	no AcOH	11%
5	1 equiv. AcOH	58%
6	2 equiv. AcOH	55%
7	add. 20 equiv. HFIP	67%
8	2.0 F/mol	(59%)[e,f]
9	3.0 F/mol	(74%)[e,g]

[a] Deviation from the conditions given in the scheme. [b] Isolated yields are given if not indicated otherwise. [c] Unreacted starting material (isolated yield: 55%). [d] Contains unidentified inseparable by-product ~15% [e] ^{1}H-NMR-yield using 1,4-bis(trichloromethyl)benzene as an internal standard. [f] Unreacted starting material (^{1}H-NMR yield: 20%) [g] Unreacted starting material (^{1}H-NMR yield: 5%).

found to be crucial reaction components (Table 2, Entry 3). Decreasing the amount of AcOH reduced the yield of product **5a** (Table 2, Entries 4–6). Addition of HFIP did not have an impact on product **5a** formation (Table 2, Entry 7). Notably, 4.0 F/mol of charge were needed to achieve complete consumption of the starting material **4a** (Table 2, Entries 8,9). This indicated a parallel competitive oxidation process since in theory only 2.0 F/mol are needed for the desired transformation (*vide infra*). In all the experiments, the formation of ester **5a** with a Z-configuration double bond was observed while *E*-isomer formation was not detected. *Z*-Configuration of ester **5a** was confirmed by characteristic coupling constant of double bond protons (J = 11.8 Hz) and their cross peaks in NOESY spectra (see Supporting Information)

Spirocycles **4b–h** were subjected to electrochemical oxidative fragmentation to esters **5b–h** using the optimized conditions found for model substrate **4a** (Scheme 2). Ethoxy substituted spirocycle **4b** gave product **5b** in a slightly lower yield compared to the methoxy analogue **5a**. Noteworthy, mixed acetal **5b** formed exclusively, indicating that no transacetalyzation with methanol takes place during the reaction. Addition of HFIP to the reaction of substrate **4b** improved the yield of product **5b** – such an effect was not observed in the reaction of the model substrate **4a** (Table 2, entry 8). Substrates **4c–f** with a substituted ethylene linker gave the desired esters **5c–f** in good yields using standard conditions with no HFIP additive. Methyl substituted substrate **4g** also gave the expected product **5g**, however, it was difficult to separate from the unreacted starting material. In this case full conversion of spirocycle **4g** could not be achieved after 4.0 F/mol of charge passed. Morpholine derivative **4h** was efficiently transformed to the *O*-acylated *N*-protected amino alcohol **5h**.

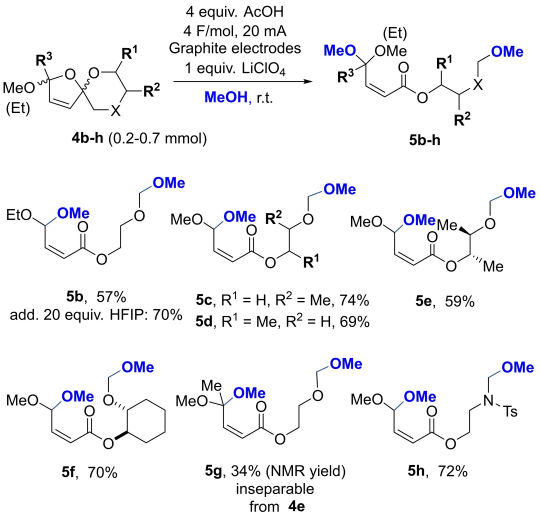

Scheme 2. Scope of oxidative fragmentation of spirocycles **4** to esters.

Diol **3i** derived from bis-hydroxymethylfuran was also successfully transformed into the spirocycle **4i** by anodic oxidation (Scheme 3). However, electrochemical oxidative fragmentation of the spirocycle **4i** gave the expected product **5i** in a relatively low yield (22%).

One-pot synthesis of esters **5** from alcohols **3** was also explored (Scheme 4). PPTS additive which was found beneficial for the transformation of substrates **3** to spirocycles **4** could not be applied for this purpose because the transformation of intermediates **4a** to ester **5a** was low yielding in the presence of this additive. Therefore, HFIP was used for the first step given the good conversion of substrate **3a** to the mixture of compounds **4a** and **5a** using this additive (Table 1, entry 8). After complete conversion of the starting material **3** at the first stage (equal to 2.2 F/mol of passed charge), acetic acid was added, and the electrolysis was continued for additional 4.0 F/mol of passed charge to obtain products **5**. This procedure led to moderate yields of esters **5a,c,d** from *O*-furfuryl ethylene glycols **3a,c,d**. Gratifyingly, this approach was more productive in the case of synthesis of esters **5h–m** containing protected amine functionality from *O*-furfuryl amino alcohols **3h–m**. It should be noted that ester **5k** synthesis was successfully performed on 0.9 g scale.

Mechanisms of electrochemical bis-alkoxylation of furan and (methoxy) anisole derivatives have been proposed previously depending on the reaction conditions.[6a,10] For the oxidative fragmentation of spirocycle **4a** to ester **5a** two possible pathways are provided in Scheme 5. Path A involves reversible S_N type methanolysis of the acetal in the dihydrofuran part of spirocycle **4a**, leading to intermediate **C**. Electrochemical oxidation of the hemi-acetal would give the *O*-centered radical **E** which fragments to α-oxy-stabilized *C*-centered radical **F**. Further oxidation of intermediate **F** would give oxonium ion **G** which reacts with methanol giving ester **5a**. The alternative path B starts with electrochemical activation of acetal group in spirocycle **4a** to give radical cation **D** after which the ring opens by methanolysis, leading to *O*-centered radical **E**. It cannot be excluded that methanolysis of activated acetal **D** and fragmentation occurs in a simultaneous fashion leading directly to intermediate **F.**

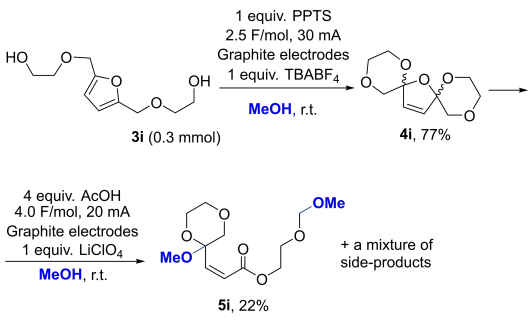

Scheme 3. Transformation of alcohol **3i** to spirocycle **4i** and its fragmentation to ester **5i**.

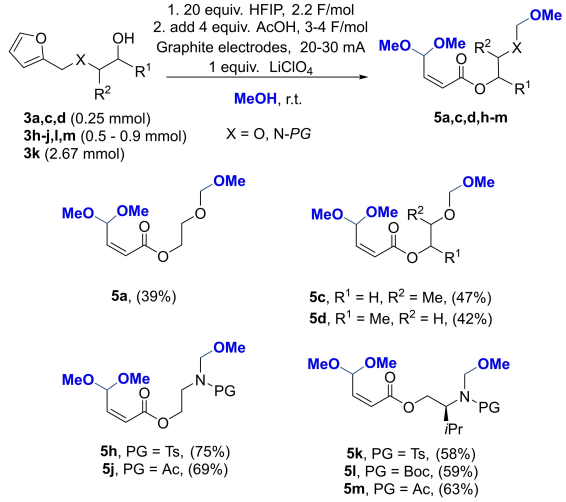

Scheme 4. One-pot synthesis of esters **5** from alcohols **3**.

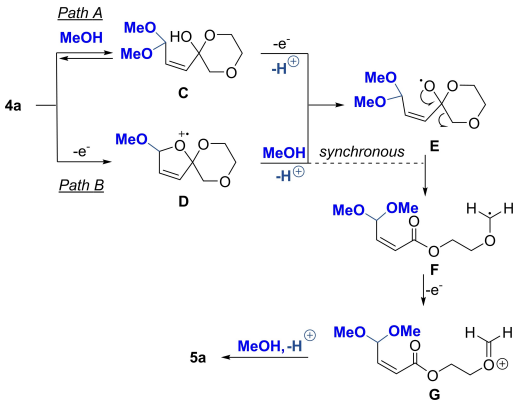

Scheme 5. Proposed mechanistic pathways for ester **5a** formation from spirocycle **4a**.

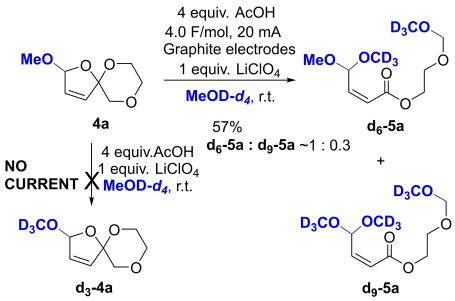

Scheme 6. Deuterium labelling experiments supporting path B of ester **5a** formation mechanism.

To establish if path A is operational, spirocycle **4a** was subjected to the reaction conditions with no current passing through the reaction mixture and using deuterated methanol as the reaction solvent (Scheme 6). In this case, no deuterium incorporation was observed by ^{1}H-NMR even after 24 hours. However, when the current was passed through the reaction mixture, incorporation of deuterated methanol took place, forming a mixture of the products ***d*$_6$-5a** and ***d*$_9$-5a** (ratio 1 : 0.3, detected by ^{1}H-NMR). These results clearly indicated the necessity of electrochemical activation for the methanolysis of spirocycle **4a** and supported path B of the product **5a** formation mechanism.

Conclusion

In summary, we have demonstrated an extended application of Torii-type ester electrosynthesis from biomass-derived furan conjugates with glycols and amino alcohols. The ester synthesis from furanoics can be done in two steps or by using one-pot protocol giving multifunctional building blocks and tailored monomers for polymerization. Notably, the reactions can be performed using undivided cell commercial electrochemical set-up using inexpensive graphite electrodes.

Demonstration of the application for the reaction products is planned as the next step of our research work.

Experimental Section

Optimized conditions for spirocycle formation: Substrate (1.0 equiv.), $TBABF_4$ (1.0 equiv.) and PPTS (1.0 equiv.) were transferred to an undivided cell (10 mL) and dissolved in freshly distilled MeOH (7 mL). Graphite electrodes were fitted to the cell and electrolysis was performed in constant current (30 mA) conditions until 2.5 F/mol of charge were passed through the cell. Afterwards the solvent was evaporated, and the product was purified using column chromatography.

Optimized conditions for α,β-unsaturated ester formation: Substrate (1.0 equiv.) and $LiClO_4$ (1.0 equiv.) were transferred to an undivided cell (10 mL) and dissolved in freshly distilled MeOH (7 mL). AcOH (4.0 equiv.) was added. Graphite electrodes were fitted to the cell and electrolysis was performed in constant current (20–30 mA) conditions until 4.0 F/mol of charge were passed through the cell. After electrolysis was done, TEA (4.0 equiv.) was added, and the reaction mixture was filtered through a silica plug. The solvent was evaporated, and product was purified using column chromatography.

Optimized conditions for one-pot transformation of alcohols to α,β-unsaturated esters: Substrate (1.0 equiv.) and $LiClO_4$ (1.0 equiv.) were transferred to an undivided cell (10 mL) and dissolved in freshly distilled MeOH (7 mL). HFIP (20.0 equiv.) was added. Graphite electrodes were fitted to the cell and electrolysis was performed using constant current (20–30 mA) conditions until 2.2 F/mol of charge were passed through the cell. Then AcOH (4.0 equiv.) was added, and electrolysis was continued for another 4.0 F/mol. After electrolysis was done, TEA (4.0 equiv.) was added, and the reaction mixture was filtered through a silica plug. The solvent was evaporated, and the product was purified using column chromatography.

Acknowledgements

We thank Dr. Dace Rasiņa and Dr. Janis Veliks for scientific discussion. The work was financially supported by LIOS student grants IG-2020-05 and IG-2021-03.

Conflict of Interest

The authors declare no conflict of interest.

Keywords: Anodic oxidation · Biomass · Electrochemistry · Furan · α,β-Unsaturated ester

[1] a) A. Corma Canos, S. Iborra, A. Velty, *Chem. Rev.* **2007**, *107*, 2411–2502; b) E. M. Karp, T. R. Eaton, V. Sànchez i Nogué, V. Vorotnikov, M. J. Biddy, E. C. D. Tan, D. G. Brandner, R. M. Cywar, R. Liu, L. P. Manker, W. E. Michener, M. Gilhespy, Z. Skoufa, M. J. Watson, O. S. Fruchey, D. R. Vardon, R. T. Gill, A. D. Bratis, G. T. Beckham, *Science* **2017**, *358*, 1307; c) H. Li, H. Guo, Z. Fang, T. M. Aida, R. L. Smith, *Green Chem.* **2020**, *22*, 582–611; d) W. Deng, Y. Wang, S. Zhang, K. M. Gupta, M. J. Hülsey, H. Asakura, L. Liu, Y. Han, E. M. Karp, G. T. Beckham, P. J. Dyson, J. Jiang, T. Tanaka, Y. Wang, N. Yan, *Proc. Natl. Acad. Sci. USA* **2018**, *115*, 5093; e) Y. Wang, S. Furukawa, S. Song, Q. He, H. Asakura, N. Yan, *Angew. Chem. Int. Ed.* **2020**, *59*, 2289–2293; *Angew. Chem.* **2020**, *132*, 2309–2313; f) J. He, L. Chen, S. Liu, K. Song, S. Yang, A. Riisager, *Green Chem.* **2020**, *22*, 6714–6747; g) A. Hommes, H. J. Heeres, J. Yue, *ChemCatChem* **2019**, *11*, 4671–4708; h) J. Iglesias, I. Martínez-Salazar, P. Maireles-Torres, D. Martin Alonso, R. Mariscal, M. López Granados, *Chem. Soc. Rev.* **2020**, *49*, 5704–5771; i) N. R. Babij, N. Choy, M. A. Cismesia, D. J. Couling, N. M. Hough, P. L. Johnson, J. Klosin, X. Li, Y. Lu, E. O. McCusker, K. G. Meyer, J. M. Renga, R. B. Rogers, K. E. Stockman, N. J. Webb, G. T. Whiteker, Y. Zhu, *Green Chem.* **2020**, *22*, 6047–6054; j) Z. Sun, K. Barta, *Chem. Commun.* **2018**, *54*, 7725–7745; k) X.-L. Li, K. Zhang, J.-L. Jiang, R. Zhu, W.-P. Wu, J. Deng, Y. Fu, *Green Chem.* **2018**, *20*, 362–368.

[2] a) Z. Zhang, G. W. Huber, *Chem. Soc. Rev.* **2018**, *47*, 1351–1390; b) V. M. Chernyshev, O. A. Kravchenko, V. P. Ananikov, *Russ. Chem. Rev.* **2017**, *86*, 357–387; c) B. R. Caes, R. E. Teixeira, K. G. Knapp, R. T. Raines, *ACS Sustainable Chem. Eng.* **2015**, *3*, 2591–2605; d) K. I. Galkin, V. P. Ananikov, *ChemSusChem* **2019**, *12*, 2976–2982; e) B. Y. Karlinskii, A. Y. Kostyukovich, F. A. Kucherov, K. I. Galkin, K. S. Kozlov, V. P. Ananikov, *ACS Catal.* **2020**, *10*, 11466–11480; f) J. M. J. M. Ravasco, C. M. Monteiro, F. Siopa, A. F. Trindade, J. Oble, G. Poli, S. P. Simeonov, C. A. M. Afonso, *ChemSusChem* **2019**, *12*, 4629–4635; g) X. Liu, Y. Li, J. Deng, Y. Fu, *Green Chem.* **2019**, *21*, 4532–4540; h) S. Song, V. Fung Kin Yuen, L. Di, Q. Sun, K. Zhou, N. Yan, *Angew. Chem. Int. Ed.* **2020**, *59*, 19846–19850; *Angew. Chem.* **2020**, *132*, 20018–20022; i) I. Scodeller, S. Mansouri, D. Morvan, E. Muller, K. de Oliveira Vigier, R. Wischert, F. Jérôme, *Angew. Chem. Int. Ed.* **2018**, *57*, 10510–10514; *Angew. Chem.* **2018**, *130*, 10670–10674; j) J.-P. Lange, S. H. Wadman, *ChemSusChem* **2020**, *13*, 5329–5337; k) K. A. Kuznetsov, G. Kumar, M. A. Ardagh, M. Tsapatsis, Q. Zhang, P. J. Dauenhauer, *ACS Sustainable Chem. Eng.* **2020**, *8*, 3273–3282; l) X. Li, P. Jia, T. Wang, *ACS Catal.* **2016**, *6*, 7621–7640; m) C. Pezzetta, L. F. Veiros, J. Oble, G. Poli, *Chem. Eur. J.* **2017**, *23*, 8385–8389; n) M. Li, X. Dong, N. Zhang, F. Jérôme, Y. Gu, *Green Chem.* **2019**, *21*, 4650–4655; o) S. P. Simeonov, M. A. Ravutsov, M. D. Mihovilovic, *ChemSusChem* **2019**, *12*, 2748–2754.

[3] a) S. Mohle, M. Zirbes, E. Rodrigo, T. Gieshoff, A. Wiebe, S. R. Waldvogel, *Angew. Chem. Int. Ed.* **2018**, *57*, 6018–6041; *Angew. Chem.* **2018**, *130*, 6124–6149; b) F. J. Holzhäuser, J. B. Mensah, R. Palkovits, *Green Chem.* **2020**, *22*, 286–301; c) J. Carneiro, E. Nikolla, *Annu. Rev. Chem. Biomol. Eng.* **2019**, *10*, 85–104; d) O. O. James, W. Sauter, U. Schroder, *ChemSusChem* **2017**, *10*, 2015–2022; e) M. Garedew, F. Lin, B. Song, T. M. DeWinter, J. E. Jackson, C. M. Saffron, C. H. Lam, P. T. Anastas, *ChemSusChem* **2020**, *13*, 4214–4237; f) F. W. S. Lucas, R. G. Grim, S. A. Tacey, C. A. Downes, J. Hasse, A. M. Roman, C. A. Farberow, J. A. Schaidle, A. Holewinski, *ACS Energy Lett.* **2021**, 1205–1270.

[4] D. Nicewicz, H. Roth, N. Romero, *Synlett* **2015**, *27*(05), 714–723.

[5] S. R. Kubota, K. S. Choi, *ACS Sustainable Chem. Eng.* **2018**, *6*, 9596–9600.

[6] a) L.-D. Syntrivanis, F. Javier del Campo, J. Robertson, *J. Flow Chem.* **2018**, *8*, 123–128; b) T. Sigeru, T. Hideo, A. Takuo, S. Yasuo, *Chem. Lett.* **1976**, *5*(5), 495–498; c) Y. matsumura, K. Shirai, T. Maki, Y. Itakura, Y. Kodera, *Tetrahedron Lett.* **1998**, *39*, 2339–2340; d) N. L. Weinberg, H. R. Weinberg, *Chem. Rev.* **1968**, *68*, 449–523; e) N. Clauson-Kaas, F. Limborg, K. Glens, E. Stenhagen, S. Östling, *Acta Chem. Scand.* **1952**, *6*, 531–534; f) T. Sigeru, T. Hideo, O. Tsutomu, *Bull. Chem. Soc. Jpn.* **1972**, *45*, 2783–2787.

[7] H. Tanaka, Y. Kobayasi, S. Torii, *J. Org. Chem.* **1976**, *41*, 3482–3484.

[8] a) T. Iwasaki, T. Nishitani, H. Horikawa, I. Inoue, *J. Org. Chem.* **1982**, *47*, 3799–3802; b) W. C. Still, H. Ohmizu, *J. Org. Chem.* **1981**, *46*, 5242–5244.

[9] A. A. Ponomarev, I. A. Markushina, N. V. Shulyakovskaya, *Khim. Geterotsikl. Soedin.* **1970**, *9*, 1155–1159.

[10] a) T. Sumi, T. Saitoh, K. Natsui, T. Yamamoto, M. Atobe, Y. Einaga, S. Nishiyama, *Angew. Chem. Int. Ed.* **2012**, *51*, 5443–5446; *Angew. Chem.* **2012**, *124*, 5539–5542; b) X. Barros-Álvarez, K. M. Kerchner, C. Y. Koh, S. Turley, E. Pardon, J. Steyaert, R. M. Ranade, J. R. Gillespie, Z. Zhang, C. L. M. J. Verlinde, E. Fan, F. S. Buckner, W. G. J. Hol, *Biochimie* **2017**, *138*, 124–136; c) M. A. Shipman, S. Sproules, C. Wilson, M. D. Symes, *R. Soc. Open Sci.* **2019**, *6*, 190336.

Manuscript received: May 18, 2021
Revised manuscript received: July 9, 2021

Briede, S.; Platnieks, O.; **Darzina, M**.; Jirgensons, A.; Gaidukovs, S.

Effect of novel furan-based ester reactive diluent on structure and properties of UV-crosslinked acrylated rapeseed oil.

J. Polym. Sci. **2023**, *61*, 3318–3328.

https://doi.org/10.1002/pol.20230451

The Supporting Information is available free of charge on the Wiley website:

https://doi.org/10.1002/pol.20230451

Received: 1 July 2023 | Revised: 9 September 2023 | Accepted: 18 September 2023

DOI: 10.1002/pol.20230451

RESEARCH ARTICLE

JOURNAL OF POLYMER SCIENCE WILEY

Effect of novel furan-based ester reactive diluent on structure and properties of UV-crosslinked acrylated rapeseed oil

Sabine Briede[1] | **Oskars Platnieks**[1] | **Madara Darzina**[2] | **Aigars Jirgensons**[2] | **Sergejs Gaidukovs**[1]

[1]Institute of Polymer Materials, Faculty of Materials Science and Applied Chemistry, Riga Technical University, Riga, Latvia

[2]Latvian Institute of Organic Synthesis, Riga, Latvia

Correspondence
Sergejs Gaidukovs, Institute of Polymer Materials, Faculty of Materials Science and Applied Chemistry, Riga Technical University, P. Valdena 3/7, Riga LV-1048, Latvia.
Email: sergejs.gaidukovs@rtu.lv

Funding information
European Social Fund, Grant/Award Number: 8.2.2.0/20/I/008; Latvian Institute of Organic Synthesis, Grant/Award Number: IG-2023-07; Latvijas Zinātnes Padome, Grant/Award Number: lzp-2022/1-0485; Rīgas Tehniskā Universitāte.Doctoral Grant Programme

Abstract

Unsaturated furan-based ester (UES) was prepared by green electrosynthesis using a single-cell setup and inexpensive graphite electrodes. The UES was validated as a reactive diluent for a bio-based acrylated rapeseed oil (ARO). UV-light photopolymerization of the bio-based resin was initiated using a diphenyl (2,4,6-trimethylbenzoyl)phosphine oxide (TPO) radical photoinitiator. The addition of 20 wt% UES to ARO dropped the resin viscosity by 1.6-fold. Incorporating 5 wt% UES into the ARO resin increased crosslinking density ν_e from 1.07 to 1.65 mol/m^3. Fourier-transform infrared spectroscopy (FT-IR) spectra revealed that ARO has been grafted with UES. The UES functional moieties promote the formation of soft mobile dangling chain end segments in the developed macromolecular network. UV-cured thermoset polymer reveals distinct morphologies in SEM micrographs, indicating notable structural changes with the addition of UES. A total of 5 wt% UES increased tensile strength from 0.49 to 0.55 MPa and storage modulus from 7.9 to 12.0 MPa at room temperature (22 ± 1 °C). The biodegradability in composting conditions was investigated, and up to 28% of the initial mass was lost after 60 days. UES was shown as to be efficient reactive diluent that can successfully replace fossil-based acrylate monomers in vegetable oil-based thermoset polymer synthesis.

KEYWORDS

bio-based, biodegradation, mechanical properties, Photopolymerization, vegetable oil

1 | INTRODUCTION

Unsaturated polyester (UPE) oligomers are used in photopolymerization because of their ability to cure upon UV irradiation.[1] UPEs can form a crosslinked network through intramolecular and intermolecular reactions. Often, monomers are combined with UPEs to increase the reactivity.[2] Styrene is the most common reactive diluent used in UPE systems to reduce viscosity, increase crosslink density, and reduce cost, but its use comes with known drawbacks, such as toxicity.[3] Nebioglu et al. synthesized UPE acrylates to evaluate the internal and terminal double bond position effects in UV-curable network formation.[4] The authors reported that the final conversion of the internal double bonds was not much lower than that of the terminal double bond. Thus, monomer structures are not limited by double bond location. With new sustainability goals set by European Union, the search for alternatives requires the integration of bio-based monomers.[5] For this purpose, we

explored bio-based monomers obtained from furan-based derivatives in a green manner via electrosynthesis as a possible reactive diluent for enhancement of UV-curable thermosets prepared from unsaturated polyester (UPE) oligomers.

White et al. reported a nonvolatile and "green" ionic liquid 4-vinylbenzyl trioctyl phosphonium bis(trifluoromethanesulfonyl)imide (VBTOP Tf_2N) as a reactive diluent for UPE oligomers containing internal double bonds from maleic acid anhydride.[6] In combination with dimethoxyethane as an unreactive diluent, they produced resins suitable for stereolithography, where 3D printed networks reached an ionic conductivity of 1×10^{-5} S cm^{-1} at 150 °C. Another grafting using maleate esters with an internal double bond was done by Esen et al.[7] First, epoxidized soybean oil was reacted with monomethyl maleate. Afterward, monomethyl maleate was treated with maleic anhydride, yielding a high unsaturation of 4.9 maleates per triglyceride. Finally, the synthesized maleates were copolymerized with styrene, vinyl acetate, and methyl methacrylate as reactive diluents. Superior properties were observed after treatment with maleic anhydride compared to monomethyl maleate due to the increased number of internal double bonds. As a result, the glass transition temperature increased from 55 °C to 90 °C for produced styrene copolymers. Bonneaud et al. observed only partial homopolymerization of synthesized maleate ester, whereas the copolymerization with oligo(hexafluoropropylene) vinyl ether was much faster.[8] The complete conversion was achieved in less than 40 s, and highly hydrophobic polymers were obtained. Wei et al. studied fumarates instead of maleates.[9] Fumarates have lower reactivity than acrylates and methacrylates, and their kinetics depend on the UV initiator, monomer molecule size, and monomer concentrations. The authors investigated electron density distribution and its influence on the copolymerization behavior of fumarate esters. The vinyl ester double bonds of divinyl fumarate are electron more affluent, and the fumarate double bonds are electron poorer compared to nonconjugated analogues; therefore, for example, thiol addition to the internal fumarate double bond of divinyl fumarate was much faster than that of diethyl fumarate. Thus, the polymerization rate of vinyl ester groups was faster than that of fumarate groups.

Recently, interest has grown in plant and vegetable oil-based UV-curable monomers with various unsaturated pendant moieties or groups synthesized and researched.[10,11] Yang et al. used the Diels-Alder process to synthesize tung oil monomer (TOA) with cyclic internal unsaturation moieties using acrylic acid.[12] The subsequent step involved a glycidylation reaction and ring-opening esterification producing a liquid monomer (TOA-GMA) with both internal and terminal unsaturation. Next, TOA-GMA was mixed with myrcene and modified with acrylic acid yielding the monomer (ADMM). High TOA-GMA content in a mixture with ADMM resulted in a strong preference for homopolymerization. In addition, TOA-GMA viscosity and branching were higher than ADMM, limiting the monomer from free movement. Despite low rates of copolymerization, the double bond conversion of copolymers was up to 95%. In another study, vegetable oil-derived dimer acid was combined with glycidyl methacrylate to create monoesters with a methacrylate group.[13] The distance between the two methacrylate groups was adjusted using a diepoxy extender. The final dimethacrylate was UV cross-linked for 10 s, reaching a double bond conversion of 82%. Meng et al. obtained castor oil-derived acrylate in a transesterification reaction with *N*-hydroxyethylacrylamide, which, after polymerization with acrylic acid, methyl methacrylic acid, and butyl acrylate, formed a multifunctional substituted polyacrylate.[14] The authors evaluated the material's performance as a wood coating with pencil hardness up to 3H, tensile strength up to 12.2 MPa and elongation up to 301.5%. Wei et al. reported castor oil-based hyperbranched acrylate (C20AA) synthesis.[15] The authors studied the potential of replacing polyurethane acrylate with bio-based C20AA and achieved the best results with 40 wt% of C20AA, which showed the highest double bond conversion of 83.7% after UV-curing. Chen et al. revealed an efficient photoredox catalytic method for radical-mediated functionalization of internal alkenes.[16] Four alkenes with internal double bonds were investigated in free-radical thiol-ene click reaction. The predicted order of reactivity of these internal alkenes was: norbornene > fumarate > maleimide > crotonate.[17]

Despite the growing research into environmentally friendly UV-curable materials, most commercial solutions rely on fossil-based monomers because of their high reactivity.[18] Our previous study showed the feasibility of the commercially available biobased components as a modifier for vegetable oil acrylate coatings.[19] In this study, we propose a novel biobased unsaturated furan-based ester (UES), which can successfully replace fossil-based reactive diluents like trimethylolpropane triacrylate (TMPTA),[20] broadly commercially available nowadays. Herein, furan-based unsaturated ester as a reactive diluent for vegetable oil acrylate is explored with 5 and 20 wt% loadings.

Vegetable oils have been used for the synthesis of polymer materials for decades. The current study focuses on the use of rapeseed oil as one of the most popular plant oils in Europe, consisting of more than 90% unsaturated acids.[21] Moreover, acrylated rapeseed oil (ARO) has

displayed much promise for developing new effective formulations used as resins for coatings, composites, foams, and 3D printing.[22–24] Herein, ARO has been grafted with UES through a UV-light-initiated photopolymerization crosslinking approach. UV curing was chosen due to its sustainability, versatility, and significant energy-saving aspects. The current research is focused on the reactivity and compatibility investigation of the lab-synthesized bio-based monomers, obtained resin properties, and light-cured thermoset biopolymer structural performance.

2 | EXPERIMENTAL SECTION

2.1 | Materials

Unrefined rapeseed oil was purchased from a local producer, "Iecavnieks" (Latvia). Acrylic acid, $BF_3{\cdot}Et_2O$, hexane, $NaHCO_3$, Na_2SO_4, acetone, and photoinitiator diphenyl(2,4,6-trimethylbenzoyl) phosphine oxide (TPO) were supplied by Sigma Aldrich. $LiClO_4$, MeOH, AcOH, and triethylamine (TEA) were supplied by Acros and Sigma-Aldrich. All chemicals were used as received unless otherwise stated.

2.2 | Synthesis of photoactive components

As described in our previous work, the furan-based unsaturated ester (UES) monomer was obtained in two electrochemical steps from furfurylated ethylene glycol X (Figure 1A).[25] First, it was electrochemically transformed to a spirocycle, which was then subjected to electrochemically induced rearrangement to form UES. Electrolysis was performed using the commercially available potentiostat Electrasyn 2.0.

The procedure is as follows: In the first electrolysis, furfurylated ethylene glycol, the supporting electrolyte $TBABF_4$, and the additive PPTS were transferred to an undivided cell, and dissolved in dry MeOH. Graphite electrodes were fitted to the cell and electrolysis was performed in constant current conditions until 2.3 F/mol of charge was passed through the cell. Afterward, the solvent was evaporated, and the product was purified using column chromatography (74% yield). During the second electrolysis, the spirocycle and supporting electrolyte $LiClO_4$ were transferred to an undivided electrochemical cell and dissolved in distilled MeOH. Then the additive AcOH was added. Graphite electrodes were fitted to the cell, and electrolysis was performed under constant current conditions. A total of 4.0 F/mol of charge was passed through the cell until all the starting material was consumed. After electrolysis, TEA was added, and the reaction mixture was filtered through a silica plug. The solvent was evaporated, and the product UES was purified using column chromatography (63% yield). The formation of UES with a *Z*-configuration double bond was observed, while *E*-isomer formation was not detected. The full synthesis procedure starting with furfuryl alcohol is available in supplementary file.

The acrylation reaction of rapeseed oil is shown in Figure 1B. Rapeseed oil, acrylic acid, and $BF_3{\cdot}Et_2O$ as catalyst were mixed in a round-bottom flask and stirred for 5 h at 80 °C before being left overnight at room

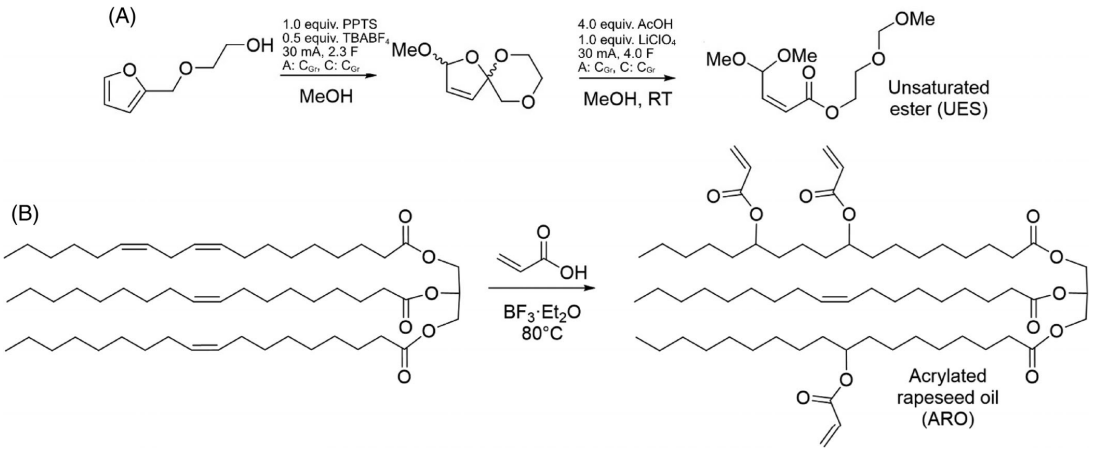

FIGURE 1 Synthesis of used materials (A) Unsaturated furan-based ester (UES) and (B) acrylated rapeseed oil (ARO).

temperature (22 ± 1 °C). In the work-up, the organic phase was dissolved in hexane, washed with a $NaHCO_3$ solution, dried over Na_2SO_4, and filtered. The solvent was removed via a rotary evaporator to obtain liquid acrylated rapeseed oil (ARO).

2.3 | Resin preparation

The UV-curable resins were prepared by mixing liquid ARO resin with 5 and 20 wt% liquid UES (approximately 1 mol ARO double bond equivalent was mixed with 0.1 and 0.4 mol UES double bond equivalent). Next, 3 wt% TPO dissolved in a small amount of acetone was added to each resin, mixed, and left overnight under the hood to allow the acetone to evaporate, yielding compositions ARO/UES5 and ARO/UES20, respectively.

2.4 | UV-curing and sample film preparation

Liquid resins were applied on a glass substrate using an applicator with a wet film thickness of 20 mils (508 μm). Then samples were cured under monochromatic conditions ($\lambda = 405$ nm) at a UV intensity of 400 μW cm^{-2} at a distance of 3 cm. The curing time was set to 70 s. After treating the samples' surfaces with acetone to remove the unreacted resins, they were peeled off and free-standing polymer films were obtained.

2.5 | Characterization

2.5.1 | Viscosity

The viscosity of liquid resins was measured on an Anton Paar MCR102 rheometer (Graz, Austria). The instrument was equipped with a 25 mm diameter spindle with plate-plate geometry. The measurement gap was set to 0.1 mm, and the shear rate range was set from 0.01 1 to 1000 s^{-1}.

2.5.2 | Fourier-transform infrared spectroscopy

Fourier-transform infrared spectroscopy (FT-IR) performed in attenuated total reflectance mode was used for the investigation. FT-IR Nicolet 6700 (ThermoScientific, Germany) was used to analyze the prepared samples. With 16 measurements, of which the average spectrum is displayed, a measurement error of 1% was achieved.

2.5.3 | UV–Vis spectroscopy

UV–Vis spectra of UV-cured samples were measured on a Shimadzu SolidSpec3700 UV–VIS–NIR spectrophotometer (Kyoto, Japan) with a 60 mm diameter integration sphere and a wavelength precision of 0.5 nm in the wavelength range of 300–700 nm. Tests were performed on UV-cured samples with a width of 250 μm in transmittance mode.

2.5.4 | Tensile tests

Tensile tests were performed on cured free-standing films to study the tensile behavior. Elongation at break, tensile strength, and tensile modulus were recorded on Tinius Olsen model 25ST (Horsham, PA, USA). All tensile tests were conducted at room temperature (22 ± 1 °C) at a 1 mm min^{-1} strain rate and repeated thrice. The average results are reported. Before measurements, samples were preconditioned for 24 h at room temperature with a RH of 40%.

2.5.5 | Scanning electron microscopy

A field emission scanning electron microscope (FE-SEM) Nova NanoSEM 650 (the Netherlands) was used to characterize the cross-sectional morphology of the cured samples. The samples were submerged in liquid nitrogen, cooled for about 60 s, removed from liquid nitrogen, and fractured with a light stroke of a hammer. Images were taken of the fractured cross-sections of the films. The samples were attached to standard 45°/90° angled aluminium pin stubs with electrically conductive double-sided carbon tape. The image was acquired with a 10 kV electron acceleration voltage in low vacuum conditions.

2.5.6 | Dynamic mechanical analysis

The cured free-standing films' storage modulus, loss modulus, and loss factor (tanδ) were recorded using a dynamic mechanical analyzer Mettler DMA/SDTA861e (Mettler Toledo, Columbus, OH, USA). The experiment was carried out in tension mode from −70 °C to 100 °C with a 3 °C min^{-1} heating rate, the applied force of 10 N and 10 μm elongation, and a frequency of 1 Hz. The photopolymerized films were prepared with dimensions of 8.5 mm (length) × 4 mm (width) × 0.2 mm (thickness).

2.5.7 | Thermogravimetric analysis

The thermal properties of cured samples were obtained using a thermogravimetric analyzer Mettler TG50 (Mettler Toledo, USA). About 10 mg of each cured sample was heated from 25 °C to 750 °C at a heating rate of 10 °C min^{-1} under an inert (N_2) atmosphere.

2.5.8 | Biodegradation

To measure the density (d) Sartorius KB BA 100 electronic scales with a Sartorius YDK 01 hydrostatic density measuring kit were set up. The following equation was used to determine the composite densities:

$$d = \frac{m_a(d_{EtOH} - d_{air})}{d_{water}(m_a - m_s)} + d_{air},$$

where m_a is the sample's measured mass in the air; m_s is the sample's measured mass when the sample is submerged in ethanol; d_{EtOH} is the density of ethanol (0.805 g/cm^3), which was measured with the aerometer; d_{air} is the density of the air (0.00120 g/cm^3), and d_{water} is the density of the water (0.99983 g/cm^3). For measurements, 10 replicates of each sample were utilized.

Soil burial tests evaluated the biodegradation of films. The weight loss of the films was studied under aerobic simulated composting conditions at 58 °C, soil humidity above 50% and a pH range between 5.7 and 6.5. Thin films were cut into rectangular shapes (10 mm × 10 mm × 0.1 mm) and sandwiched between sieves. Specimens were submerged in a commercial compost soil of local Latvian swamp peat (Formoss, Latvia) and packed in plastic containers. Recovered samples were cleaned with a brush and washed with distilled water. Before the measurements, specimens were vacuum dried for 4–6 h at 37 °C. The specimen's weight was measured before the test (reference abbreviated as 0 days) and on days 30, 40, 50, and 60. The remaining mass in percentage was calculated after measurements.

3 | RESULTS AND DISCUSSION

3.1 | Chemical structure, reaction analysis, and physical properties

The radical photopolymerization crosslinking between ARO and UES is shown in Figure 2A. Reaction (1) occurs between ARO and UES vinyl groups, forming dangling chains. The free radical generation is mainly restricted to a terminal double bond, whereas the conversion of internal double bonds usually remains challenging because the increased steric congestion hampers the intermolecular addition of radicals.[16] UES contains an internal double bond; therefore, reaction (2) between two unsaturated bonds of UES should be the slowest and occurs with a low probability. Internal alkenes are linked to more carbons along the chain, where the surrounding carbons stabilize their π bonds. This makes them more stable and less reactive than terminal alkenes.[26] The third crosslinking reaction (3) is between two ARO molecules and is likely to be favored and occur faster than other reactions. This could be explained by the terminal double bonds in the ARO structure. Since the terminal double bond is located at the end of the chain, it is only connected to primary carbon, which is the least stable. In addition, more rotational energy and higher steric freedom enable the terminal double bond to react more efficiently.[27]

Figure 2B visualizes the possible macromolecular chain network structure. The formation of the resulting macromolecular chain network with incorporated mobile pendant dangling chain ends may be explained by the many factors that affect crosslinking polymerization reactions.[28] The fatty acid composition, the nature of the oil, and the number of carbon–carbon double bonds, and dangling chains strongly impact the developed macromolecular structure and crosslinking quality. The long dangling chains present in the triglyceride structures have been reported to act as plasticizers, which can lower the mechanical properties (e.g., elastic modulus and tensile strength) of the polymer-based material. While the short dangling chains, resulting from furan-based unsaturated ester, cannot be counted as elastically effective chains but contribute to the free volume of the material and chain relaxation phenomena.[29] In turn, the observed dangling chains account for the crosslinking network degree and decrease in the glass transition temperature of the developed polymer. The crosslinking density ν_e, calculated by the Flory–Rehner equation as reported elsewhere,[30,31] increased significantly from $1.07 \cdot 10^3$ to $1.65 \cdot 10^3$ mol/m^3 for ARO and ARO/UES5 (ARO with 5 wt% UES), respectively. The improved crosslinking density after incorporating 5 wt% of UES enhances the polymer materials' tensile strength, storage modulus and glass transition temperature (discussed in the following sections). The materials' measured density is 1.009 ± 0.0029, 1.013 ± 0.0017, and 1.003 ± 0.0056 g/cm^3 for ARO, ARO/UES5, and ARO/UES20, respectively. The proposed reactive diluent UES facilitates the crosslinking of chains; it also significantly decreases the resin viscosity, as shown in Figure 2C. With 20 wt% UES, the resin viscosity drops approximately 1.6 times. A biobased diluent, cardanyl acrylate, was used as a reactive diluent for UV-curable castor oil-based polyfunctional

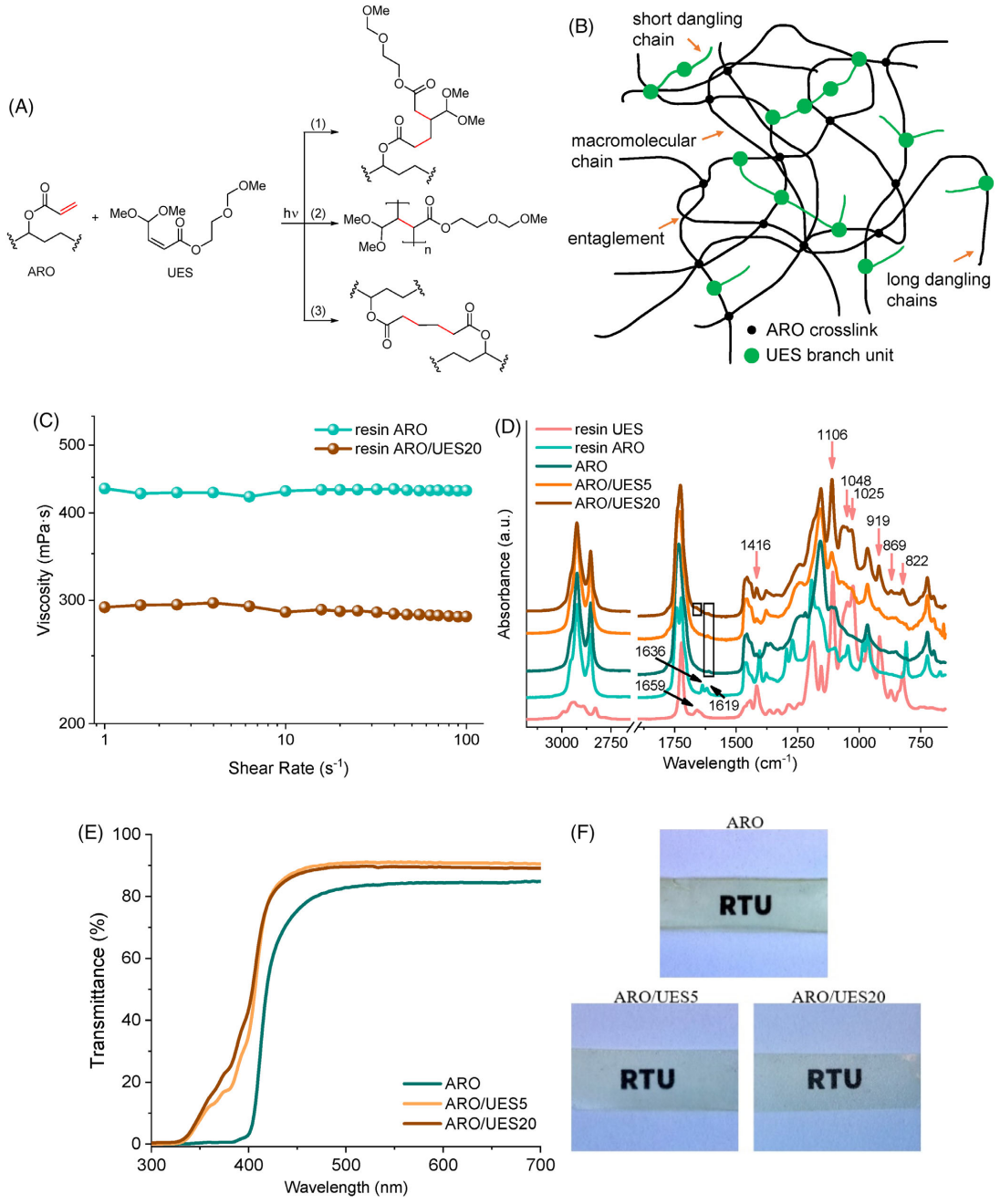

FIGURE 2 (A) Possible reactions between ARO and UES; (B) schematic illustration of ARO and UES crosslinked network; (C) viscosity dependence on shear rate; (D) FT-IR spectra of UES and ARO liquid resins and polymerized samples; (E) UV–VIS transmittance spectra of sample films; (F) Optical images of sample films.

polyurethane acrylate resin.[32] With the addition of 20 wt% cardanyl acrylate, viscosity dropped from 1360 to 340 mPa s. Dipak et al. used a bio-based castor oil-based reactive diluent as an additive to lower the viscosity of UV-curable urethane acrylate oligomer.[33] The authors showed that viscosity dropped from about 1070 mPa·s (neat) to about 560 mPa·s for resin that contained 20 wt% reactive diluent. Zhang et al. reported the successful use of bio-based of methacrylated eugenol as a reactive diluent for maleinated acrylated epoxidized soybean oil.[34] While viscosities between matrices vary significantly, it can be noted that methacrylated eugenol has a viscosity of about 110 mPa s (shear rate up to 100 s^{-1}). Hence, UES acts as an effective reactive diluent, achieving viscosity values comparable to those presented in the literature.

Figure 2D reveals the FT-IR spectra of liquid resins ARO and UES (resin ARO, and resin UES, respectively) and respective UV-cured polymers (ARO, ARO/UES5, and ARO/UES20). The characteristic UES vibrational type peaks can be seen in ARO/UES5 and ARO/UES20 samples (marked with pink arrows). Characteristic peaks of ARO are described in detail elsewhere.[23] We are interested in the internal double bond peak for UES and ARO's terminal double bond peak. Double bond peaks at 1636 and 1619 cm^{-1} in ARO resin spectra and 1659 cm^{-1} in UES resin spectra (black arrows) almost fully disappear after UV curing.[23] From two ARO peaks, only a minimal peak remains at 1619 cm^{-1}, while in the ARO/UES20 spectra at 1659 cm^{-1} some traces of unreacted UES double bonds can be observed. Thus, FTIR serves as an indication of the high conversion rate of double bonds. It is also testified by boosting up to 90% optical transmittance in the UV–VIS region of the developed polymer film when the UES monomer is incorporated (Figure 2E). The excellent optical transparency of the obtained films can be seen in the optical images in Figure 2F. Some reactive groups remain in the polymer after complete photopolymerization and absorb in specific regions (i.e., below 400 nm).[35] At the same time, UES enhances the polymer's overall optical transparency, which could also be related to the observations that reactive diluent increases the crosslinking density of the developed polymer network.

3.2 | Tensile properties

Tensile test stress–strain curves are shown in Figure 3. With the addition of UES, tensile strength increased from 0.49 to 0.55 MPa for ARO/UES5, while a decrease was observed for ARO/UES20 showing a value of 0.31 MPa. Two distinct stress–strain patterns are visible, with ARO/UES20 following the curve of ARO, while ARO/UES5 becomes noticeably stiffer. This observation is complemented by tensile modulus values of 9.2, 16.2, and 7.9 MPa for ARO, ARO/UES5, and ARO/UES20, respectively. This can be explained by an increased crosslink density in ARO/UES5. The content of long fatty acid aliphatic chains is lowered by adding UES. Small molecules of UES can find the optimal placements in the structure and provide strong intermolecular bonding. It should be noted that the ARO double bond reactivity is limited by steric interference; thus, ARO cannot reach 100% of double bond conversion. However, smaller UES molecules can overcome these limitations and add denser intermolecular bonding on top of chemical crosslinking; as such, a material's tensile strength and tensile modulus increase.

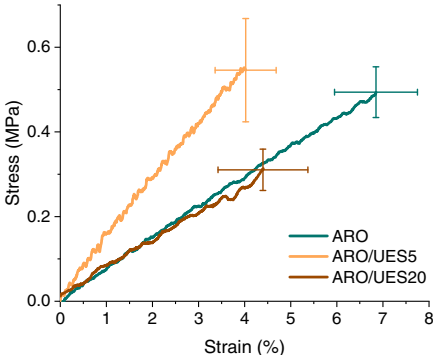

FIGURE 3 Stress–strain curves of UV-cured polymers.

Adding 20 wt% of UES introduces a notable amount of the second component. This opens several routes of possible interactions. As a smaller molecule, UES can more easily find double bonds to react with, hindering the formation of a strong crosslinked network of ARO, resulting in lower chemical cross-linking. Thus, reducing crosslinking between ARO and adding too many dangling chains and a plasticizing effect.[29] While a notable amount of the second component can also yield the formation of an additional phase in the thermoset structure.[36] If the material's phase interface is weak, then a drop in mechanical properties is observed.[37] The decreased elongation (strain) values for ARO/UES5 match the observed increase in tensile modulus, thus clearly indicating structural changes attributed to enhanced crosslinking. While for ARO/UES20, the decrease in strain is assigned to disrupted ARO network, which cannot achieve the conformation changes required for elongation due to interference of the second phase or dangling chains.

3.3 | Morphology of sample films

The morphology of the UV-cured films was examined with SEM. The micrographs of cured samples are shown in Figure 4. The incorporation of UES increased the

overall roughness of the fracture surface. No visible phase separation can be observed, indicating that both components are cross-linked. The enhanced fracture roughness indicates structural changes related to increased crosslinked network complexity. Thus, fracture forms and finds a route that spreads through the weakest structural links. The pronounced cracks of ARO/UES5 indicate elongation of the fracture route, which matches the observed increase in tensile strength. In the case of ARO/UES20, the uneven fracture surface could be explained by stress concentrations and very loosely connected regions in the thermoset structure, which serves as multiple failure points that connect during fracture. The complex nature of the observable surface for ARO/UES20 also indicates that components did not react in balanced proportions, creating local defects, which explain the decrease in tensile properties.

3.4 | Dynamic mechanical analysis

Storage modulus, loss modulus, and loss factor (tanδ) graphs for ARO and ARO/UES5 are shown in Figure 5. Tensile test results showed that adding 5 wt% UES increased storage modulus. Given the similarities between the storage modulus and tensile modulus, the increase observed for ARO/UES5 matches the abovementioned observations. ARO showed 7.9 MPa and ARO/UES5 12.0 MPa at 22 °C (Figure 5A). The difference in storage modulus values reached as high as 583 MPa at −60 °C. The loss modulus shows the materials dissipated energy, which peaks at the glass transition, where large segmental motions start to occur.[38,39] The ARO/UES5 saw an increase of the glass transition temperature by 2 °C and had an increased peak maximum and broader overall shape compared to ARO. This indicates that crosslinking between ARO molecules was enhanced, while UES chains restricted segmental rearrangements, as indicated by increased loss modulus value. In the tanδ graph, the narrower peak of ARO/UES5 indicates the structural changes in the ARO network as molecular relaxations take place at slightly lower temperatures. Also, a slightly lower tanδ peak maximum of ARO indicates a more rigid structure of the macromolecular network. Still, in a viscoelastic state, the material proved to have higher resistance to deformation, as indicated by increased storage modulus and

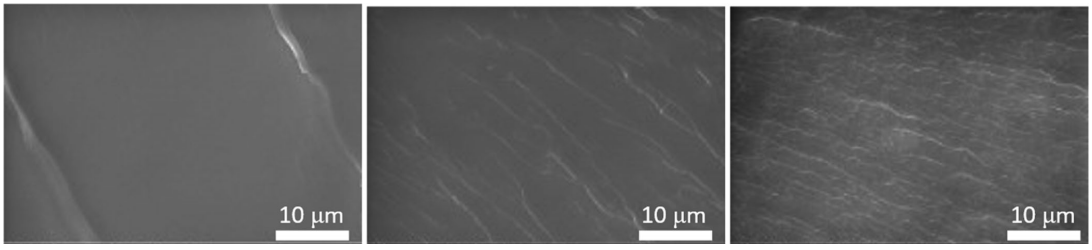

FIGURE 4 Fracture surface SEM images at 2500× magnification: (A) ARO; (B) ARO/UES5; and (C) ARO/UES20.

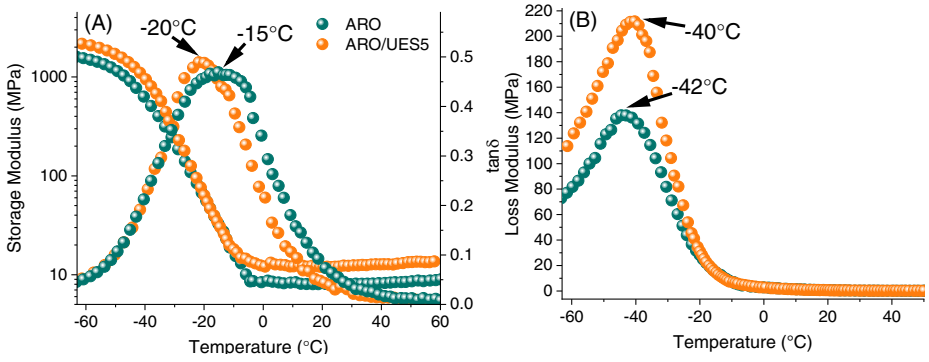

FIGURE 5 Dynamic mechanical analysis (DMA) curves for cured samples: (A) Storage modulus and tanδ and (B) Loss modulus.

crosslinking degree. This could be explained by changes in chain structural packing, augmented chain intermolecular entanglements and enhanced crosslinking degree.

Tensile tests and dynamic mechanical analysis (DMA) both indicate that ARO-based polymers in this study yield relatively soft materials. At the same time, if more rigid properties are desired, several modification strategies can be applied. First, aimed at increased glass transition, which can be achieved by increasing crosslinking density, for example, by the use of additional polyfunctional reactive diluents, additional steps to enhance acrylation degree of vegetable oil, and improve post-curing processes.[40] Second, the use of reinforcement via the preparation of biocomposites could be considered. This can be achieved with the use of nanofillers like nanocellulose.[41]

3.5 | Thermogravimetric analysis

Thermogravimetric analysis (TGA) and derivative thermogravimetric (DTG) curves for the samples are shown in Figure 6. The initial thermal decomposition temperature of crosslinked ARO/UES was lower than that of neat ARO. With the addition of UES, the $T_{5\%}$, which indicates the weight loss at 5 wt%, decreased from 289 to 271 and 204 °C for ARO/UES5 and ARO/UES20, respectively (Figure 6A). TGA revealed a linear decrease in $T_{5\%}$ temperature, proportional to UES content (Figure 6A inset plot).

A three-step degradation pattern is observed for all samples in Figure 6B. The first peak is attributed to the degradation of the crosslinked ester-ether moieties in the UES side chain.[42] The maximum rate of ester decomposition is reached at around 205 °C. While the first notable weight drop in ARO is attributed to more loosely connected sections of the network. The second visible peak with a maximum of around 350 °C is assigned to the degradation of acrylic moieties and the polymer backbone. The maximum degradation rate (T_{max}) is achieved between 370 and 430 °C, resulting from chain scission in the oil-based ester groups.[43] The remaining degradation products are further carbonized at a higher temperature. Over 600 °C, pyrolysis occurs with little weight loss.[42]

3.6 | Biodegradation studies in the composting conditions

Reactive diluents are typically fossil vinyl monomers, and their addition into the formulation increases the non-degradable component of the product.[44] In the literature, there is no evidence for the commonly used crosslinked reactive diluents like (2-hydroxyethyl methacrylate (HEMA) to be biodegradable.[45]

The percentage weight loss in composting conditions for ARO and ARO/UES films is presented in Figure 7A. Furthermore, Figure 7B visualizes the samples after removal from the soil. Although ARO showed 28% weight loss after 2 months, the degradation rate remained relatively stable but slightly decreased over time. The compositions with UES showed a similar degradation rate during the initial 30 days compared to ARO but afterwards saw a significant drop in degradation speed. We assume that fatty acid hydrolysis is the primary reaction that occurs during biodegradation, and the presence of UES obstructs microbial activity and limits access to ester bonds. The ARO/UES20 degraded slightly faster than ARO/UES5. This could be explained by the looser structure that lacks

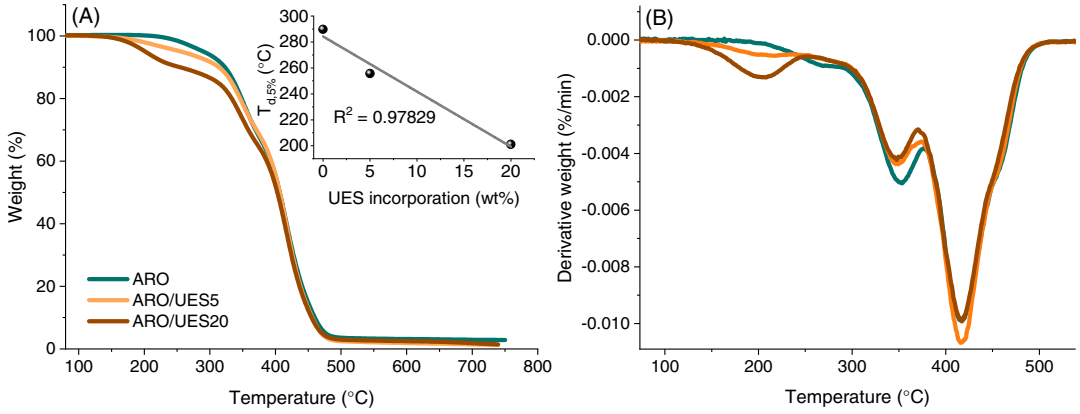

FIGURE 6 TGA of photocured polymers containing varied amounts of UES: (A) TGA thermogram (the inset plot reveals the trend in $T_{d,5\%}$ with increasing UES content); (B) Derivative thermogram (DTG).

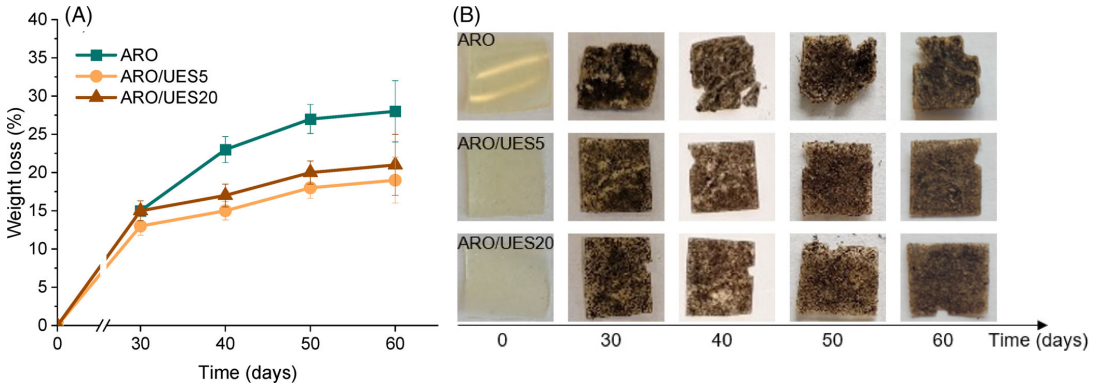

FIGURE 7 (A)) Weight loss of ARO and ARO/UES during soil burial test and (B) Optical images of samples before and after biodegradation.

the dense crosslinking in the ARO/UES5 structure, making the water migration easier, exposing more surface, and losing the structural integrity faster.

It has been reported before that the increase in double bond content does not significantly affect the biodegradability of acrylated epoxidized soybean oil (AESO).[46] After a 3-month biodegradation test in the garden soil, AESO showed a weight loss of approximately 16%. Adding a co-monomer lowered the degradation by about 2%. In another study, 3D printed objects from waste cooking oil collected from McDonald's restaurant demonstrated a weight loss of around 20% in only 2 weeks when buried in soil and kept at 25 °C and 30% relative humidity.[47]

4 | CONCLUSIONS

This work focuses on a polymer material made from two bio-based photoactive components, presenting the influence of UES as a reactive diluent on the ARO matrix. Three proposed reactions can occur during photopolymerization between the two components.

A correlation between tensile and DMA results showed a notable performance increase with the addition of 5 wt% UES. With the addition of relatively low loadings, UES can potentially tune the mechanical properties of ARO towards stiffer structures. Furthermore, the thermal degradation temperature of UES is notably lower than ARO's. Still, this should not limit most applications and uses.

The biodegradability of compositions was explored, and a maximum mass loss of 28 wt% was achieved in 60 days for ARO. The addition of UES slightly reduced the biodegradation rate. Follow-up studies with evolved carbon dioxide measurements are needed to evaluate the degradation rate further.

ACKNOWLEDGMENTS

This work was supported by Latvian Council of Science in the framework of FLPP "Printed biopolymer 4D TENG device for mechanical energy harvesting" (lzp-2022/1-0485). Sabine Briede was funded by the European Social Fund within the Project No 8.2.2.0/20/I/008 «Strengthening of PhD students and academic personnel of Riga Technical University and BA School of Business and Finance in the strategic fields of specialization» of the Specific Objective 8.2.2 «To Strengthen Academic Staff of Higher Education Institutions in Strategic Specialization Areas» of the Operational Programme «Growth and Employment». Sabine Briede was supported by Riga Technical University's Doctoral Grant programme. The authors would like to thank their parental institutions for their support. Madara Darzina was supported by Latvian Institute of Organic Synthesis student grant no. IG-2023-07.

CONFLICT OF INTEREST STATEMENT

The authors declare that they have no conflict of interest.

DATA AVAILABILITY STATEMENT

Data is available upon request from corresponding author as it is part of larger ongoing study.

ORCID

Oskars Platnieks https://orcid.org/0000-0001-5529-0912
Aigars Jirgensons https://orcid.org/0000-0002-8937-8792
Sergejs Gaidukovs https://orcid.org/0000-0001-8638-5009

REFERENCES

[1] W. Shi, B. Rånby, *UV J. Appl. Polym. Sci.* **1994**, *51*, 1129.

[2] Z. Dai, Q. Li, Z. Chen, R. K. Shawon, Y. Zhu, H. Lv, F. Fu, Y. Zhu, Y. Fu, X. Liu, *ACS Sustain. Chem. Eng.* **2020**, *8*, 17379.
[3] S. Cousinet, A. Ghadban, E. Fleury, F. Lortie, J.-P. Pascault, D. Portinha, *Eur. Polym. J.* **2015**, *67*, 539.
[4] A. Nebioglu, M. D. J. Soucek, *Polym. Sci., Part A: Polym. Chem.* **2006**, *44*, 6544.
[5] S. RameshKumar, P. Shaiju, K. E. O'Connor, *Curr. Opin. Green Sustain. Chem.* **2020**, *21*, 75.
[6] B. T. White, V. Meenakshisundaram, K. D. Feller, C. B. Williams, T. E. Long, *Polymer* **2021**, *223*, 123727. https://doi.org/10.1016/j.polymer.2021.123727
[7] H. Esen, S. Küsefoğlu, R. Wool, *J. Appl. Polym. Sci.* **2007**, *103*, 626.
[8] C. Bonneaud, M. Decostanzi, J. Burgess, G. Trusiano, T. Burgess, R. Bongiovanni, C. Joly-Duhamel, C. M. Friesen, *RSC Adv.* **2018**, *8*, 32664.
[9] H. Wei, T. Y. Lee, W. Miao, R. Fortenberry, D. H. Magers, S. Hait, A. C. Guymon, S. E. Jönsson, C. E. Hoyle, *Macromolecules* **2007**, *40*, 6172.
[10] S. K. Yadav, K. M. Schmalbach, E. Kinaci, J. F. Stanzione, G. R. Palmese, *Eur. Polym. J.* **2018**, *98*, 199.
[11] S. Briede, A. Barkane, M. Jurinovs, V. K. Thakur, S. Gaidukovs, *Curr. Opin. Green Sustain. Chem.* **2022**, *35*, 100626.
[12] X. Yang, S. Li, J. Xia, J. Song, K. Huang, M. Li, *Ind. Crop. Prod.* **2015**, *63*, 17.
[13] M. Fei, T. Liu, B. Zhao, A. Otero, Y.-C. Chang, J. Zhang, *ACS Appl. Polym. Mater.* **2021**, *3*, 2470.
[14] L. Meng, H. Qiu, D. Wang, B. Feng, M. Di, J. Shi, S. Wei, *Prog. Org. Coat.* **2020**, *140*, 105492.
[15] D. Wei, X. Huang, J. Zeng, S. Deng, J. Xu, *J. Appl. Polym. Sci.* **2020**, *137*, e49054.
[16] Y. Chen, J. Wang, X. Wu, C. Zhu, *ACS Org. Inorg. Au* **2022**, *2*, 392.
[17] B. H. Northrop, R. N. Coffey, *J. Am. Chem. Soc.* **2012**, *134*, 13804.
[18] L. Dall Agnol, F. T. G. Dias, H. L. Ornaghi, M. Sangermano, O. Bianchi, *Prog. Org. Coat.* **2021**, *154*, 106156.
[19] S. Briede, O. Platnieks, A. Barkane, I. Sivacovs, A. Leitans, J. Lungevics, S. Gaidukovs, *Coatings* **2023**, *13*, 657.
[20] A. Barkane, O. Platnieks, M. Jurinovs, S. Kasetaite, J. Ostrauskaite, S. Gaidukovs, Y. Habibi, *Polymer* **2021**, *13*, 1195.
[21] E. Woźniak, E. Waszkowska, T. Zimny, S. Sowa, T. Twardowski, *Front. Plant Sci.* **2019**, *10*, 1423.
[22] Y. Su, H. Lin, S. Zhang, Z. Yang, T. Yuan, *Polymer* **2020**, *12*(5), 1165.
[23] S. Briede, M. Jurinovs, S. Nechausov, O. Platnieks, S. Gaidukovs, *Mol. Syst. Des. Eng.* **2022**, *7*, 1434.
[24] M. Kolář, J. Machotová, M. Hájek, J. Honzíček, T. Hájek, Š. Podzimek, *Coatings* **2023**, *13*(2), 262.
[25] M. Darzina, A. Lielpetere, A. Jirgensons, *Eur. J. Org. Chem.* **2021**, *2021*, 4224.
[26] Y. Li, H. Liu, Z. Huang, H. Wang, Z. Yu, *Tetrahedron Lett.* **2021**, *82*, 153396.
[27] Z. P. Vang, A. Reyes, R. E. Sonstrom, M. S. Holdren, S. E. Sloane, I. Y. Alansari, J. L. Neill, B. H. Pate, J. R. Clark, *J. Am. Chem. Soc.* **2021**, *143*, 7707.
[28] T. S. Omonov, V. Patel, J. M. Curtis, *J. Am. Oil Chem. Soc.* **2019**, *96*, 1389.
[29] D. P. Pfister, Y. Xia, R. C. Larock, *ChemSusChem* **2011**, *4*, 703.
[30] P. J. Flory, J. Rehner, *J. Chem. Phys.* **1943**, *11*, 512.
[31] S. Gaidukovs, A. Medvids, P. Onufrijevs, L. Grase, *Express Polym Lett* **2018**, *12*, 918.
[32] Y. Hu, Q. Shang, J. Tang, C. Wang, F. Zhang, P. Jia, G. Feng, Q. Wu, C. Liu, L. Hu, W. Lei, Y. Zhou, *Ind. Crop. Prod.* **2018**, *117*, 295.
[33] D. S. Tathe, R. N. Jagtap, *J. Coat. Technol. Res.* **2015**, *12*(1), 187.
[34] Y. Zhang, Y. Li, L. Wang, Z. Gao, M. R. Kessler, *ACS Sustain. Chem. Eng.* **2017**, *5*(10), 8876.
[35] F. Masson, C. Decker, S. Andre, X. Andrieu, *Prog. Org. Coat.* **2004**, *49*(1), 1.
[36] M. J. Stevens, *J. Chem. Phys.* **2021**, *155*, 054905.
[37] D. A. Jesson, J. F. Watts, *Polym. Rev.* **2012**, *52*, 321.
[38] P. Lall, M. Kasturi, H. Wu, E. Davis, Proceedings of 2020 19th IEEE Intersociety Conference on Thermal and Thermomechanical Phenomena in Electronic Systems (ITherm), pp. 1389–1394. **2020** https://doi.org/10.1109/ITherm45881.2020.9190482
[39] Y. Sun, Z. Zhang, K.-S. Moon, C. P. J. Wong, *Polym. Sci. B: Polym. Phys.* **2004**, *42*, 3849.
[40] M. Lebedevaite, V. Talacka, J. Ostrauskaite, *J. Appl. Polym. Sci.* **2021**, *138*(16), 50233.
[41] A. Barkane, M. Jurinovs, S. Briede, O. Platnieks, P. Onufrijevs, Z. Zelca, S. Gaidukovs, *3D Print. Addit. Manuf.* **2022**. https://doi.org/10.1089/3dp.2021.0294
[42] X. Yang, Y. Li, W. Lei, X. Liu, Q. Zeng, Q. Liu, W. Feng, K. Li, P. Wang, *Polym. Degrad. Stab.* **2021**, *191*, 109668.
[43] S. K. Sahoo, V. Khandelwal, G. Manik, *Polym. Adv. Technol.* **2018**, *29*, 2080.
[44] Y. Bao, N. Paunović, J. C. Leroux, *Adv. Funct. Mater.* **2022**, *32*(15), 2109864.
[45] G. Mabilleau, M. Moreau, R. Filmon, M. Baslé, D. Chappard, *Biomaterials* **2004**, *25*(21), 5155.
[46] J. Chen, H. Liu, W. Zhang, L. Lv, Z. Liu, *J. Appl. Polym. Sci.* **2020**, *137*, 48827.
[47] B. Wu, A. Sufi, R. Ghosh Biswas, A. Hisatsune, V. Moxley-Paquette, P. Ning, R. Soong, A. P. Dicks, A. J. Simpson, *ACS Sustain. Chem. Eng.* **2019**, *8*, 1171.

SUPPORTING INFORMATION

Additional supporting information can be found online in the Supporting Information section at the end of this article.

How to cite this article: S. Briede, O. Platnieks, M. Darzina, A. Jirgensons, S. Gaidukovs, *J. Polym. Sci.* **2023**, 1. https://doi.org/10.1002/pol.20230451

Darzina, **M**.; Jirgensons, A.

Electrochemical Formation of Oxazolines by 1,3-Oxyfluorination of Non-activated Cyclopropanes.

Org. *Lett*. **2024**, *26*, 2158–2162.

https://doi.org/10.1021/acs.orglett.4c00143

The Supporting Information is available free of charge on the American Chemical Society Publications website:

https://doi.org/10.1021/acs.orglett.4c00143

OL | Organic Letters

pubs.acs.org/OrgLett Letter

Electrochemical Formation of Oxazolines by 1,3-Oxyfluorination of Non-activated Cyclopropanes

Madara Darzina and Aigars Jirgensons*

Cite This: https://doi.org/10.1021/acs.orglett.4c00143 Read Online

ACCESS | Metrics & More | Article Recommendations | Supporting Information

ABSTRACT: The C−C bond in non-activated cyclopropanes can be intramolecularly cleaved with an electrochemically generated amidyl radical forming oxazolines. In the presence of $TBABF_4$, this provides 1,3-oxyfluorination products. C−C bond cleavage of cyclopropane proceeds with inversion of the configuration, suggesting an intramolecular homolytic substitution (S_Hi) mechanism. The performance of $TBABF_4$ as an efficient fluoride source was explained by accumulation of the BF_4^- anion at the anode surface, at which a carbocation is formed by the oxidation of the C-centered radical.

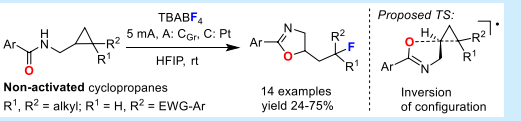

Functionalization of the C−C bond has high potential to access value-added compounds.[1] However, the inertness of the C−C σ bond renders such transformations a very challenging task. The cyclopropane C−C bond is relatively more reactive compared to larger cyclic or acyclic systems as a result of a weaker overlap of the C−C bond forming orbitals.[2] Several approaches have been used to achieve the ring cleavage of cyclopropanes, including the reactions of donor−acceptor cyclopropanes,[3,4] metal insertion,[5] reaction with electrophiles[6] and radical cations,[7] and oxidation-induced activation.[8] Activation by electrochemical oxidation is feasible for cyclopropane derivatives with lowered oxidation potential.[9] Among them, anodic oxidation of arylcyclopropane **1** to a cation radical **A** has enabled transformations to access a range of the useful 1,3-difunctionalization reaction product **2** (Figure 1). Seminal work by Shono and Matsamura has demonstrated dimethoxylation of phenylcyclopropanes in methanol using undivided cell electrolysis.[10] The group of Lei has developed electrochemical oxyfluorination, amino fluorination, and difluorination reactions of arylcyclopropanes using $Et_3N{\cdot}3HF$ as a fluorine source.[11] Oxyamination of arylcyclopropanes was established by Zhou et al., using electrochemical oxidation conditions.[12] The same approach was used for oxyhalogenation and oxyalkynylation reactions of arylcyclopropanes by Sheng et al.[13] as well as the green synthesis method of β-hydroxy ketones by Huang et al.[14] and 1,3-diols by Cai et al.[15] A few examples for electrochemical oxidation of cyclopropane integrated into polycyclic systems are known; however, these are limited to the strained compounds with an increased highest occupied molecular orbital (HOMO) level.[16,17] Because the high oxidation potential of non-activated cyclopropanes prevents their selective electrochemical activation in the presence of other functional groups,[11] we envisioned electrochemical generation of a reactive species, which would be engaged in the reaction with a C−C bond. For this purpose, we explored cyclopropane substrate **3** bearing benzamide functionality, which could be oxidized to an amidyl radical (Figure 1).[18] Initial electrolysis of amide **3a** (Ar = Ph and R^1 and R^2 = Me) in methanol using $TBABF_4$ as an electrolyte provided a mixture of oxazolines **4a** and **5** (Ar = Ph and R^1 and R^2 = Me). This indicated a competitive reaction of $TBABF_4$ as a fluoride source and methanol as an oxygen nucleophile. Further attempts were directed to optimize the formation of oxazoline **4a** (Table 1).

Performing the electrolysis of amide **3a** in less nucleophilic solvent HFIP with $TBABF_4$ as an electrolyte provided oxazoline **4a** in a good yield (entry 1 in Table 1). The use $TBAPF_6$ as an electrolyte also enabled the formation of fluorinated product **4a**, although a slight increase of byproduct

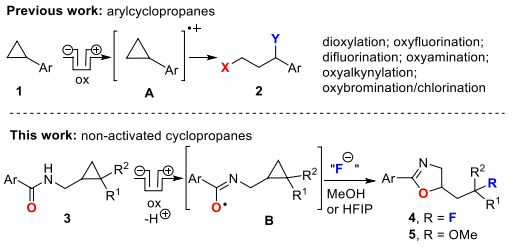

Figure 1. 1,3-Difunctionalization of arylcyclopropanes and non-activated cyclopropanes.

Received: January 12, 2024
Revised: March 5, 2024
Accepted: March 6, 2024

Table 1. Investigation of the Fluorine Source for Electrochemical Oxyfluorination of Cyclopropane 3a

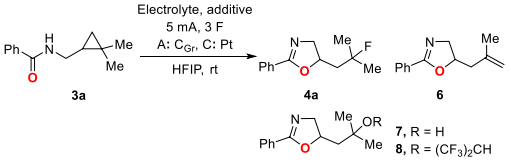

entry	electrolyte, additive[a]	conversion of compound 3a (%)	product ratio of compounds 4a/6/7/8[b]	yield of compound 4a (%)[c]
1	$TBABF_4$, none	100	95:2:2:0	82
2	$TBAPF_6$, none	100	79:7:9:5	68
3	$TBAClO_4$, TASF	100	41:34:5:19	nd
4	$TBAClO_4$, CsF	74	8:40:6:20	nd
5	$TBAClO_4$, $TBAF{\cdot}3H_2O$	100	11:31:40:18	nd
6	$TBAClO_4$, $n Bu_3SnF$	28	6:15:7:0	nd

[a]A total of 1 equiv of electrolyte and 2 equiv of an additive. [b]Determined by ultra-performance liquid chromatography−mass spectrometry (UPLC−MS). [c]NMR yield using 4,4′-difluorobenzophenone (0.5 equiv) as an internal standard.

6−**8** formation was observed (entry 2 in Table 1). Other nucleophilic fluorine sources, such as TASF and CsF, in the presence of $TBAClO_4$ as an electrolyte were explored; however, these performed less efficiently compared to $TBABF_4$ to produce fluorinated product **4a** (entries 3 and 4 in Table 1). These conditions induced the formation of considerably higher amounts of olefin **6** and oxylated product **8**. Introduction of water to the reaction media using TBAF hydrate led to an increased formation of hydroxylated product **7** (entry 5 in Table 1). Poor conversion of amide **3a** and a trace amount of fluorinated product **4a** were observed when $n Bu_3SnF$ was used as an additive (entry 6 in Table 1).

The use of 3 equiv of $TBABF_4$ was optimal to achieve a high yield of the product **4a** formation. Decreasing the amount of electrolyte to 2 equiv reduced the yield of oxazoline **4a** to 69%, while increasing to 5 equiv caused damage to the graphite anode (see the Supporting Information for the full set of optimization experiments).

With optimized electrochemical conditions in hand, the scope of the oxyfluorination reaction was investigated for substrates **3a**−**3p** (Scheme 1). Benzamide **3a** and its analogues **3b** and **3c** containing a halogen group at the arene ring provided oxazolines **4a**−**4c** in a good yield. Introduction of an electron-donating metoxy group in benzamide of substrate **3d** reduced the yield of product **4d**, probably as a result of competitive oxidation of the aromatic ring (see the Supporting Information for cyclic voltammetry studies). Trifluoromethyl-substituted analogue **3e** provided oxazoline **4e** in a good yield. Another electron-poor benzamide **3f**, containing a nitro group, provided product **4f** in a lower yield, presumably as a result of electrochemical side reactions. Spirocyclic substrates **3h** and **3i** comprising cyclobutane, cyclopentane, and cyclohexane provided oxazolines **4h** and **4i** in moderate to good yields. Electrolysis of spirocycle **3j** bearing tetrahydropyrane gave oxazoline **4j** in a good yield; however, a similar substrate **3k** with *N*-tosyl-protected piperidine produced product **4k** in a

Scheme 1. Substrate Scope for 1,3-Oxyfluorination of Cyclopropanes

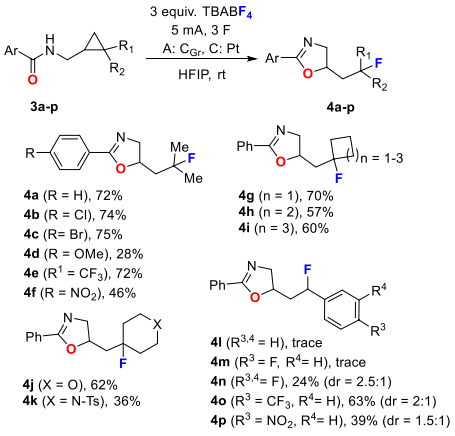

reduced yield, which was due to difficult separation from the electrolyte. Arylcyclopropanes **3l**−**3p** were also explored as substrates for oxyfluorination to produce oxazolines **4l**−**4p**. Phenyl and fluorophenyl cyclopropane derivatives **3l** and **3m** failed to give the oxazolines **4l** and **4m**; instead, the formation of a complex product mixture was observed. Cyclopropane derivative **3l** has a lower oxidation potential compared to substrate **3a** (see the Supporting Information), implying that the activation of substrates **3l** and **3m** might be triggered by the oxidation of the aryl group rather than the amide group. Substrates **3n**−**3p** bearing more electron-deficient difluoro, trifluoromethyl, or nitro phenyl groups produced the expected oxazolines **4n**−**4p** as mixtures of diastereomers. In the case of electrolysis of substrate **3o**, the major diastereomer *S**,*S**-**4o** was separated, and its relative configuration was determined by X-ray analysis (Figure 2)

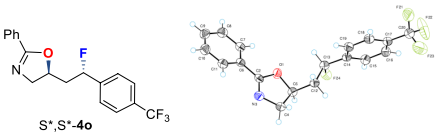

Figure 2. ORTEP diagram of compound *S**,*S**-**4o** with 50% ellipsoid contour probability.

An interesting result was obtained when using a penta-substituted cyclopropane derivative **3q** as a substrate for oxyfluorination (Scheme 2). Dihydrooxazine **9** was obtained as the major product instead of oxazoline **4q** [see the Supporting Information for the proof by two-dimensional (2D) nuclear

Scheme 2. 1,3-Oxyfluorination of Penta-substituted Cyclopropane 3q

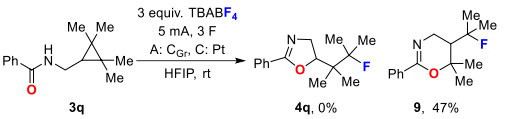

https://doi.org/10.1021/acs.orglett.4c00143
Org. Lett. XXXX, XXX, XXX−XXX

magnetic resonance (NMR) spectra]. The change in the reaction course can be explained by the preferred cleavage of the most strained C−C bond in substrate **3q**.

An attempt was also made to perform 1,3-thiofluorination of cyclopropane **3r**, bearing thioamide functionality, which has considerably reduced oxidation potential compared to amide.[19] Unfortunately, a low yield of product **4r** was observed in the electrolysis of substrate **3r** (Scheme 3).

Scheme 3. 1,3-Thiofluorination of Cyclopropane 3r

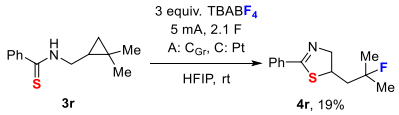

An enantioenriched substrate (*S*)-**3c** was subjected to electrochemical oxyfluorination to establish the stereochemical course of cyclopropane C−C bond cleavage (Scheme 4). The

Scheme 4. Chirality Transfer in 1,3-Oxyfluorination of Cyclopropane 3c

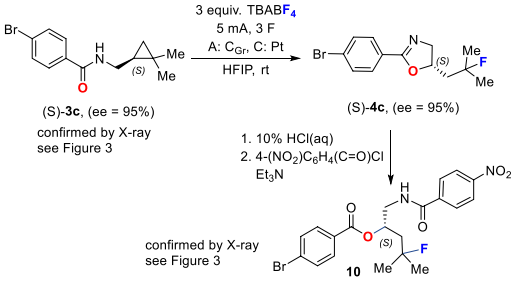

reaction product (*S*)-**4c** was obtained with a complete inversion of configuration as determined by X-ray analysis of its derivatization product **10**. Compound **10** was obtained by hydrolysis of oxazoline (*S*)-**4c** in acidic conditions followed by N-acylation. The absolute configuration of starting material (*S*)-**3c** was also confirmed by X-ray analysis (Figure 3).

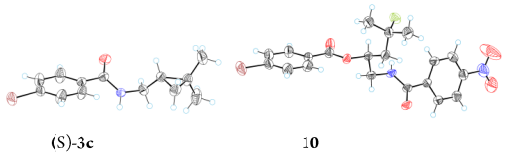

Figure 3. ORTEP diagrams of compounds (*S*)-**3c** and **10** with 50% ellipsoid contour probability.

The transfer of chirality with inversion of the newly formed stereocenter as well as the substrate scope with the requirement of electron-poor phenyl substituents at cyclopropane for a successful reaction supports the following proposed mechanism (Scheme 5): Anodic oxidation of the amide group provides amidyl radical **A**, which in its oxygen-centered mesomeric form attacks the C−C bond to form an oxazoline ring via a stereospecific intramolecular homolytic substitution (S_Hi) process.[20] The cyclopropane ring cleavage

Scheme 5. Proposed Mechanism for the Formation of Oxazoline 4 from Cyclopropane 3

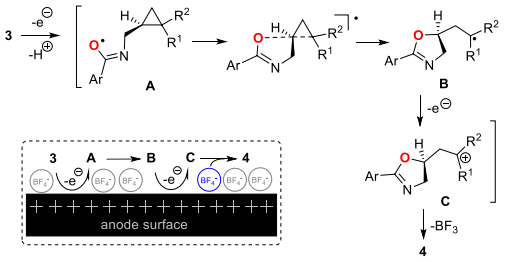

leads to a C-centered radical **B**, which is electrochemically oxidized to a carbocation **C**. Capturing of the fluoride ion from $TBABF_4$ by the carbocation **C** leads to product **4**.

Salts with the BF_4^- anion are known to act as a fluoride sources in several electrochemical reactions;[21] however, the reported conditions use non-protic chlorinated solvents as the reaction media. It was surprising to observe that $TBABF_4$ competed with HFIP and even MeOH as the reaction solvents delivering fluoride to the carbocation **C**. An explanation to this could be a high concentration of anionic $TBABF_4$ at the positively charged anode surface in analogy to a hypothesis by Xiong et al. explaining increased selectivity of the reaction of alkenes with organotrifluoroborates.[22] Because carbocation **C** forms at the surface of the anode, it is exposed to a high concentration of BF_4 anions, thus facilitating selective fluoride transfer. This corroborates with the observation that using the mixture of $TBABF_4$ and $TBAClO_4$ (2:1) reduces the yield of product **4a** formation to 46% (see the Supporting Information)

In summary, we have shown that non-activated cyclopropanes can be cleaved by an electrochemically generated intramolecular amidyl radical in the presence of $TBABF_4$ as an electrolyte to generate oxazolines as 1,3-oxyfluorination products. This transformation demonstrates a proof of concept that the ring cleavage of non-activated cyclopropanes is feasible under electrochemical conditions using an undivided cell setup. The approach has potential to be extended to a wide range of 1,3-difunctionalization reactions of non-activated cyclopropanes by C−C bond cleavage.

■ ASSOCIATED CONTENT

Data Availability Statement

The data underlying this study are available in the published article and its Supporting Information.

Supporting Information

The Supporting Information is available free of charge at https://pubs.acs.org/doi/10.1021/acs.orglett.4c00143.

Optimization of the fluorine source and electrochemical reaction conditions, synthesis and characterization of substrate **3**, electrolysis of cyclopropane **3**, synthesis of compound **4**, synthesis of compound **10**, copies of NMR spectra, list of unsuccessful substrates, X-ray description for compounds *S**,*S**-**4o**, (*S*)-**3c**, and **10**, and cyclic voltammetry studies (PDF)

https://doi.org/10.1021/acs.orglett.4c00143
Org. Lett. XXXX, XXX, XXX−XXX

Accession Codes

CCDC 2323671−2323673 contain the supplementary crystallographic data for this paper. These data can be obtained free of charge via www.ccdc.cam.ac.uk/data_request/cif, or by emailing data_request@ccdc.cam.ac.uk, or by contacting The Cambridge Crystallographic Data Centre, 12 Union Road, Cambridge CB2 1EZ, UK; fax: +44 1223 336033.

AUTHOR INFORMATION

Corresponding Author

Aigars Jirgensons − *Latvian Institute of Organic Synthesis, LV-1006 Riga, Latvia*; orcid.org/0000-0002-8937-8792; Phone: +371-29334948; Email: aigars@osi.lv

Author

Madara Darzina − *Latvian Institute of Organic Synthesis, LV-1006 Riga, Latvia*

Complete contact information is available at: https://pubs.acs.org/10.1021/acs.orglett.4c00143

Notes

The authors declare no competing financial interest.

ACKNOWLEDGMENTS

This project was supported by the Latvian Institute of Organic Synthesis Student Grant IG-2023-07. The authors thank Dr. Sergejs Belakovs from the Latvian Institute of Organic Synthesis for the X-ray structure analysis, Dr. Anna Lielpetere from the Latvian Institute of Organic Synthesis for scientific discussions, Dmitrijs Cernobrovkins from the Latvian Institute of Organic Synthesis for the assistance in synthesis of starting materials, and Georgijs Stakanovs from the Latvian Institute of Organic Synthesis for the assistance in crystallization of compounds for X-ray analysis.

REFERENCES

(1) (a) Liang, Y.-F.; Bilal, M.; Tang, L.-Y.; Wang, T.-Z.; Guan, Y.-Q.; Cheng, Z.; Zhu, M.; Wei, J.; Jiao, N. Carbon−Carbon Bond Cleavage for Late-Stage Functionalization. *Chem. Rev.* **2023**, *123*, 12313−12370. (b) Deb, M. L.; Saikia, B. S.; Rahman, I.; Baruah, P. K. Metal-Free Catalysis in C−C Single-Bond Cleavage: Achievements and Prospects. *Top. Curr. Chem.* **2022**, *380*, 38. (c) Wang, B.; Perea, M. A.; Sarpong, R. Transition Metal-Mediated C−C Single Bond Cleavage: Making the Cut in Total Synthesis. *Angew. Chem., Int. Ed.* **2020**, *59*, 18898−18919. (d) Yu, X.-Y.; Chen, J.-R.; Xiao, W.-J. Visible Light-Driven Radical-Mediated C−C Bond Cleavage/Functionalization in Organic Synthesis. *Chem. Rev.* **2021**, *121*, 506−561. (e) Shi, S.-H.; Liang, Y.; Jiao, N. Electrochemical Oxidation Induced Selective C−C Bond Cleavage. *Chem. Rev.* **2021**, *121*, 485−505. (f) Nairoukh, Z.; Cormier, M.; Marek, I. Merging C−H and C−C Bond Cleavage in Organic Synthesis. *Nat. Rev. Chem.* **2017**, *1*, 0035. (g) Murakami, M.; Ishida, N. Potential of Metal-Catalyzed C−C Single Bond Cleavage for Organic Synthesis. *J. Am. Chem. Soc.* **2016**, *138*, 13759−13769. (h) Ruhland, K. Transition-Metal-Mediated Cleavage and Activation of C−C Single Bonds. *Eur. J. Org. Chem.* **2012**, *2012*, 2683−2706.

(2) (a) Wiberg, K. B. The Concept of Strain in Organic Chemistry. *Angew. Chem., Int. Ed.* **1986**, *25*, 312−322. (b) Wong, H. N. C.; Hon, M. Y.; Tse, C. W.; Yip, Y. C.; Tanko, J.; Hudlicky, T. Use of Cyclopropanes and Their Derivatives in Organic Synthesis. *Chem. Rev.* **1989**, *89*, 165−198. (c) Cohen, Y.; Cohen, A.; Marek, I. Creating Stereocenters within Acyclic Systems by C−C Bond Cleavage of Cyclopropanes. *Chem. Rev.* **2021**, *121*, 140−161.

(3) Schneider, T. F.; Kaschel, J.; Werz, D. B. A New Golden Age for Donor-Acceptor Cyclopropanes. *Angew. Chem., Int. Ed.* **2014**, *53*, 5504−5523.

(4) Pirenne, V.; Muriel, B.; Waser, J. Catalytic Enantioselective Ring-Opening Reactions of Cyclopropanes. *Chem. Rev.* **2021**, *121*, 227−263.

(5) (a) Shaw, M. H.; Bower, J. F. Synthesis and Applications of Rhodacyclopentanones Derived from C−C Bond Activation. *Chem. Commun.* **2016**, *52*, 10817−10829. (b) He, Z.; Yudin, A. K. Palladium-Catalyzed Oxidative Activation of Arylcyclopropanes. *Org. Lett.* **2006**, *8*, 5829−5832. (c) Masarwa, A.; Didier, D.; Zabrodski, T.; Schinkel, M.; Ackermann, L.; Marek, I. Merging Allylic Carbon−Hydrogen and Selective Carbon−Carbon Bond Activation. *Nature* **2014**, *505*, 199−203. (d) Bruffaerts, J.; Vasseur, A.; Singh, S.; Masarwa, A.; Didier, D.; Oskar, L.; Perrin, L.; Eisenstein, O.; Marek, I. Zirconocene-Mediated Selective C−C Bond Cleavage of Strained Carbocycles: Scope and Mechanism. *J. Org. Chem.* **2018**, *83*, 3497−3515. (e) Cormier, M.; de la Torre, A.; Marek, I. Total Synthesis of C30 Botryococcene and epi-Botryococcene by a Diastereoselective Ring Opening of Alkenylcyclopropanes. *Angew. Chem., Int. Ed.* **2018**, *57*, 13237−13241.

(6) (a) Rösner, C.; Hennecke, U. Homohalocyclization: Electrophilic Bromine-Induced Cyclizations of Cyclopropanes. *Org. Lett.* **2015**, *17* (13), 3226−3229. (b) Coxon, J. M.; Smith, W. B. Polar Bromination of Cyclopropane: A DFT Study. *J. Org. Chem.* **2000**, *65*, 2192−2194. (c) Ilchenko, N. O.; Hedberg, M.; Szabó, K. J. Fluorinative Ring-Opening of Cyclopropanes by Hypervalent Iodine Reagents. An efficient Method for 1,3-Oxyfluorination and 1,3-Difluorination. *Chem. Sci.* **2017**, *8*, 1056−1061. (d) Banik, S. M.; Mennie, K. M.; Jacobsen, E. N. Catalytic 1,3-Difunctionalization via Oxidative C−C Bond Activation. *J. Am. Chem. Soc.* **2017**, *139*, 9152−9155. (e) Zhang, Z.-Y.; Liu, Z.-Y.; Guo, R.-T.; Zhao, Y.-Q.; Li, X.; Wang, X.-C. $B(C_6F_5)_3$-Catalyzed Ring Opening and Isomerization of Unactivated Cyclopropanes. *Angew. Chem., Int. Ed.* **2017**, *56*, 4028−4032. (f) Gieuw, M. H.; Ke, Z.; Yeung, Y.-Y. Lewis Base-Promoted Ring-Opening 1,3-Dioxygenation of Unactivated Cyclopropanes Using a Hypervalent Iodine Reagent. *Angew. Chem., Int. Ed.* **2018**, *57*, 3782−3786. (g) Skvorcova, M.; Jirgensons, A. Amide-Group-Directed Protonolysis of Cyclopropane: An Approach to 2,2-Disubstituted Pyrrolidines. *Org. Lett.* **2017**, *19*, 2478−2481. (h) Skvorcova, M.; Lukasevics, L. T.; Jirgensons, A. Amination of Carbenium Ions Generated by Directed Protonolysis of Cyclopropane. *J. Org. Chem.* **2019**, *84*, 3780−3792.

(7) Pitts, C. R.; Ling, B.; Snyder, J. A.; Bragg, A. E.; Lectka, T. Aminofluorination of Cyclopropanes: A Multifold Approach through a Common, Catalytically Generated Intermediate. *J. Am. Chem. Soc.* **2016**, *138*, 6598−6609.

(8) (a) Ge, L.; Wang, D.-X.; Xing, R.; Ma, D.; Walsh, P. J.; Feng, C. Photoredox-Catalyzed Oxo-amination of Aryl Cyclopropanes. *Nat. Commun.* **2019**, *10*, 4367. (b) Petzold, D.; Singh, P.; Almqvist, F.; König, B. Visible-Light-Mediated Synthesis of β-Chloro Ketones from Aryl Cyclopropanes. *Angew. Chem., Int. Ed.* **2019**, *58*, 8577−8580. (c) Yang, S.; Wang, L.; Zhang, H.; Liu, C.; Zhang, L.; Wang, X.; Zhang, G.; Li, Y.; Zhang, Q. Copper-Catalyzed Asymmetric Aminocyanation of Arylcyclopropanes for Synthesis of γ-Amino Nitriles. *ACS Catal.* **2019**, *9*, 716−721. (d) Zuo, Z.; Daniliuc, C. G.; Studer, A. Cooperative NHC/Photoredox Catalyzed Ring-Opening of Aryl Cyclopropanes to 1-Aroyloxylated-3-Acylated Alkanes. *Angew. Chem., Int. Ed.* **2021**, *60*, 25252−25257. (e) Zhao, H.; Fan, X.; Yu, J.; Zhu, C. Silver-catalyzed ring-opening strategy for the synthesis of β- and γ-fluorinated ketones. *J. Am. Chem. Soc.* **2015**, *137*, 3490−3493. (f) Fan, X.; Zhao, H.; Yu, J.; Bao, X.; Zhu, C. Regiospecific synthesis of distally chlorinated ketones via C−C bond cleavage of cycloalkanols. *Org. Chem. Front.* **2016**, *3*, 227−232. (g) Feng, T.; Liu, C.; Wu, Z.; Wu, X.; Zhu, C. Redox-neutral manganese-catalyzed synthesis of 1-pyrrolines. *Chem. Sci.* **2022**, *13*, 2669−2673.

(9) (a) Klehr, M.; Schäfer, H. J. Anodic Oxidation of Cyclopropane Derivatives. *Angew. Chem., Int. Ed.* **1975**, *14*, 247−248. (b) Kumar, R.; Banerjee, N.; Kumar, P.; Banerjee, P. Electrochemical Synthesis and

Reactivity of Three-Membered Strained Carbo- and Heterocycles. *Chem. - Eur. J.* **2023**, *29*, No. e202301594.
(10) Shono, T.; Matsumura, Y. Organic Synthesis by Electrolysis. VI. Anodic Oxidation of Arylcyclopropanes. *J. Org. Chem.* **1970**, *35*, 4157−4160.
(11) Peng, P.; Yan, X.; Zhang, K.; Liu, Z.; Zeng, L.; Chen, Y.; Zhang, H.; Lei, A. Electrochemical C−C Bond Cleavage of Cyclopropanes Towards the Synthesis of 1,3-Difunctionalized Molecules. *Nat. Commun.* **2021**, *12*, 3075.
(12) Zhou, W.; Chen, P.; Li, Z.-Q.; Xiao, L.-T.; Bai, J.; Song, X.-R.; Luo, M.-J.; Xiao, Q. Electrochemical 1,3-Alkyloxylimidation of Arylcyclopropane Radical Cations: Four-Component Access to Imide Derivatives. *Org. Lett.* **2023**, *25*, 6919−6924.
(13) Sheng, W.; Huang, X.; Cai, J.; Zheng, Y.; Wen, Y.; Song, C.; Li, J. Electrochemical Oxidation Enables Regioselective 1,3-Hydroxyfunctionalization of Cyclopropanes. *Org. Lett.* **2023**, *25*, 6178−6183.
(14) Huang, X.; Cai, J.; Zheng, Y.; Song, C.; Li, J. Electrochemical-Induced 1,3-Oxohydroxylation of Arylcyclopropanes. *Adv. Synth. Catal.* **2024**, *366*, 201.
(15) Cai, J.; Wen, Y.; Sheng, W.; Huang, X.; Zheng, Y.; Song, C.; Li, J. Electrochemical Ring-Opening 1,3-Dihydroxylation of Arylcyclopropanes with H_2O. *Green Chem.* **2023**, *25*, 6618−6622.
(16) (a) Gassman, P. G.; Yamaguchi, R. Electrochemical Oxidation of Strained Hydrocarbons. *J. Am. Chem. Soc.* **1979**, *101*, 1308−1310. (b) Shono, T.; Matsumura, Y.; Nakagawa, Y. Electroorganic chemistry. VII. Anodic Oxidation of Cyclopropanes. *J. Org. Chem.* **1971**, *36*, 1771−1775. (c) Matsubara, Y.; Uchida, T.; Ohnishi, T.; Kanehira, K.; Fujita, Y.; Hirashima, T.; Nishiguchi, I. Selective Cleavage of Polycyclic Cyclopropanes by Electrochemical Oxidation. *Tetrahedron Lett.* **1985**, *26*, 4513−4516.
(17) Uchida, T.; Matsubara, Y.; Nishiguchi, I.; Hirashima, T.; Ohnishi, T.; Kanehira, K. Electrochemical Oxidation of Polycyclic Cyclopropanes and Camphene. Novel Synthesis of exo-5,5-Dimethyl-6-methylenebicyclo[2.2.1]heptan-2-ol (nojigiku alcohol). *J. Org. Chem.* **1990**, *55*, 2938−2943.
(18) Xiong, P.; Xu, H.-C. Chemistry with Electrochemically Generated *N*-Centered Radicals. *Acc. Chem. Res.* **2019**, *52*, 3339−3350.
(19) Bordwell, F. G.; Algrim, D. J.; Harrelson, J. A. The relative ease of removing a proton, a hydrogen atom, or an electron from carboxamides versus thiocarboxamides. *J. Am. Chem. Soc.* **1988**, *110*, 5903−5904.
(20) Walton, J. C. Homolytic Substitution: A Molecular Ménage à Trois. *Acc. Chem. Res.* **1998**, *31*, 99−107.
(21) (a) Yoshida, J.; Ishichi, Y.; Isoe, S. Intramolecular Carbon-Carbon Bond Formation by the Anodic Oxidation of Unsaturated.alpha.-stannyl Heteroatom Compounds. Synthesis of Fluorine Containing Heterocyclic Compounds. *J. Am. Chem. Soc.* **1992**, *114*, 7594−7595. (b) Yoshida, J.-i.; Sugawara, M.; Kise, N. Organothio Groups as Electroauxiliaries: Electrooxidative Inter- and Intramolecular Carbon-Carbon Bond Formation. *Tetrahedron Lett.* **1996**, *37*, 3157−3160. (c) Leech, M. C.; Nagornïi, D.; Walsh, J. M.; Kiaku, C.; Poole, D. L.; Mason, J.; Goodall, I. C. A.; Devo, P.; Lam, K. eFluorination Using Cheap and Readily Available Tetrafluoroborate Salts. *Org. Lett.* **2023**, *25*, 1353−1358. (d) Kiaku, C.; Martinage, D.; Sicim, Y.; Leech, M. C.; Walsh, J. M.; Poole, D. L.; Mason, J.; Goodall, I. C. A.; Devo, P.; Lam, K. eFluorination of Activated Alcohols Using Collidinium Tetrafluoroborate. *Org. Lett.* **2023**, DOI: 10.1021/acs.orglett.3c00976. (e) Yue, Y.; Song, Y.; Zhao, S.; Zhang, C.; Zhu, C.; Feng, C. Electrooxidative Fluorofunctionalization of Arylcyclopropanes. *Org. Lett.* **2023**, *25*, 7385−7389.
(22) Xiong, P.; Long, H.; Song, J.; Wang, Y.; Li, J.-F.; Xu, H.-C. Electrochemically Enabled Carbohydroxylation of Alkenes with H_2O and Organotrifluoroborates. *J. Am. Chem. Soc.* **2018**, *140*, 16387−16391.

https://doi.org/10.1021/acs.orglett.4c00143
Org. Lett. XXXX, XXX, XXX−XXX

Darzina, **M**.; Lielpetere, A.; Jirgensons, A.

Preparation of furfural derived enantioenriched vinyl oxazoline building block and exploring its reactivity.

Beilstein J. Org. Chem. **2025,** *21,* 1737–1741.

https://doi.org/10.3762/bjoc.21.136

The Supporting Information is available free of charge on the Beilstein Journal of Organic Chemistry website:

https://doi.org/10.3762/bjoc.21.136

BEILSTEIN JOURNAL OF ORGANIC CHEMISTRY

Preparation of a furfural-derived enantioenriched vinyloxazoline building block and exploring its reactivity

Madara Darzina[1,2], Anna Lielpetere[1] and Aigars Jirgensons[*1]

Full Research Paper

Open Access

Address:
[1]Latvian Institute of Organic Synthesis Aizkraukles 21, Riga, LV-1006, Latvia and [2]Faculty of Natural Sciences and Technology, Riga Technical University, 3 P. Valdena Street, Riga LV-1048, Latvia

Email:
Aigars Jirgensons[*] - aigars@osi.lv

[*] Corresponding author

Keywords:
aza-Diels–Alder reaction; electrosynthesis; furfural; valinol; vinyloxazoline

Beilstein J. Org. Chem. **2025,** *21,* 1737–1741.
https://doi.org/10.3762/bjoc.21.136

Received: 28 May 2025
Accepted: 21 August 2025
Published: 29 August 2025

Associate Editor: J. A. Murphy

Abstract

N-Alloc-protected furfuryl amino alcohols derived from furfural and L- or D-valinol were subjected to Torii-type ester electrosynthesis to obtain the corresponding unsaturated esters. These served as key intermediates to prepare (*S*)- and *(R)*-enantioenriched unsaturated amides by *N*-Alloc deprotection which induced concomitant methoxymethyl group cleavage, *O*-to-*N* rearrangement, and isomerization of the double bond. An oxazoline ring formation in the resulting unsaturated amides provided the corresponding enantioenriched vinyloxazoline. The reactivity of the electron-deficient double bond in the vinyloxazoline was explored in several reactions. Out of these, the aza-Diels–Alder reaction with TsNCO was successful, leading to a highly diastereoselective formation of an oxazolo[3,2-*c*]pyrimidine derivative.

Introduction

The utilization of biomass as an alternative to fossil feedstock is central to circular economy for the production of value-added products [1-7]. Furfural [furan-2-carbaldehyde (**1**)], a platform compound derived from lignocellulosic biomass, has been utilized to obtain a range of versatile chemicals with applications to functional materials, pharmaceutically relevant compounds, and agrochemicals [8-17]. In our recent work, we have developed a Torii-type electrosynthesis of unsaturated esters **3a–c** starting from furfural (**1**) and amino alcohol conjugates **2a–c** [18]. The process involves an electrooxidative dialkoxylation of the furan ring providing spirocycles **4a–c** which undergo a further electrooxidative fragmentation to products **3a–c**. However, the further transformation of products **3a–c** was hampered by the problematic removal of the protecting groups (Ts, Boc, Ac) under the conditions compatible with the double bond and acetal functions. In this work, we present Torii-type electrosynthesis of ester **3d** (PG = Alloc) and its transformation to the enantioenriched vinyloxazoline building block **6**, which can be used for the asymmetric synthesis of complex molecules [19-24] (Scheme 1).

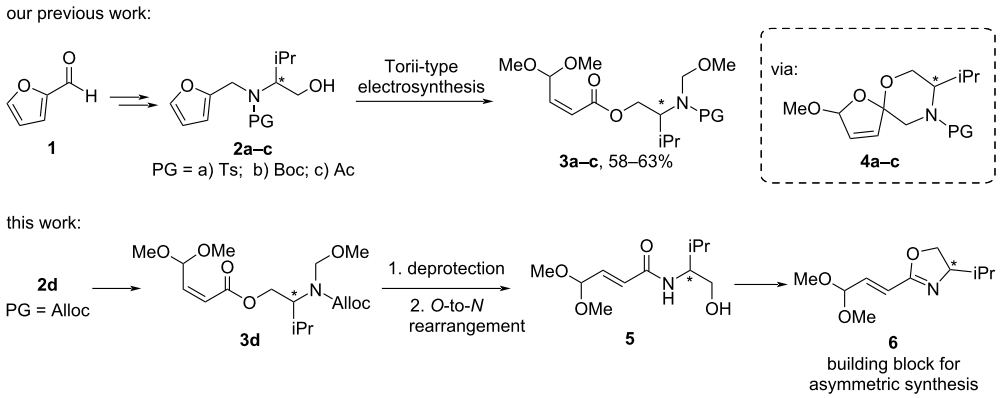

Scheme 1: Proposed approach for the preparation of vinyloxazoline **6**.

The proposed strategy relied on the *N*-deprotection of the intermediate ester **3d** inducing *O*-to-*N* rearrangement to form amide **5** as a precursor of vinyloxazoline **6**. For this purpose, Alloc (allyloxycarbonyl) turned out to be a suitable *N*-protecting group as it was compatible with the electrolysis conditions and its removal was compatible with the double bond and acetal functions in ester **3d** (see Supporting Information File 1 for attempts of other protecting groups such as Boc, Troc, and tfa). However, Pd-catalyzed *N*-Alloc deprotection induced isomerization of the double bond leading to the *trans*-isomer of amide **5**.

Results and Discussion

The protected furfuryl amino alcohols *S*-**2d** and *R*-**2d** were prepared by reductive amination of furfural (**1**) with L- and D-valinol followed by *N*-protection with Alloc-Cl (Scheme 2). The amino alcohols *S*-**2d** and *R*-**2d** were then subjected to electrochemical oxidation in methanol in batch electrolysis conditions, providing unsaturated esters *S*-**3d** and *R*-**3d**, respectively (Scheme 2). The previously used one-reactor two-step conditions were found to be productive for the electrosynthesis of *S*-**3d**, requiring the addition of acetic acid for the intermediate spiroketal **4d** oxidation (Table 1, entry 1). We found that substrate *S*-**2d** can be transformed to ester *S*-**3d** in a single step with a reduced amount of HFIP as the only additive (Table 1, entries 2 and 3). Given the high cost of HFIP, we examined if it could be replaced with other proton donors for the cathode reaction, and we found that acetic acid served well for this purpose (Table 1, entry 4). Using the reaction conditions with acetic acid as additive, the reaction could be performed also in a 0.5 g scale for the synthesis of both ester enantiomers *S*-**3d** and *R*-**3d** (Table 1, entries 5 and 6). In the absence of acetic acid or HFIP the electrochemical oxidation also provided the desired product **3d**, although in reduced yield (Table 1, entry 7). An increased amount of acetic acid (1 mL or ≈ 18 equiv) also reduced the yield (Table 1, entry 8). The attempt to use LiOAc as electrolyte instead of $LiClO_4$ was not successful as the reaction was stopped at the spirocycle **4d** formation stage (Table 1, entry 9).

The removal of the *N*-Alloc group in unsaturated ester *S*-**3d** was performed using a Pd catalyst and pyrrolidine as a nucleophile. The use of $Pd(PPh_3)_4$ as the catalyst led to a fast consumption of the starting material *S*-**3d** but provided a mixture of *cis*- and *trans*-amides *cis*-*S*-**5** and *trans*-*S*-**5** (Scheme 3). The use of $PdCl_2$(*S*-BINAP) complex as a precatalyst resulted in a longer reaction time and an exclusive formation of amide *trans*-*S*-**5** with isomerized double bond (Scheme 4). The amide *trans*-*R*-**5** was prepared analogously from ester *R*-**3d**.

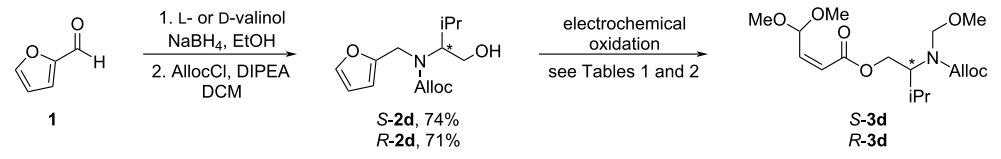

Scheme 2: Synthesis of furfuryl amino alcohols *S*-**2d** and *R*-**2d** and their electrochemical oxidation to esters *S*-**3d** and *R*-**3d**.

Table 1: Electrochemical oxidation of protected amino alcohol **2d** to ester **3d**.

Entry	Conditions[a]	Yield of **3d**
1[b]	1st step: MeOH/HFIP (10:4 mL), $LiClO_4$ (1 equiv), 2.0 F; 2nd step: add AcOH (4 equiv), 3.5 F	72% (*S*-**3d**)
2	single step: MeOH/HFIP (13:1 mL), $LiClO_4$ (1 equiv), 5.5 F	71% (*S*-**3d**)
3	single step: MeOH/HFIP (13.5:0.5 mL), $LiClO_4$ (1 equiv), 5.5 F	70% (*S*-**3d**)
4	single step: MeOH (14 mL), AcOH (3 equiv), $LiClO_4$ (1 equiv), 5.5 F	72% (*S*-**3d**)
5[b]	single step: MeOH (14 mL), AcOH (3 equiv), $LiClO_4$ (0.5 equiv), 5.5 F	68%[c] (*S*-**3d**)
6[b]	single step: MeOH (14 mL), AcOH (3 equiv), $LiClO_4$ (0.5 equiv), 5.5 F	68% (*R*-**3d**)
7	single step: MeOH (14 mL), $LiClO_4$ (1 equiv), 5.5 F	60% (*S*-**3d**)
8	single step: MeOH/AcOH (13:1 mL), $LiClO_4$ (1 equiv), 5.5 F	55% (*S*-**3d**)
9	single step: MeOH (14 mL), AcOH (3 equiv), LiOAc (1 equiv), 5.5 F	0%[d] (*S*-**3d**)

[a]Scale: 1 mmol. [b]Scale: 2 mmol. [c]Faradaic efficiency 49.5%; cell productivity 0.09 mmol/h. [d]Major product is spirocycle **4d** (PG = Alloc).

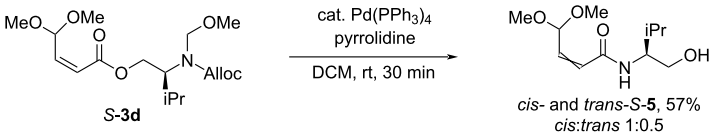

Scheme 3: Cleavage of the *N*-Alloc group leading to a mixture of isomers *cis*-*S*-**5** and *trans*-*S*-**5**.

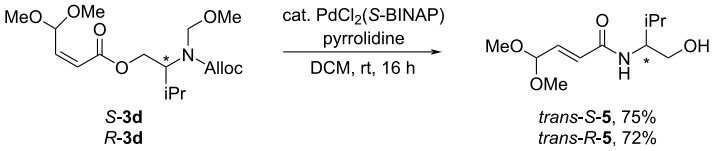

Scheme 4: Cleavage of the *N*-Alloc group with $PdCl_2$(*S*-BINAP) leading to *trans*-*S*-**5** and *trans*-*R*-**5**.

Thus, Alloc was validated as non-expensive and relatively small *N*-protecting group, removal of which is compatible with double bond and acetal function of amides *S*-**5** and *R*-**5**. The removal of the Pd catalyst at laboratory scale was done by chromatography. For large scale synthesis, Pd scavengers have to be considered at the work-up.

Unsaturated amides *trans*-*S*-**5** and *trans*-*R*-**5** were transformed to oxazolines *S*-**6** and *R*-**6** in good yields by mesylation of the hydroxy group (Scheme 5). Having both enantiomers in hand, the enantiomeric excess of oxazolines *S*-**6** and *R*-**6** was determined by chiral HPLC. This confirmed that no erosion of enantiomeric purity had happened during the deprotection stage.

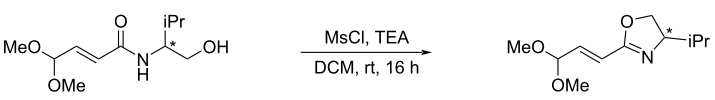

Scheme 5: Cyclization of amides *trans*-*S*-**5** and *trans*-*R*-**5** to oxazolines *S*-**6** and *R*-**6**.

With the enantioenriched vinyloxazoline *S*-**6** in hand, we explored the reaction scope involving its electron-deficient double bond. Unfortunately, the olefin appeared unreactive or gave a mixture of products in copper-catalyzed 1,4-addition of phenylmagnesium bromide, Giese reaction with 2-iodopropane, Simmons–Smith or Johnson–Corey–Chaykovsky cyclopropanation, hydroboration reaction with 9-BBN, and Diels–Alders reaction with Danishevsky diene. Gratifyingly, it was found that vinyloxazoline *S*-**6** is a good substrate for an aza-Diels–Alder reaction with tosylisocyanate (TsNCO) providing the oxazolo[3,2-*c*]pyrimidine derivative **7** as the only detectable diastereomer (Scheme 6) [22-24]. Oxazolo[3,2-*c*]pyrimidines are substructures in several pharmaceutically relevant compounds such as potent gonadotropin-releasing hormone receptor antagonists with potential application as anticancer drugs [25] and as nucleoside analogs with antiviral potency [26].

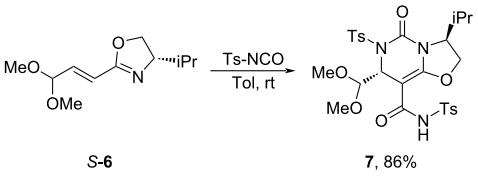

S-**6** **7**, 86%

Scheme 6: aza-Diels–Alder reaction of vinyloxazoline *S*-**6** with TsNCO.

According to the reaction mechanism proposed by Elliott et al., the aza-Diels–Alder reaction of vinyloxazoline *S*-**6** with TsNCO is a step-wise process [22]. The first step involves addition of the oxazoline nitrogen to TsNCO leading to a zwitterionic intermediate **A**, which undergoes 1,4-conjugate addition forming a cyclic intermediate **B**. Subsequently, the electron-rich double bond in intermediate **B** reacts with a second equivalent of TsNCO to form oxazolo[3,2-*c*]pyrimidine derivative **7** (Scheme 7).

The highly diastereoselective formation of product **7** can be explained based on the theoretical calculations by Elliott et al. of aza-Diels–Alder reaction of vinyloxazoline with TsNCO [19]. According to their investigations, the aza-nucleophile attack to the double bond in intermediate **A** is kinetically preferred from the face forming the *R*-configured carbon of the C–N bond as a result of a minimized steric interaction of the oxygen in zwitterion with iPr substituent of oxazoline.

Conclusion

Unsaturated ester obtained by Torii-type ester electrosynthesis from the conjugate of two biobased starting materials furfural and valinol serves as an intermediate to prepare an enantioenriched vinyl oxazoline **6** with atom economy 24.5% over 5 steps (>75% average per step). The electrochemical oxidation of *N*-Alloc can be performed as a single step operation in MeOH with acetic acid as an additive. This is a step toward the large scale synthesis of enantioenriched vinyloxazolines **6** from biomass-derived furfural, however, several challenges remain such as replacing $LiClO_4$ as electrolyte at the oxidation step and avoiding chromatography for purification. Further scale-up could be achieved by switching to flow conditions, or designing a continuous tank reactor [27].

Several attempts were made to explore enantioenriched vinyloxazoline **6** as a chiral building block. While additions to the double bond were not successful, vinyloxazoline **6** was found to be a competent substrate for the aza-Diels–Alder reaction in with TsNCO to give oxazolo[3,2-*c*]pyrimidine derivative **7** as a single diastereomer.

Supporting Information

Supporting Information File 1

Experimental procedures, characterization data and copies of NMR spectra.
[https://www.beilstein-journals.org/bjoc/content/supplementary/1860-5397-21-136-S1.pdf]

Funding

This project has received funding from the European Union's Horizon Europe research and innovation program under grant

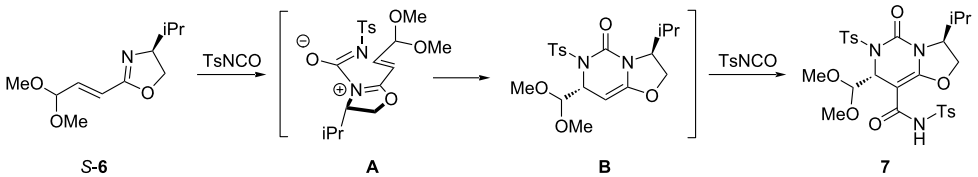

S-**6** **A** **B** **7**

Scheme 7: The proposed mechanism of product **7** formation.

agreement No 101057816 – TRANSPHARM. M. Darzina acknowledges financial support from LIOS internal student grant IG-2021-03 and Recovery and Resilience Facility (RRF) (5.2.1.1.i.) grant Nr. 34/OSI/DG (2025).

Author Contributions

Madara Darzina: investigation; writing – original draft. Anna Lielpetere: investigation; writing – original draft. Aigars Jirgensons: conceptualization; funding acquisition; project administration; writing – original draft; writing – review & editing.

ORCID® iDs

Anna Lielpetere - https://orcid.org/0000-0002-4727-0935
Aigars Jirgensons - https://orcid.org/0000-0002-8937-8792

Data Availability Statement

All data that supports the findings of this study is available in the published article and/or the supporting information of this article.

Preprint

A non-peer-reviewed version of this article has been previously published as a preprint: https://doi.org/10.3762/bxiv.2025.35.v1

References

1. Corma, A.; Iborra, S.; Velty, A. *Chem. Rev.* **2007,** *107,* 2411–2502. doi:10.1021/cr050989d
2. Li, H.; Guo, H.; Fang, Z.; Aida, T. M.; Smith, R. L. *Green Chem.* **2020,** *22,* 582–611. doi:10.1039/c9gc03655e
3. He, J.; Chen, L.; Liu, S.; Song, K.; Yang, S.; Riisager, A. *Green Chem.* **2020,** *22,* 6714–6747. doi:10.1039/d0gc01869d
4. Hommes, A.; Heeres, H. J.; Yue, J. *ChemCatChem* **2019,** *11,* 4671–4708. doi:10.1002/cctc.201900807
5. Iglesias, J.; Martínez-Salazar, I.; Maireles-Torres, P.; Martin Alonso, D.; Mariscal, R.; López Granados, M. *Chem. Soc. Rev.* **2020,** *49,* 5704–5771. doi:10.1039/d0cs00177e
6. Sun, Z.; Barta, K. *Chem. Commun.* **2018,** *54,* 7725–7745. doi:10.1039/c8cc02937g
7. Li, X.-L.; Zhang, K.; Jiang, J.-L.; Zhu, R.; Wu, W.-P.; Deng, J.; Fu, Y. *Green Chem.* **2018,** *20,* 362–368. doi:10.1039/c7gc03125d
8. Liu, X.; Li, Y.; Deng, J.; Fu, Y. *Green Chem.* **2019,** *21,* 4532–4540. doi:10.1039/c9gc01767d
9. Song, S.; Fung Kin Yuen, V.; Di, L.; Sun, Q.; Zhou, K.; Yan, N. *Angew. Chem., Int. Ed.* **2020,** *59,* 19846–19850. doi:10.1002/anie.202006315
10. Scodeller, I.; Mansouri, S.; Morvan, D.; Muller, E.; de Oliveira Vigier, K.; Wischert, R.; Jérôme, F. *Angew. Chem., Int. Ed.* **2018,** *57,* 10510–10514. doi:10.1002/anie.201803828
11. Mariscal, R.; Maireles-Torres, P.; Ojeda, M.; Sádaba, I.; López Granados, M. *Energy Environ. Sci.* **2016,** *9,* 1144–1189. doi:10.1039/c5ee02666k
12. Lange, J.-P.; Wadman, S. H. *ChemSusChem* **2020,** *13,* 5329–5337. doi:10.1002/cssc.202001376
13. Kuznetsov, A.; Kumar, G.; Ardagh, M. A.; Tsapatsis, M.; Zhang, Q.; Dauenhauer, P. J. *ACS Sustainable Chem. Eng.* **2020,** *8,* 3273–3282. doi:10.1021/acssuschemeng.9b06881
14. Li, X.; Jia, P.; Wang, T. *ACS Catal.* **2016,** *6,* 7621–7640. doi:10.1021/acscatal.6b01838
15. Li, M.; Dong, X.; Zhang, N.; Jérôme, F.; Gu, Y. *Green Chem.* **2019,** *21,* 4650–4655. doi:10.1039/c9gc02206f
16. Simeonov, S. P.; Ravutsov, M. A.; Mihovilovic, M. D. *ChemSusChem* **2019,** *12,* 2748–2754. doi:10.1002/cssc.201900601
17. Babij, N. R.; Choy, N.; Cismesia, M. A.; Couling, D. J.; Hough, N. M.; Johnson, P. L.; Klosin, J.; Li, X.; Lu, Y.; McCusker, E. O.; Meyer, K. G.; Renga, J. M.; Rogers, R. B.; Stockman, K. E.; Webb, N. J.; Whiteker, G. T.; Zhu, Y. *Green Chem.* **2020,** *22,* 6047–6054. doi:10.1039/d0gc02063j
18. Darzina, M.; Lielpetere, A.; Jirgensons, A. *Eur. J. Org. Chem.* **2021,** 4224–4228. doi:10.1002/ejoc.202100605
19. Barluenga, J.; Suárez-Sobrino, A. L.; Tomás, M.; García-Granda, S.; Santiago-García, R. *J. Am. Chem. Soc.* **2001,** *123,* 10494–10501. doi:10.1021/ja010719m
20. Mitsui, K.; Sato, T.; Urabe, H.; Sato, F. *Angew. Chem., Int. Ed.* **2004,** *43,* 490–492. doi:10.1002/anie.200352769
21. Meyers, A. I.; Stoianova, D. *J. Org. Chem.* **1997,** *62,* 5219–5221. doi:10.1021/jo970429h
22. Elliott, M. C.; Kruiswijk, E.; Willock, D. J. *Tetrahedron Lett.* **1998,** *39,* 8911–8914. doi:10.1016/s0040-4039(98)01949-2
23. Elliott, M. C.; Kruiswijk, E. *J. Chem. Soc., Perkin Trans. 1* **1999,** 3157–3166. doi:10.1039/a905700e
24. Elliott, M. C.; Kruiswijk, E. *Chem. Commun.* **1997,** 2311–2312. doi:10.1039/a705571d
25. Pontillo, J.; Chen, C. *Bioorg. Med. Chem. Lett.* **2005,** *15,* 1407–1411. doi:10.1016/j.bmcl.2005.01.009
26. Folkers, G.; Junginger, G.; Müller, C. E.; Schloz, U.; Eger, K. *Arch. Pharm. (Weinheim, Ger.)* **1989,** *322,* 119–123. doi:10.1002/ardp.19893220213
27. Lehnherr, D.; Chen, L. *Org. Process Res. Dev.* **2024,** *28,* 338–366. doi:10.1021/acs.oprd.3c00340

License and Terms

Madara Dārziņa dzimusi 1994. gadā Rīgā. Latvijas Universitātē ieguvusi dabaszinātņu bakalaura (2018) un maģistra (2020) grādu ķīmijā. 2021. gadā saņēmusi Latvijas Zinātņu akadēmijas Jauno zinātnieku balvu par maģistra darbu "Elektroķīmiska α,β-nepiesātinātu esteru iegūšana no 2-(hidroksimetil)furāna atvasinājumiem" (vadītājs prof. A. Jirgensons). 2024. gada vasarā kā viespētniece viesojās SynBioC grupā Gentes Universitātē (Beļģija). Patlaban strādā Latvijas Organiskās sintēzes institūta Organiskās sintēzes metodoloģijas grupā. Zinātniskās intereses saistītas ar elektroorganisko un organisko sintēzi. Ir piecu zinātnisko oriģinālpublikāciju līdzautore.

Madara Dārziņa was born in Riga in 1994. She obtained a Bachelor's degree (2018) and a Master's degree (2020) in Natural Sciences in Chemistry from the University of Latvia. In 2021, she received the Latvian Academy of Sciences Young Scientist Award for her Master's Thesis "Electrochemical synthesis of α,β-unsaturated esters from 2-(hydroxymethyl)furan derivatives" (supervisor Prof. A. Jirgensons). In the summer of 2024, she was a visiting researcher at the SynBioC group at Ghent University, Belgium. She currently works in the Organic Synthesis Methodology Group at the Latvian Institute of Organic Synthesis. Her scientific interests are related to electroorganic and organic synthesis. She is the co-author of five original scientific publications.